Titre: Title:	Fluorescent Gold-Silver Alloy Core Silica Shell Nanoparticles for Bioimaging Applications
Auteur: Author:	Siyu Tu
Date:	2016
Type:	Mémoire ou thèse / Dissertation or Thesis
Référence: Citation:	Tu, S. (2016). Fluorescent Gold-Silver Alloy Core Silica Shell Nanoparticles for Bioimaging Applications [Master's thesis, École Polytechnique de Montréal]. PolyPublie. https://publications.polymtl.ca/2393/

UNIVERSITÉ DE MONTRÉAL

FLUORESCENT GOLD-SILVER ALLOY CORE SILICA SHELL NANOPARTICLES FOR BIOIMAGING APPLICATIONS

SIYU TU

DÉPARTEMENT DE GÉNIE PHYSIQUE

ÉCOLE POLYTECHNIQUE DE MONTRÉAL

MÉMOIRE PRÉSENTÉ EN VUE DE L'OBTENTION

DU DIPLÔME DE MAÎTRISE ÈS SCIENCES APPLIQUÉES

(GÉNIE PHYSIQUE)

DÉCEMBRE 2016

UNIVERSITÉ DE MONTRÉAL

ÉCOLE POLYTECHNIQUE DE MONTRÉAL

Ce mémoire intitulé:

FLUORESCENT GOLD-SILVER ALLOY CORE SILICA SHELL NANOPARTICLES FOR BIOIMAGING APPLICATIONS

présenté par: TU Siyu

en vue de l'obtention du diplôme de : Maîtrise ès sciences appliquées

a été dûment accepté par le jury d'examen constitué de :

M. DESJARDINS Patrick, Ph. D., président

M. MEUNIER Michel, Ph. D., membre et directeur de recherche

M. BROUARD Danny, Ph. D., membre et codirecteur de recherche

Mme BOUDOUX Caroline, Ph. D., membre

DEDICATION

This thesis is dedicated to my parents. As the first time of my overseas study, I encounter so many challenges culturally, linguistically, physically and mentally. They supported me all the way as always and gave me suggestions to tackle problems and to be, for the first time, independent on my own.

ACKNOWLEDGEMENTS

First and foremost, my thanks and appreciations go to my supervisor Professor Michel Meunier, for accepting me in his group and gave me the chance to work in Laser processing and plasmonics laboratory after we have met in 2013 in China. During the last two years and a half, he provided significant advices for my research project and offered me the chance to undertake a summer research internship to Hema-Quebec, where I considerably advanced my master project.

I would thank equally my co-supervisor Dr. Danny Brouard. He proposed very interesting ideas and shared his strong background in this field. As a scientist at Héma-Quebec, he guided me tremendously on experiments not only on the optimization of fabrication but also on the biomedical applications. He also showed great patience and spared no efforts performing my presentation skills.

The members of the jury for the thesis, Patrick Desjardins and Caroline Boudoux have generously spent their time and expertise on revision of my work. I thank them for their contribution and support.

Thanks to my colleague David Rioux, who offered me important technical supports and precious scientific discussions. I appreciated very much the time he spent with me for troubleshooting my own experimental problems.

I’m also grateful to many people who shared their experience with me, especially Adrien Dagallier on Matlab programming, Josée Perreault, Mengjiao Qi on cell culture, and Weimeng Ding on tackling culture shock.

Last but not least, I would like to thank MEDITIS for its financial support and the personnel of Polytechnique for its hospitality, support, and resources so that I could learn so much during my master study.

RÉSUMÉ

Les nanomatériaux représentent un domaine de recherche en pleine expansion depuis quelques décénies. Plusieurs études portent sur le développement de nouveaux matériaux présentant de remarquables propriétés physiques, optiques ou mécaniques qui peuvent être exploitées avantageusement dans la conception d'architectures innovantes à l'échelle du nanomètre. La taille et la composition des nanoparticules d'alliages or-argent (Au / Ag), présentées dans ce mémoire, peuvent être modifiées ce qui permet d'accorder leurs propriétés plasmoniques en fonction des besoins d'une application. Ces mêmes alliages nanoparticulaires peuvent présenter des propriétés de fluorescence lorsqu'elles sont enrobées d'une couche de silice dopée de fluorophores. Ainsi, les alliages nanoparticulaires fluorescents offres plusieurs avantages par rapport à une utilisation en tant qu'agents de contrastes versatiles pour des applications biomédicales.

L'objectif principal de ce projet de maîtrise est le développement d'une architecture nanoparticulaires composé d'un cœur en alliage or-argent recouvert par une couche de silice fluorescente. Dans un second temps, la démonstration de l'applicabilité de cette nouvelle gamme de marqueurs cellulaires pour des expériences de reconnaissance et de marquage cellulaire sera effectuée.

On sait depuis longtemps que l'immunofluorescence, en tant que technique standard pour marquer les cellules, présente certains inconvénients tels que la limite d'intensité, les limites de multiplexage et le photoblanchiment. Alors que la diffusion de lumière par une nanoparticule plasmonique ne s'épuise jamais. Le noyau d'alliage Au/Ag exploite non seulement les mérites d'un signal de diffusion accordable mais aussi l'effet de rehaussement de la fluorescence par un métal. L'idée est de fabriquer les nanoparticules (NP) et de démontrer qu'elles permettent une nouvelle stratégie d'analyse en multiplex à l'aide d'une plate-forme multidétection

Au cours de cette étude de maîtrise, les NP d'Au/Ag@SiO_2 ont été fabriqués avec succès et reproductibilité. Plusieurs types de fluorophores avec des propriétés de fluorescence différentes ont été incorporés dans la coquille de silice de Au/Ag@SiO_2 NP. En utilisant une chimie relativement simple, il a même été possible d'augmenter les performances des fluorophores grâce à la présence de cœurs métalliques augmentant ainsi le signal de fluorescence. Pendant le

procédé de revêtement de la silice, un effet d'attaque au noyau métallique a été noté et il était plus sévère pour les noyaux riches en argent, créant un espace entre la surface du coeur métallique et la coquille de silice de la nanoparticule affectant par le fait même les propriétés photophysiques du système. Quatre types de NPs ont été préparés, en combinant deux rapports de composition Au / Ag différents (Ag pur et 50/50 Au/Ag) et deux types de fluorophore (fluorescéine et rhodamine). Un test d'identification des nanoparticules par microcopie optique a permis de démontrer que la reconnaissance des particules sur la base de leurs signatures spectrales uniques était possible. Lors du test, 86% des NPs déposées sur une surface de verre ont pu être correctement identifiées en utilisant un algorithme d'identification simple. En outre, les NPs ont été fonctionnalisées avec des anticorps et ciblés sur les cellules pour vérifier leur capacité à être marqueur cellulaire spécifique. Les résultats de la cytométrie de flux indiquent une fonctionnalisation réussie des NPs et le potentiel d'être des marqueurs cellulaires. Des travaux restent pour améliorer l'efficacité de dopage du fluorophore dans la coquille de silice et pour optimiser le processus de fonctionnalisation des anticorps.

ABSTRACT

Nanomaterials have been a popular research field for decades and scientists are always trying to develop novel materials. This can be achieved with a hybrid of existing material to either significantly improve the performance for certain applications or generate new properties which can be exploited for new applications. Two perfect examples are gold-silver (Au/Ag) alloy nanoparticles (NPs) with strong and tunable extinction spectra in the visible range and superluminescent NPs with a metallic core and dye-doped silica shell. Both of them can be used as contrast agents for biomedical imaging applications.

This research is based on the combination of these two types of NPs: the demonstration of a multiplexed bioimaging application with fluorescent NPs composed of a Au/Ag alloy core and a fluorophore-doped silica shell(Au/Ag@SiO_2). It has long been known that immunofluorescence, as the standard technique to label cells, has some drawbacks such as intensity limit, limited multiplexing and loss of signal due to photobleaching. Plasmonic NPs do not photobleach and do not lose their scattering signal. The Au/Ag alloy NPs with a core-shell structure not only exploit the merits of a tunable scattering signal from the core but also the metal enhanced fluorescence (MEF) effect from the shell near a metallic surface. In this research, we have fabricated the hybrid NPs and applied them in a multimodal platform to detect both scattering and fluorescence signals in order to improve the multiplexing capability.

During the master study, Au/Ag@SiO_2 NPs were successfully fabricated with high reproducibility. Different fluorophores with different emission wavelengths were incorporated in the silica shell of Au/Ag@SiO_2 NPs resulting in a stronger fluorescence signal in the presence of a metallic core. An etching effect of the metallic core was noted during the silica shell growth, creating a spacer between the surface of the metallic core and silica shell resulting in a slight blueshift of the plasmonic peak. This effect is more severe for silver-rich cores. Four types of NPs were prepared, with two different Au/Ag composition ratios (pure Ag and 50/50 Au/Ag) and two different fluorophores (fluorescein and rhodamine B) were incorporated into the silica shell for a bimodal multiplexed imaging test in scattering and fluorescence. A proportion of 86% of NPs on a glass slide can be identified and a similar result was obtained for NPs on cells. Furthermore, the NPs were functionalized with antibodies to target cells and flow cytometry

results indicate a successful functionalization of NPs which confirms their potential as cell markers. Future work will aim to improve the fluorophore doping efficiency and to optimize the antibody functionalization process.

TABLE OF CONTENTS

LIST OF TABLES

LIST OF FIGURES

LIST OF SYMBOLS AND ABBREVIATIONS

$Ag@SiO_2$	silver core silica shell
APC	Allophycocyanin
APTES	Aminopropyl triethoxysilane
AOT	Dioctyl sodium sulfosuccinate
$Au@SiO_2$	Gold core silica shell
$Au/Ag@SiO_2$	Gold-silver alloy core silica shell
CF647	Cyanine-based far-red fluorophore 647
CTAB	Cetrimonium bromide
DF	Darkfield
EtOH	Ethanol
FITC	Fluorescein
LSPR	Local surface plamsonic resonance
MEF	Metal enhanced fluorescence
NHS	N-Hydroxysuccinimide
NP	Nanoparticle
PE	Phycoerythrin
QD	Quantum dot
Rcf	Relative centrifugal force
RBITC	Rhodamine B isothiocyanate
SEF	Surface enhanced fluorescence
TEM	Transmitted electronic microscope
TEOS	Tetraethyl orthosilicate
W/O	water/oil

LIST OF APPENDICES

CHAPTER 1 INTRODUCTION

For the last decades, nanotechnology, as a growing field, has not only attracted a significant attention of researchers, but also made a considerable impact on the economy. Until the year of 2010, the value of products related to nanotechnology is estimated as high as 254 billion USD worldwide. Actually, by 2020, it is estimated that 6 million workers will be involved in nanotechnology product market[1]. According to a recent report of the symposium on assessing the economic impact[2], before the year of 2011, the focus of nanotechnology research was mainly on theoretical investigation and interdisciplinary study, while after 2011, a shift occurred from a more fundamental research to a more application-oriented research, with increasing complexity and multidisciplinary. With the development of various synthesis methods and full characterization techniques for all types of nanomaterials, such as nanoparticles (NPs), nanotubes, graphene, core-shell, etc., scientists can now design and optimise the performance and properties of nanomaterials in various fields of applications, such as: (i) energy, for example the noble metal NPs as photocatalysts[3-5]; (ii) health, for example mesoporous nanostructure for the drug delivery[6-9]; (iii) environment, for example by using photocatalytic copper tungsten oxide nanoparticles to clean up oil spills[10-12] and so on.

Optical imaging systems are necessary tools to help biologists and medical doctors to characterize cell phenotype in physiological and pathological conditions. There is a need to develop more sensitive, accurate and economical methods for detecting and treating cells such as cancer ones[13]. The selective cell labeling according to different cell types is of great interest because with such technique, certain kinds of cells can be distinguished from other types in the tissue. In order to efficiently target cells with specificity and easily observe them under microscope, it is important to develop efficient biomarkers of different optical properties such as different colors as contrast agents for multiplexed imaging.

The essential method in biology to visualize cells is to label proteins with specific antibodies and fluorescent dyes[14]. While fluorophores having an emission peak wavelength ranging from ultraviolet to near infrared, are commonly used in this identification, these molecules have however some problems. First, they suffer from photobleaching, a quick decay of emission intensity under strong exposure of light, limiting their use to very short observation time. Second, the intensity of the fluorescent signal from targeted cells is restricted to the number of fluorescent

molecules labeling on antibodies[15]. Since the fluorescent intensity is weak per fluorophore-labeled antibody, large quantities of antibodies are needed, thus increasing the cost of this approach. Moreover, if the investigated cells have only a few specific receptors, this technique may not function well due to the same problem. In addition, the fluorescent emission bandwidth of fluorescent molecule is usually quite broad and can easily cause spectra overlapping, making it harder to do multiplexed imaging. The upper limit of its multiplexed imaging capacity is around 7 colors at the same time[16].

Quantum dots(QDs) can be a good candidate for multiplexed imaging contrast agent because they have a narrow bandwidth and high photostability [17, 18]. Although being as an attractive alternative[19, 20], QDs have an universally observed fluorescence intermittency, namely blinking of QDs, which greatly influence the observation. As for the toxicity issue, many researchers are convinced that QDs will never be used for treating patients because of their potential toxicity[21].

Metallic NPs are of great interest for biomedical applications, mostly based on their extraordinary optical properties. When a metallic NP is irradiated, the light can induce an oscillation of free electrons in the NP and a resonance may happen at certain wavelength, which is called localized surface plasmon resonance (LSPR). This LSPR effect results in a strong absorption, scattering of light by NPs and an enhancement of electric field near NPs. Among metals, Au and Ag have the strongest LSPR effect and are frequently used for biomedical applications, such as photothermal therapy[22-24] and biomarkers for cells and tissues[13, 25-29].

Plasmonic NPs such as Au, Ag, and Au/Ag alloy, with different gold/silver composition ratios, present different plasmonic spectra and colors[30]. The Au/Ag alloy NPs were recently developed by our group and is a subject of a provisional patent[31]. Based on these noble metal NPs, more complex structures, core-shell for instance, can be synthesize to achieve specific goals. Researchers designed Ag core silica shell ($Ag@SiO_2$) NPs and Au core silica shell ($Au@SiO_2$) NPs to exploit the LSPR effect of the core on the shell coupling with different kinds of molecules, such as fluorescent molecules to enhance its properties. Based on plasmonic NPs, the advent of plasmonic metal core, silica shell structure[32, 33] multifunctional NPs take advantage of the facile silica chemistry to perform surface functionalization and the possibility of covalently

bonding fluorescent molecules (called plasmon-coupled fluorescent probes[34]) or loading drugs in the porous silica matrix[7-9].

In this master thesis we propose to design and synthesize a new hybrid biomarker combining fluorescent dyes with the Au/Ag alloy NPs by a core-shell structure with an alloy core resulting in a tunable scattering signal and a silica shell embedded with fluorescent dyes. We propose to adapt the silica shell growth chemistry developed for Au and Ag core to Au/Ag NPs and perform optical and structural characterization of the new hybrid NPs . Then, the use of our new hybrid biomarkers in multiplexed imaging with both scattering and fluorescence signal will be demonstrated.

Objectives and thesis plan

The objectives of this master research are based on the synthesis and characterization of fluorescent Au/Ag alloy core silica shell nanoparticles. The sub-objectives are:

1. Fabricate Au/Ag alloy nanoparticles with different Au/Ag composition ratio, develop silica coating afterward and change the size of particles for the convenience of coating and further imaging application;
2. Incorporate different fluorescent dyes into silica shell of NPs and ameliorate the synthesis process to obtain a uniform core-shell structure;
3. Demonstrate multiplexed imaging ability of the product to make the identification of single NP on cells for further cell labeling applications.

In order to demonstrate the research work done to fulfill the above objectives, the thesis is written with the following plan:

Chapter 2 includes the literature review of the relevant topics. The first part covers the synthesis methods of both noble metallic NPs and silica shell coating. The second part reviews the theoretical background of physics to explain the unique optical properties of such NPs. The third part proposes several applications in imaging where such NPs can be exploited

Chapter 3 is a transcription of article “Fluorescence and scattering dual-mode multiplexed imaging with gold-silver alloy core silica shell nanoparticles”. It also includes the supporting information of the article. This chapter corresponds to the first and third objectives showing the

proof of principle of multiplexed imaging with 4 different biomarkers in both scattering and fluorescence mode.

Chapter 4 focuses on improvements of synthesis method, quality controls and exploration of possible extension of dual-mode based multiplexing nanostrutures. More results and discussions are demonstrated to obtain the second objective above, covering the selection of structure, Au/Ag ratios, fluorescent molecules and the elimination of core-free silica NPs.

Chapter 5 presents the conclusion and proposes some future works based on Au/Ag alloy core silica shell nanoparticles.

This thesis also contains an annex that clarifies the multistage optical imaging set up.

CHAPTER 2 LITERATURE REVIEW

The objective of this master study is to fabricate gold-silver alloy core fluorescent silica shell NPs (Au/Ag@SiO_2 NPs) for bioimaging applications. This nanostructure is schematically presented in Figure 2.1 and involves the Au/Ag alloy NP fabrication and silica coating on noble metal surface incorporating fluorescent dyes. This chapter presents the methods of synthesis, characterization and applications of these hybrid plasmonic NPs. The first section is focused on different synthesis techniques, including chemical and physical approaches for metallic NPs formation and growth of silica layer. The second section covers the basic theory of plasmonic effect related to LSPR of noble metal NPs, including the optical properties, such as extinction spectrum, the color of NPs and near field enhancement of particles and their interaction with molecules such as fluorophores for metal enhanced fluorescence (MEF) application and other molecules for surface enhanced Raman spectroscopy (SERS). The third section introduces the use of these plasmonic nanostructures in bioimaging applications.

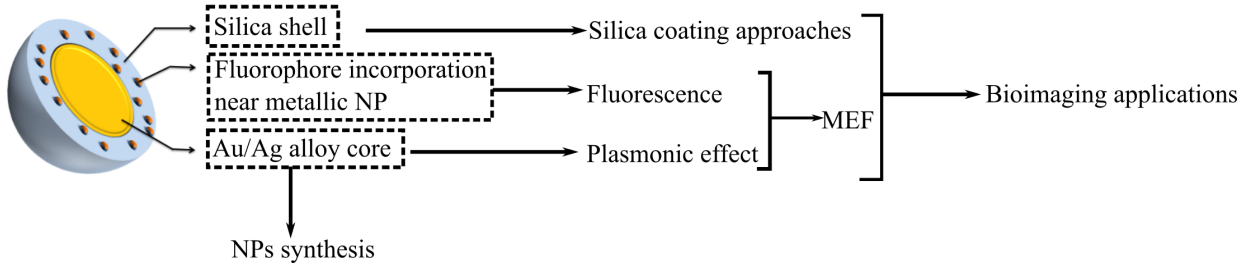

Figure 2.1 Schematics of the Au/Ag alloy core fluorescent silica shell NPs structure and the background topics to be discussed in this chapter.

2.1 Synthesis of gold-silver (Au/Ag) alloy NPs

The optical properties of NPs depend strongly on their geometry and chemical composition which in turn also strongly depend on the synthesis method used. For NPs, the synthesis methods are generally grouped into either a “bottom-up” or a “top-down” route (Figure 2.2). The first subsection of this part contains several popular methods of noble metal NPs fabrication and the second subsection introduces the silica coating process on the metallic surface (mostly gold and silver) to construct the core-shell structure.

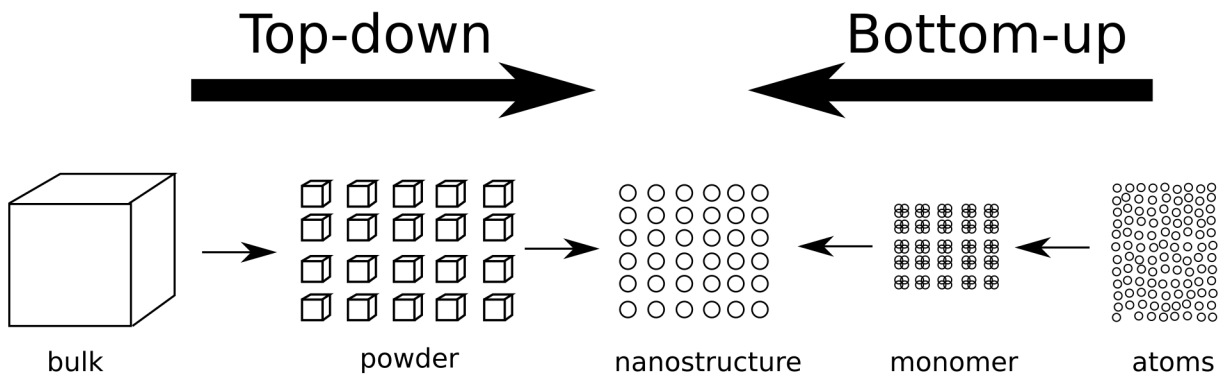

Figure 2.2 Schematics of top-down approaches and bottom-up approaches of nanomaterial synthesis.

Several gold-silver alloy nanoparticles synthesis methods have been introduced over the last decades. Dating back to 1976, Papavassilou[35] synthesized Au/Ag alloy NPs in colloidal solution through evaporating gold-silver alloy with different composition using a high-frequency electric bridge. In fact, Au/Ag alloy NPs are relatively hard to synthesize because of the existence of the phase separation at the atomic level, resulting in a preferable core-shell structure.[36] However, Papavassilou observed the extinction spectra of such NPs with only one resonance peak, indicating that gold and silver atoms were not in a core-shell structured phase separation. He also reported the linear correspondence of plasmonic peak position and chemical composition ratio (Au/Ag) of NPs.

In general, all synthesis of a material can be sorted into physical routes or chemical routes. In the case of Au/Ag alloy NPs synthesis, laser can be utilized to fabricate Au/Ag alloy NPs in both ways. For instance, the laser ablation can take place in a liquid medium where there is a target of Au/Ag alloy piece with a specified composition ratio. Similar to the method of evaporation used by Papavassilou, laser ablation is also a “top-down” approach, where the macroscopic material is broken down to NPs. Laser ablation method has been used by Lee and his coworkers[37] in liquid water with a Nd:YAG nanosecond laser at 1064nm. Since the optical energy delivered per unit area of the laser pulse is high enough to evaporate the alloy target, stoichiometric Au/Ag alloy NPs are formed with ejected atoms in the liquid.[38] Laser can also be used to assist a chemical route. For instance, Peng *et al*. [39] prepared Au/Ag alloy NPs with gold NPs in a solution of Ag^{+} ions by 532nm (or 355nm) laser irradiation. It is a “bottom-up” method, where the nanoparticles are formed originally from the separated atoms such as gold and silver ions.

Although the laser-ablation method is facile and synthesis is rapid, the laser-based set-up is not very available and alternative techniques have been considered, such as ultrasound[40], UV light[41], or simply heating. The essence of such chemical routes, apart from different irradiation approaches, is the same: mixed metallic component ions are reduced in the liquid simultaneously to form alloy NPs. The most frequently appearing reduction of gold and silver salts tetrachlorauric acid ($HAuCl_4$) and silver nitrate with a citrate acid. Link et al, among other pioneers, firstly used this co-reduction method to fabricate Au/Ag alloy NPs at 100℃.[42] Mallin et al conducted the sub-10nm Au/Ag alloy NPs synthesis at room temperature by using the reducing agent sodium borohydride ($NaBH_4$). [43]

Since the chemical route is used throughout this master work, we now cover the mechanism of formation of monodispersed Au/Ag alloy NPs as an example. The silica coating of NP will be discussed later in section 2.2.

2.1.1 Mechanism of chemical synthesis route

The most widely used synthesis technique of NPs is the Turkevich method.[44, 45] For Au NPs, it involves the chemical reduction of $HAuCl_4$ in a sodium citrate solution. Based on this method, Frens and his coworkers[46] have investigated the synthesis of 16-150nm gold NPs and concluded that the ratio citrate/metal affects largely the magnitude of NPs size and the size distribution. To understand this better, let us look at the mechanism of NPs formation. In general, as shown in Figure 2.3 there are three phases for NPs synthesis following the chemical route:

1. The reduction of ions of gold and silver to form monomers. This will continue until there is little ions left for reduction. In the meantime, the concentration of monomers keeps increasing and cross a critical value when the nucleation takes place.
2. The nucleation happens when the concentration of monomers exceed the critical value. The speed of nucleation mostly depends on the concentration of monomer. With the consumption of the monomers during nucleation, the concentration of monomers drops again within the critical value.
3. The growth involves monomers adhering on the nuclei to form the NPs. Ideally, a clear separation in time of the nucleation and growth will result in a very fine size distribution (monodispersed) of NPs. However, nucleation might continue during growth resulting in some smaller nuclei and non-monodispersed NPs.

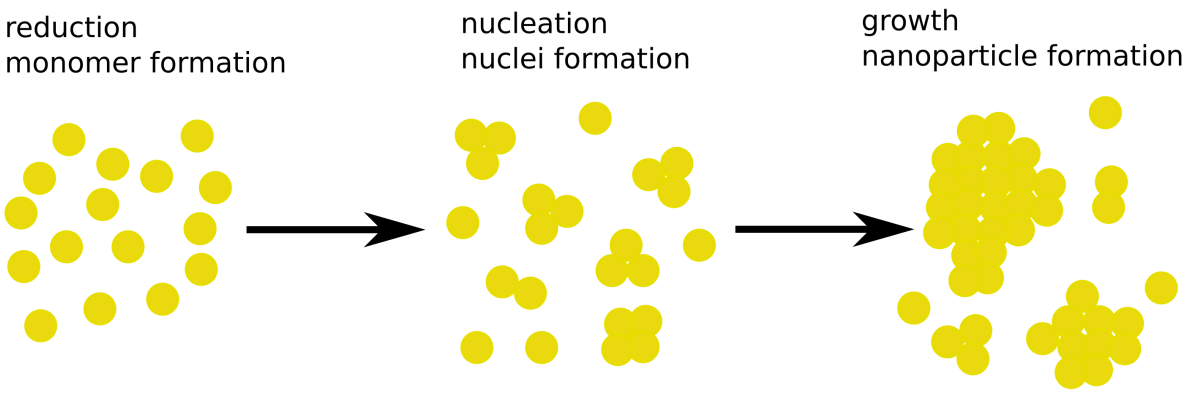

Figure 2.3 Schematics of 3 steps for the formation of NPs from metallic ions in solution. The metallic ions such as Au^{3+} are reduced to Au atom to form gold monomer dispersed in solution. The monomers aggregate to form Au nuclei and they grow larger with monomers sticking on the nuclei surface.

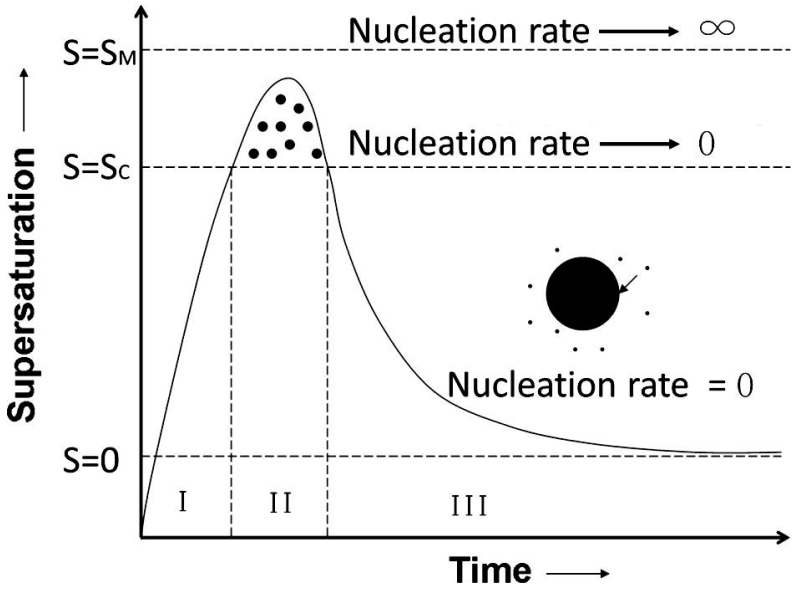

Figure 2.4: LaMer diagram illustrating NPs formation steps.[47] Phase I, II and III correspond respectively to the reduction state, nucleation state and NPs growth in Figure 2.3.

For most applications, it is preferable to have monodispersed NPs. We can use LaMer diagram shown in Figure 2.4 [48] to study how reaction conditions affect the NPs size and its distribution. The factors to modify conveniently are temperature and the concentration ratio of citrate and metallic ions (C_c/C_m). The former one, is usually fixed at 100℃. The discussion of C_c/C_m is as follows:

1. For a high C_c/C_m, the reducing rate is quite high and the concentration of monomer, in a short time, results in a high supersaturation ratio S. Shown in Figure 2.4, supersaturation is defined as current concentration of solute over the saturated concentration. When S is significantly greater than the critical value (S_c in the Figure 2.4), nucleation occurs. A large quantity of nuclei are quickly formed in this case, significantly reducing metallic ions or monomer concentration. The final sample contains many small NPs. Since the nucleation happens so fast, there is little time for growth during nucleation, thus resulting in monodispersed NPs formation with larger quantity but a smaller dimension.
2. For a small C_c/C_m, on the contrary, the low reducing rate will keep the supersaturation ratio narrowly above S_c thus providing a low nucleation rate. In this case, the growth of nuclei happens simultaneously with the generation of new nuclei. The early-generated nuclei result in larger NPs while the later-generated nuclei end up smaller, yielding to a polydispersity. Therefore, it is extremely hard to fabricate in a one-step synthesis relatively large nanoparticles with a narrow size distribution. Indeed, we need to have a relatively high concentration of gold and silver ions to be reduced in order to grow a larger nanoparticle, but restricted by the too low C_c/C_m to get large and monodispersed NPs. Frequently, the solution to such problem is a multi-step synthesis.

The next section covers a typical multi-step synthesis method named seed-mediated growth.

2.1.2 Seed-mediated growth

The seed-mediated growth is a "bottom-up" synthesis method that requires a proper concentration of seeds in the solution system so that the monomer formed through reduction can be easily grown onto their surface. Since the existing surface of the seed can provide the nucleation position with less surface energy, there is a better chance to nucleate onto the surface of seed when the concentration of monomers is low enough. Ideally, if all the monomers formed are on the surface of seeds equally distributed, the size of final NPs can be easily deduced according to the proportional relation between the volume of single nanoparticles and precursor ion numbers.

Gold and silver NPs with a large size ranging from tens to hundreds of nanometers were synthesized with seed-mediated growth method [49-52]. However, the monodispersed Au/Ag alloy NPs were recently obtained by Rioux et al [30] using the seed-mediated growth technique. In this case, the Au/Ag alloy NPs were fabricated from a gold seed of 13-15nm, and the precalculated Au^{3+}/Ag^{+} ions were added into a boiling water bath with citrate as reducing agent (see figure 2.5). Typically, the first growth step has a "Seeding Ratio (R)" of 10, which is defined as

$$R = \left(\frac{D_{final}}{D_{seed}}\right)^3 = \frac{N_{seed} + N_{metal}}{N_{seed}} = 1 + \frac{C_{final} V_{final}}{C_{seed} V_0} \quad (2.1)$$

Where D is the diameter of NPs, N denotes the total metallic atoms (Au and Ag), and C is the concentration of metallic atoms. Therefore, for R=10, the final NPs has an expected average diameter of 28.0 nm-32.3 nm according to different sizes of gold seeds.

Subsequently, the as-prepared alloy NPs were used as "Seeds" to fabricate larger NPs. This process keeps the C_c/C_m to an appropriate value favoring growth rather than nucleation, resulting in a relatively monodispersive large Au/Ag alloy NPs. The linear dependence of composition ratio between gold and silver were validated again.

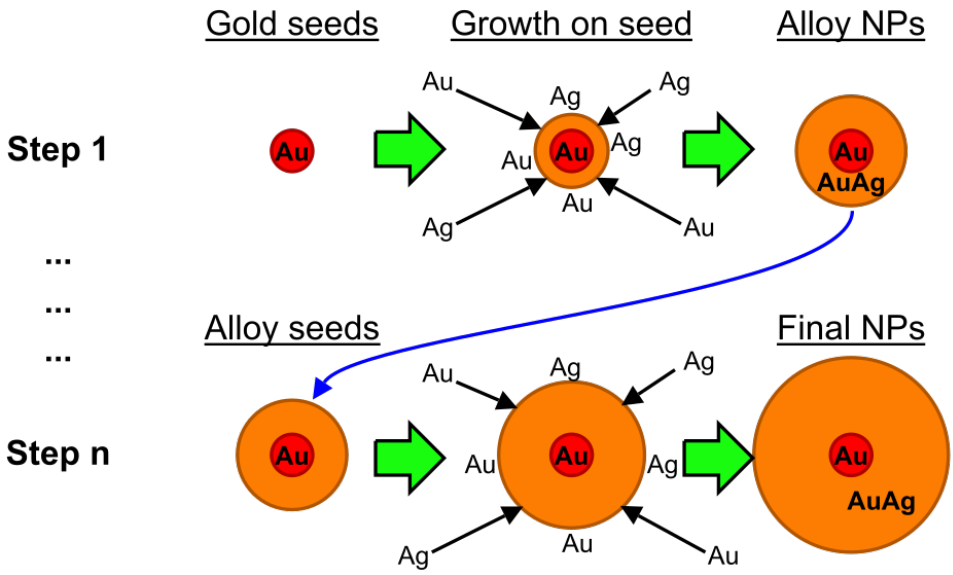

Figure 2.5 Schematic of multi-step Au/Ag alloy NPs synthesis. A ~15nm gold seed is grown to be Au/Ag alloy NP with Au^{3+} and Ag^{+} ions reduced on the surface of seed. Greater size (up to 150nm) alloy NPs are grown from smaller size alloy NPs.[30] Copyright © 2015, American Chemical Society

2.2 Synthesis of metallic core silica shell nanostructure

A core-shell nanostructure is composed of a core material and another material of shell, all at a nanoscale, which can be semiconductor-semiconductor, metal-semiconductor, metal-metal nanocomposite and so forth. The advantages of core-shell structures are frequently pertinent to

different properties of each component of the structure, such as the adjustment of surface properties, modification of surface charging and surface functionalization, which can increase the stability of the nanocomposite in complex media[53-55]. In addition, these core-shell structures could also show advantages of multifunctional physical properties, such as combination of optical[56-58], catalytic[59-63] and magnetic properties[7, 59, 64]. Accordingly, core-shell nanocomposite has been applied as devices in various fields, such as biomedical, chemistry, electronics, etc [65].

Plasmonic nanoparticles, such as gold, silver and Au/Ag alloy, are of great significance of being the core of a core-shell structure. The excellent plasmonic properties of noble metal nanoparticles can be further exploited when embedded in the oxide layer to have surface modification. Typically, for $Ag@SiO_2$, $Au@SiO_2$, we can choose a surface chemistry to tailor the dielectric and optical properties by adjusting the thickness and coating or doping materials [66-68]. The advantages of coating a silica shell onto plasmonic nanoparticles are to provide not only a stabilizer on the surface, which prevent severe aggregation, but also a stable optical spacer for its property being chemically inert and optically transparent.[69] In this section, some common synthesis methods such as sol-gel, reverse micelles are reviewed to fabricate $Ag@SiO_2$, $Au@SiO_2$ and other similar core-shell nanostructures.

2.2.1 Sol-gel

As a well-applied synthesis method for inorganic material, sol-gel process is well-known for its mild conditions (temperature and pH) to fabricate nanomaterials with high-level homogeneity and purity[70]. This process is based on the hydrolysis of metal alkoxide and afterward condensation in an acidic or basic environment. Stöber process, as regarded as the pioneering work for the synthesis of monodispersed silica particles (see Figure 2.6), is a typical sol-gel process that can also be used to produce silica shell coating. It involves hydrolysis of tetraethyl orthosilicate (TEOS, $Si(OC_2H_5)_4$) for coating an uniform layer onto the nanoparticles while the silica sols are used to induce condensation of TEOS and nucleation of silica monomer near the surface of metallic nanoparticles to form conformal silica shell. The typical thickness can be controlled from several to hundreds of nanometers by hydrolysis and condensation reaction of the alkoxide, for example TEOS, which is very useful and has been mentioned in numerous papers[71].

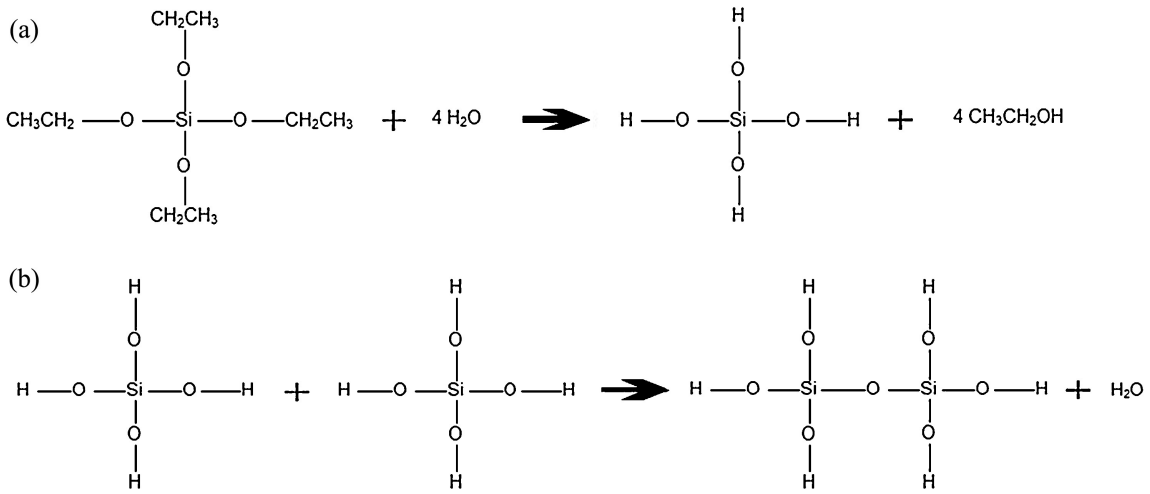

Figure 2.6 The hydrolysis and polycondensation reaction routes of TEOS. (a) Hydrolysis of TEOS to generate $Si(OH)_4$; (b) dehydrated condensation of $Si(OH)_4$ to form SiO_2 matrix.[72]

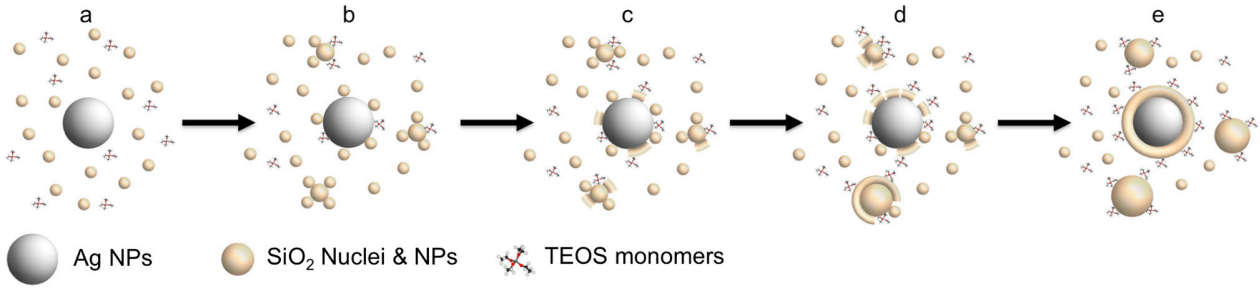

Figure 2.7 Schematic representation of the SiO_2 shell growth mechanism on Ag core. The formation of core-free SiO_2 happens when the concentration of silica precursor (TEOS) or the hydrolysis rate is too high, resulting in the nucleation of SiO_2 taking place not on the surface of silver NPs.[73]

It is important to control the morphology of the silica matrix during the synthesis in order to fabricate fibres, thin films or nanoparticles. Factors, such as the concentration of silica precursor, water and acid or base, could influence the silica growth process having different morphologies.

During silica shell coating on the surface of metallic nanoparticles, for instance, silver nanoparticles, different experimental conditions can result in various groups of products such as core-free silica nanoparticles and multicore nanoparticles. Since the alkoxysilane has a poor

miscibility with water but not alcoholic solvents, it was found that ethanol, methanol or isopropanol needed to be involved in the synthesis[74]. In fact, the type of solvent is also a factor that affects the silica shell formation. Since silica precursor hydrolysis rates and the tendency for metallic nanoparticles to aggregate are different in each solvent, the selection of the solvent is vital. For $Ag@SiO_2$ nanoparticles synthesis, the effect of alcoholic solvents has been systematically studied by Niitsoo et al[75]:

1. In methanol, with the comparatively higher hydrolysis rate, the possibility of appearance of SiO_2 core-free nanoparticles is higher and some of the silver nanoparticles may remain uncoated.
2. In ethanol on the other hand, where the hydrolysis of the silica precursor is not as high as in methanol, the core-free nanoparticles appear only if the surface area of silver nanoparticles are not sufficient for silica nucleation. Therefore the ratio of Ag/TEOS plays an important role in terms of silica nanoparticle formation. Shown in Figure 2.7, the Ag core-free nanoparticles are formed as the Ag surface does not have enough position for SiO_2 nucleus.
3. In 2-propanol, only the $Ag@SiO_2$ nanoparticles are formed but multicore nanoparticles (several Ag nanoparticles are enclosed in silica shell) also exist in the products.

As for the effect of catalyst, the acidic conditions (HCl for example) and basic conditions (ammonia for example), with different catalyzing mechanism, generate different form of condensed silica. Buckley[76] reported that slower hydrolysis occurred under acidic conditions where silica chains are formed preferably while faster hydrolysis was involved with higher pH where more clusters were formed as discrete species. Indeed, the rate of the hydrolysis is largely affected by the radius of negative ions[77]. Under the basic conditions, OH^- ions directly attack the silicon nuclei, resulting in a higher hydrolysis rate and it can be regarded that the whole condensation process begins after the finish of hydrolysis. The similar situation takes place under acidic condition when more water is added in the system so that the hydrolysis rate increases while condensation rate decreases due to the lower precursor concentration.

Taken into account the influence of catalyst on the metallic core, silver nanoparticles are affected by both HCl and ammonia. The Cl^- can attack the silver core to cause the etching effect and the similar process has been used with the addition of NaCl in $Ag@SiO_2$ to intentionally etch silver core in order to fabricate hollow silica shell[25, 78]. The etching mechanism of ammonia-

catalyzed process is due to the reaction of silver with dioxygen and forming the dissolvable $[Ag(NH_3)_2]^+$. Frequently, the yolk structure can be obtained with partial Ag core etched. Experimental procedure, such as the swift addition of silica precursor after ammonia with dropwise addition has been reported to succeed in synthesizing $Ag@SiO_2$[66].

On the other hand, coating silica onto gold nanoparticles is more challenging compared to the case of silver cores. The main problem is the stability of the colloidal solution in organic solvent, methanol or ethanol for instance. During the preparation of gold nanoparticles, it is well known that the citrate ions are finally attached to the surface of NPs as a stabilizer. However, in an organic solvent, the citrate amount is insufficient to stabilize the nanoparticles and they agglomerate within seconds to minutes[79].

The synthesis of $Au@SiO_2$ can be accomplished through a sol-gel process by using a silica precursor such as TEOS or sodium silicate, after a premier surface activation (shown in figure 2.6) with, typically, aminopropyl triethoxysilane (APTES)[69], followed by a dehydration condensation of TEOS on the colloid surface to form a silica layer. As shown in the schematic (figure 2.6), APTES, a silane coupling agent surface primer, plays a role of transferring citrate stabilized gold surface from vitriophobic to vitriophilic[80], which enables the further Stöber process. The citrate ions are replaced by APTES due to a strong adsorption of amine on the gold colloid surface. The hydrolysis of these APTES occurs to render silane triols which stabilize the gold colloid with ionized silane triols that are negatively charged[69].

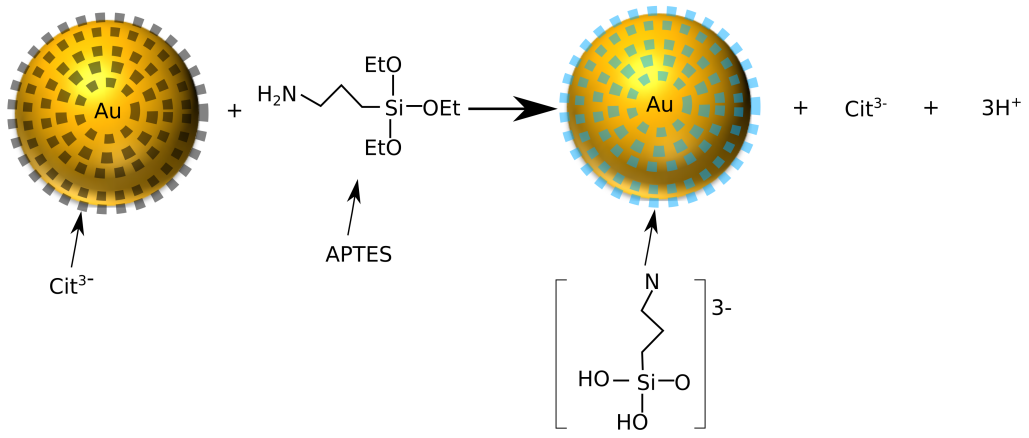

Figure 2.8 Schematics for surface primer attachment to citrate-stabilized gold colloid for further silica coating. The figure does not show the number of primer on the surface of Au NP.

Liu and Han[79] have also introduced a method to increase the citrate concentration on the surface of gold nanoparticles in order to transfer the gold nanoparticles into organic solvent for silica coating. In this case, the extra citrate has been added to the boiling gold colloid solution and cool down so that more citrate ions are on the surface of gold. Then, it can be safely transferred for subsequent silica coating.

2.2.2 Reverse Micelles

A micelle is an assembly of amphiphilic molecules (surfactant molecules) in equilibrium with a surrounding solvent and dispersed in the solution. Typically, the particle-shaped micelles gather together with a hydrophobic tail towards the center while hydrophilic head sticks to the surface.

Reverse micelles, on the other hand, are water droplets with tunable size dispersed in continuous organic solution automatically enclosed by surfactants. The polar side of the surfactant is hydrophilic and soluble in water, which turns into the droplet while the apolar side stays in contact with the organic solvent.[81] The frequently used surfactants include Cetrimonium bromide (CTAB)[82], Dioctyl sodium sulfosuccinate(Aerosol-OT or AOT)[83]. The microemulsion solution (water-in-oil) can be prepared to template nanoparticles to be fabricated with the help of the surfactant. Hybrid nanoparticle synthesis can also be conducted by using the reverse micelle method. The main advantage of this method is to delicately control the silica nucleation and polymerization inside the droplets of the reverse micelle.[84]

Tuo Li and coworkers reported a synthesis method of $Ag@SiO_2$ nanoparticles by using reverse micelle and sol-gel processing, where the microemulsion with TEOS hydrolysis and condensation rate control the size of particles and thickness of silica shell[83]. Typically, the coating of in situ synthesized nanocrystal, such as Ag NPs, begins with the reduction Ag+ ions in the reverse micelles to firstly form Ag NPs. TEOS with base is subsequently added to lead the sol-gel process so that SiO_2 shell can be coated onto the Ag NPs due to hydrolysis and condensation of TEOS. The microemulsion keeps NPs separated instead of aggregating. Igepal CO-520 was used in Li's experiment as surfactant. The molar ratio of water to TEOS was studied to determine the thickness of the silica shell while the ratio of water/surfactant was also an important factor to control the resulting size of the NPs. Yang and Holloway[85] have also shown that QDs could also be coated with silica shell in the microemulsion. More recently, Huang Lu

and co-workers studied in details a synthesis route of $Ag@SiO_2$ hybrid NPs with nonionic surfactant Triton X-100, 1-hexanol, cyclohexane and water. By using various amounts of reducing agent $NaBH_4$, H_2 was produced during the reduction of the Ag+ and led to the formation of cavities inside of Ag core, of which the number can be controlled by optimizing the experimental conditions[86].

2.2.3 Summary

Both sol-gel process and reverse micelle method are facile, inexpensive and controllable method to perform the synthesis of $metal@SiO_2$ hybrid nanoparticles. By sol-gel process, high purity and homogeneous chemical properties can be obtained whereas some clustered products may exist. By the reverse micelle method, the small radius can be controlled through the size of water-in-oil microemulsion by adjusting the water/oil (W/O) ratio. It can be applied to coating on pre-synthesized nanocrystals as well as in situ synthesized nanocrystals such as Ag, Au, Fe_2O_3, quantum dots, etc. For unstable nanoparticles in water/ethanol/TEOS mixture, the latter method is more popular. However, the microemulsion formation requires plenty of surfactants, which can raise more issues of factors such as pH, temperature and its concentration that affect the stability of microemulsion.

2.3 Surface plasmonic effect

Plasmons are collective excitation of electrons in a solid irradiated by an electromagnetic field. Surface plasmonic effect happens when an electromagnetic field interacts with free electrons at the surface of a metal. Among metals, the noble metals, such as gold, silver, copper, etc, have outstanding plasmonics properties, which attracted more attention as materials to be studied and used in various applications, including in medicine and biology.

2.3.1 Localized surface plasmon resonance (LSPR)

When the surface plasmon is confined in a metallic nanoparticle in three dimensions, it is called a localized surface plasmon and under a resonance, it is called a localized surface plasmon resonance or LSPR. The frequency of the oscillation depends mainly on the composition, size and geometry of the nanomaterial as well as the medium. When the size of nanoparticles is small enough comparing to the incident wavelength ($d<20nm$[87, 88]), the incident field exerted on NP

can be considered as a constant and can be approximately regarded as a dipole where the free electrons of the particle are polarized with the wave front of the light[89]. However, when the size of nanoparticles is not small enough to consider a constant electric field over the particle, we cannot apply the dipolar approximation whereas one side of the particle can be charged both positively and negatively so that it should be characterized more properly as multipole. In this project the NPs used are larger than 60nm, therefore Mie theory[87] must be applied.

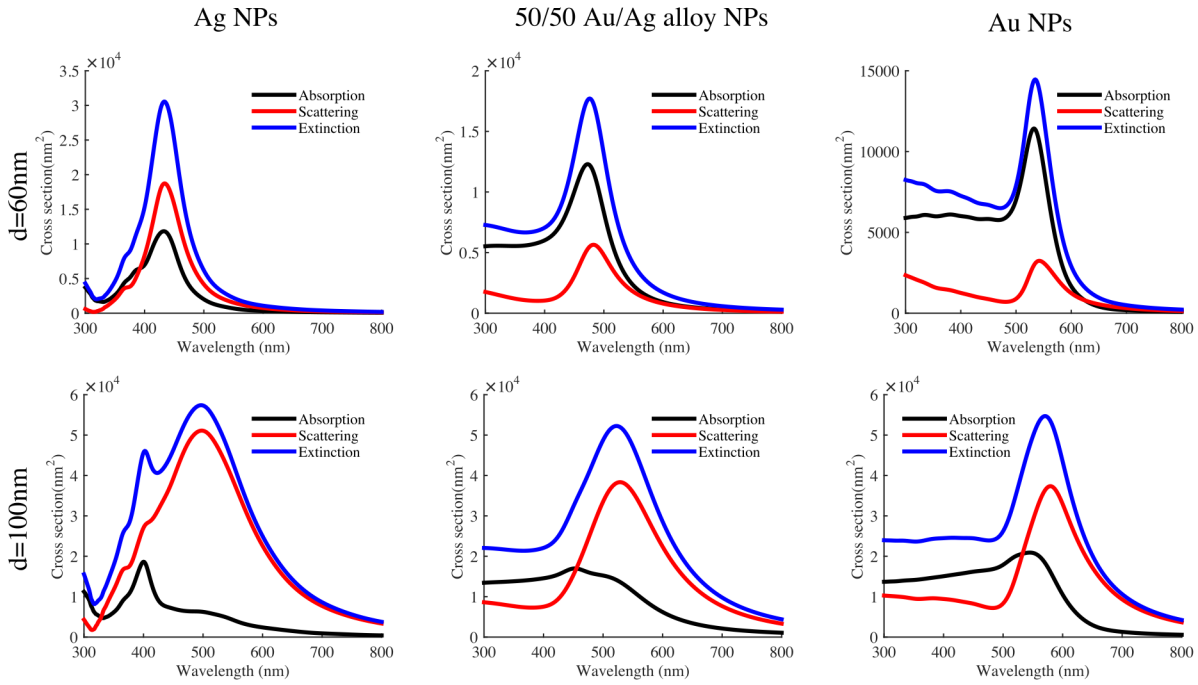

Figure 2.9 Absorption, scattering and extinction spectra of Ag, 50/50 Au/Ag alloy and Au NP with diameter 60nm (top row) and diameter 100nm (bottom row). Water is the medium. Figure is produced based on Mie theory[87] and dielectric functions of Au/Ag alloy NPs giving in [90].

Figure 2.9 shows the absorption, scattering and extinction calculated cross sections of plasmonics NPs having two different sizes (diameter 60nm and diameter 100nm) and three different compositions (Ag, 50/50 Au/Ag and Au) in water. The calculations are based on Mie theory[87] and dielectric functions of Au, Ag and Au/Ag alloy NPs are obtained from Rioux et al[90]. Note that for smaller 60nm alloy and Au NPs, the absorption overweighs the scattering while the full width at half maximum (FWHM) of scattering spectrum of 60nm NPs is smaller than the one of 100nm. However, from Figure 2.9 we can see that for the same size, the scattering cross section of Ag is higher than absorption, showing a stronger LSPR property. Actually, for multiplexed

imaging, NPs with a high scattering intensity and a small FWHM would be excellent cell labeller providing high contrast and ease of identification. Therefore, a compromise needs to be made for appropriate NP size to limit broad spectra, requiring relatively small NPs and intense scattering signal of large NPs.

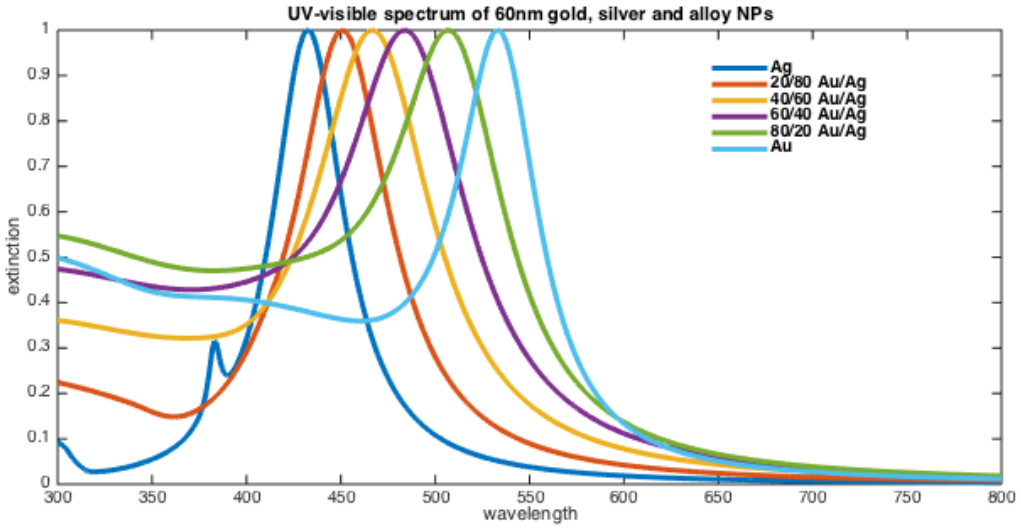

Figure 2.10 UV-visible spectra of 60nm gold, silver and alloy NPs with Au/Ag ratios 20/80, 40/60, 60/40 and 80/20. All spectra were normalised to 1.0. Figure is produced based on Mie theory[87] and dielectric functions of Au/Ag alloy NPs from [90].

The conductive band structure of NP also plays a role in determining the plasmonic peak position. For Au/Ag alloy NPs with different composition, the extinction spectra peaks vary from blue to green, for example for 60nm Ag to 60nm Au: from 433nm to 535nm as calculated by Mie theory[87] (Figure 2.10).

As discussed above, the plasmonic NP can absorb light and scatter it strongly. The optical cross section of the NP could be in some cases larger than the physical cross section. For example 60nm Ag, 50/50 Au/Ag alloy and Au NPs (Figure 2.9) have respectively scattering cross-sections 6.6, 2.0, 1.1 times larger than their actual physical cross sections at resonance. With the incident electric field, the oscillation of free electrons also generates a polarized electric near-field enhancement[87, 91], as shown in Figure 2.11. This field enhancement is affected by the NP size, the composition, the geometry and the wavelength and polarisation of incident light. In this figure, we can see that 80nm Au/Ag alloy NP shows more asymmetrical field enhancement, which indicates that multipolar effect is playing a role due to the relative scale ratio between NP and

wavelength. The field enhancement can be more than 5 times and the intensity accordingly can be enhanced more than 25 times depending on the position near the NP. This near field enhancement may be used in some applications such as surface enhanced fluorescence (SEF) or surface enhanced Raman spectroscopy (SERS), which will be briefly introduce later.

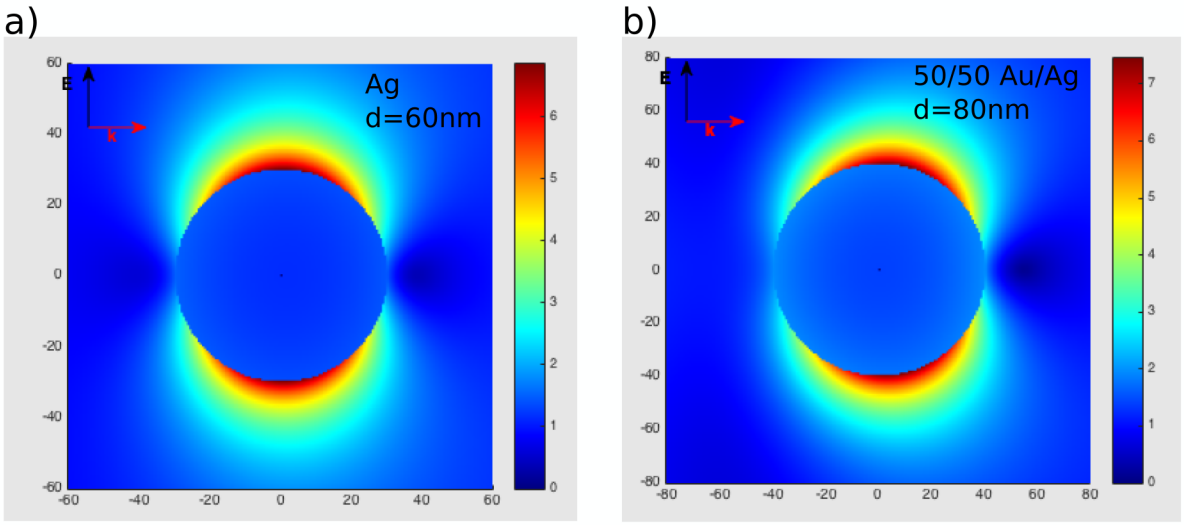

Figure 2.11 Near electric field enhancement under an irradiation of a linearly polarised 514nm wavelength light for (a) 60nm Ag NP and (b) 80nm 50/50 Au/Ag NP.

2.3.2 Metal enhanced fluorescence (MEF)

Fluorescent molecules (or fluorophores), when exited by a light near their maximum excitation wavelength, can re-emit light by photoluminescence near their maximum emission wavelength. It is vastly used as biomarker or dye in imaging. The metal enhanced fluorescence (MEF), in short, is the fluorescent intensity as well as photostability enhancement of a fluorophore near a metallic surface. Before going into details, the basic concepts for fluorescence need to be reviewed.

The maximum excitation and emission wavelength corresponds to the position of excitation peak and emission peak. The quantum yield, describing the efficiency of the energy transferred from incident light to emission of fluorescence, is defined as $Q = \Gamma/(\Gamma + \Gamma_{nr})$, where Γ is the emission rate of electrons at first excited state after being excited by the incident light and Γ_{nr} denotes the non-radiative decay rate of the electrons to the ground state. The lifetime refers to the time during which the electrons stay in the excited state, defined as $\tau = 1/(\Gamma + \Gamma_{nr})$.

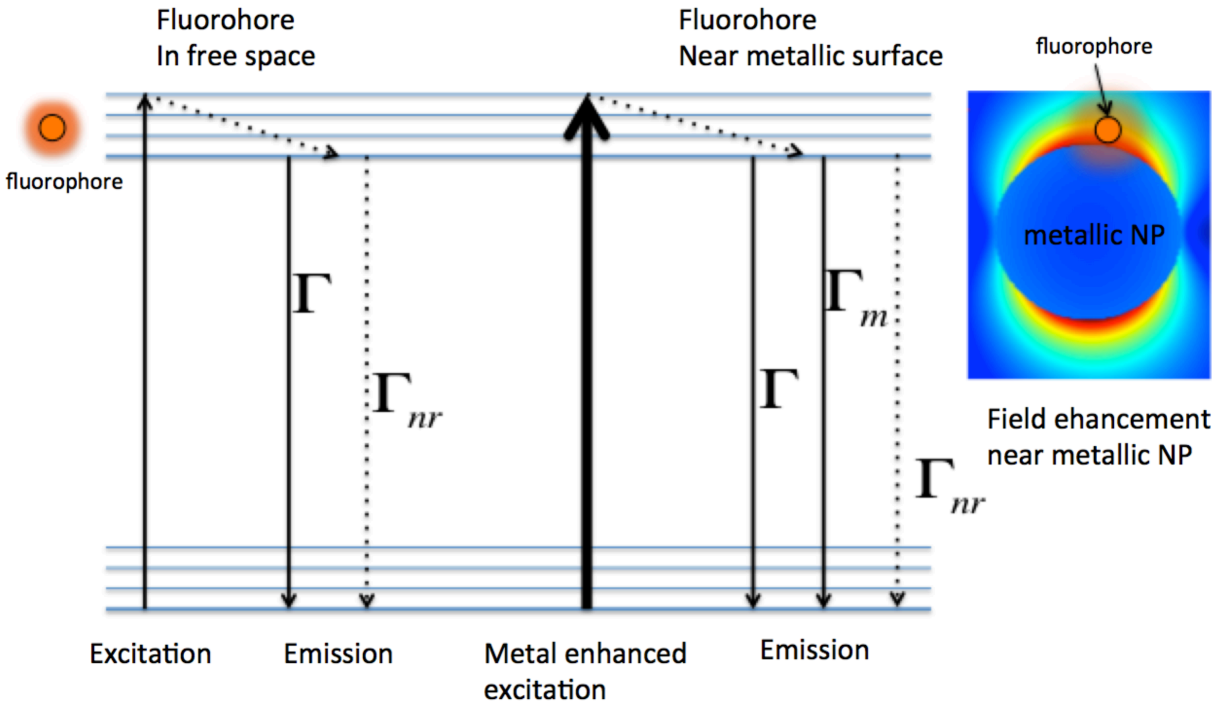

Figure 2.12 Jablonski diagram of fluorescence excitation and emission when the fluorophore is in free space and near a metallic NP. The enhanced field near the metallic NP surface is shown at the right top of the schematics.

Near a plasmonic nanoparticle surface, the field enhancement can be felt by the fluorophore, resulting in an increase of the emission intensity. In fact, the plasmonic nanoparticle can manipulate light below the diffraction limit[92] by concentrating it at near-field as a "nanolens". Moreover, the presence of the metal surface can induce an increase of the radiative rate of nearby fluorophore thus providing a shorter lifetime and greater quantum yield, which leads to a larger fluorescent intensity[27]. In this case an increase of photonic mode density enhances the radiative decay pathways due to the existence of the metal as shown in schematically in Figure 2.12. In this case, the emission rate Γ of the fluorophore is modified as $(\Gamma + \Gamma_m)$, where Γ_m corresponds to the emission rate increase in the presence of the metal. [93] The quantum yield and lifetime become:

$$Q = \frac{\Gamma + \Gamma_m}{\Gamma + \Gamma_m + \Gamma_{nr}}$$

$$\tau = \frac{1}{\Gamma + \Gamma_m + \Gamma_{nr}}$$

From the equations, one can see that the metal enhancement (Γ_m) becomes important on Q when the non-radiative decay (Γ_{nr}) is relatively large. However, we must consider the local distribution of the fluorophores near the plasmonic NP surface. Frequently, a fluorophore is considered as a dipole model, and its orientation plays a role in the emission intensity. When the fluorophore is located near the polarized field maximum, its dipole can be enhanced to be further excited and emit more photons. The distance between the metal surface and fluorophore is also important for the fluorescent rate[94]. If the distance between the metallic surface and the fluorophore is R_F, and assuming a dipole-dipole interaction, then the non-radiative decay rate is proportional to R_F^6 but only valid when $R_F \geq r_{NP}/10$. In fact, if the molecule is too close to or even attached to the metallic surface, there is a much higher non-radiative energy transfer from the molecule to metal and the fluorophore is quenched by the metal.[95]

The core-shell structure with a metallic core is very convenient for MEF effect, for the vicinity of fluorescent molecule doped in silica shell all over metallic nanoparticle. It is reported that silver colloid surfaces have yielded up to 50-fold enhancement[96]. The similar magnitude of fluorescence enhancement factor was also obtained with a gold core. This factor was calculated by obtaining the ratio of fluorescence intensity between fluorescent core-shell NPs and core-free NPs[78].

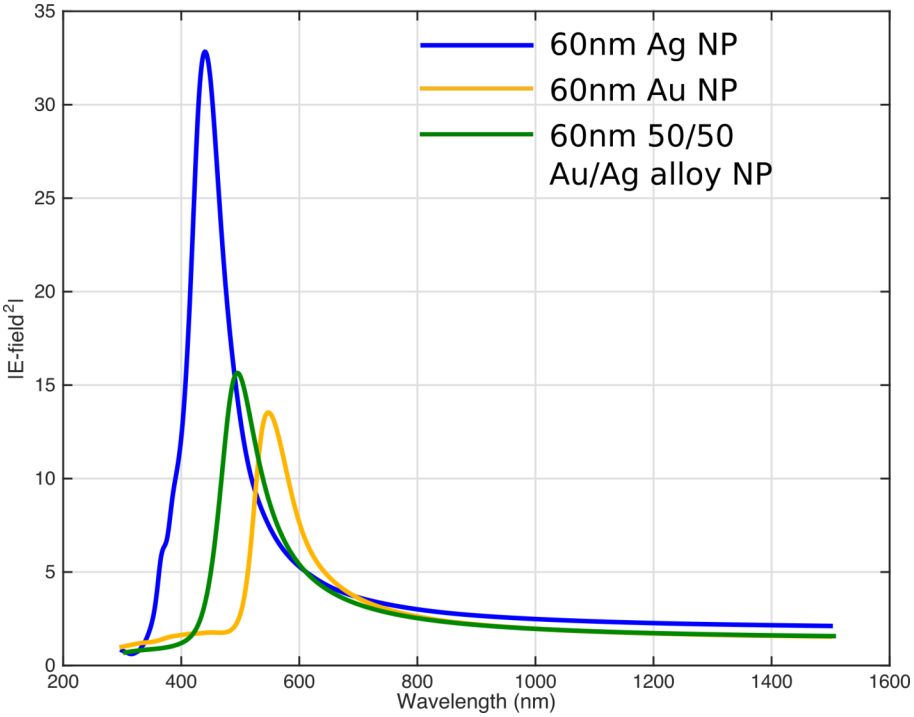

Figure 2.13 Nearfield enhancement of 60nm Ag NPs, Au NPs and 50/50 Au/Ag alloy NPs as a function of wavelength.. Calculation with dielectric function of Au/Ag alloy in water[90].

Since it is possible to control the plasmonic resonance peak wavelength for gold-silver alloy NPs according to their Au/Ag composition ratio, it is also possible to design the NPs that would fit the excitation or emission wavelengths of fluorescent molecules so that the fluorescent intensity could be even more amplified. Figure 2.13 shows the near-field enhancement as a function of the incident wavelength and can be used to determine the choice of flurophore and irradiation conditions. Some typical studies of other conditions with plasmonic-based nanostructure and different fluorophores are shown in Table 2.1.

Table 2.1 Pertinent studies of MEF in literature with different conditions.

Material and geometry	Dimension	Fluorophore	Enhancement factor	reference
Au NP	40nm	FITC	1.75	[97]
	200nm		2.5	
	14nm	TAMRA-SE−PLL	9.2	[98]
	50nm	IR800	40	[99]
Au nanorod	80×13nm	Cyanine 5	7.6	[100]
	46×11nm	IR800	9	[99]
Ag nanoprism	100nm edges	Alexa Fluor 488	9-30	[101]
Ag NP	75nm	FITC	12.5	[102]
	40nm	Alexa Fluor 350 (AL350), FITC, pacific blue (PB), Alexa Fluor 514 (AL514), Rhodamine 6G (Rh6G), Alexa Fluor 647 (AL647), Alexa Fluor 680 (AL680)	2-17	[34]
Ag nanorod	50×25nm	ICG	10-50	[103]

2.3.3 Surface enhanced Raman spectroscopy (SERS)

Similar to MEF, SERS occurs when a molecule is near the surface of a plasmonic material, resulting in an amplified Raman scattering signal of this molecule by $(E_{local}/E_{incident})^4$, where E_{local} and $E_{incident}$ are electromagnetic fields respectively at the molecule position and of the incident light, as shown in Figure 2.14. The index 4 comes from the field enhancement by both excitation and emission, which normally generates an enhancement factor of 10^4-10^6[104]. The application of plasmonic NP, especially gold and silver NP, for SERS application is a hot research topic. [29, 105] In fact, a SERS enhancement factor of ~10^7 is sufficient for single molecule detection[106]. Moreover, by modifying the structure of plasmonic material, namely with optimized geometry, the field enhancement can be further increased. For instance, dimers of silver spheres increase an addition 100-1000 fold of enhancement of Raman signal if the molecule is positioned between two closed nanospheres.[107]

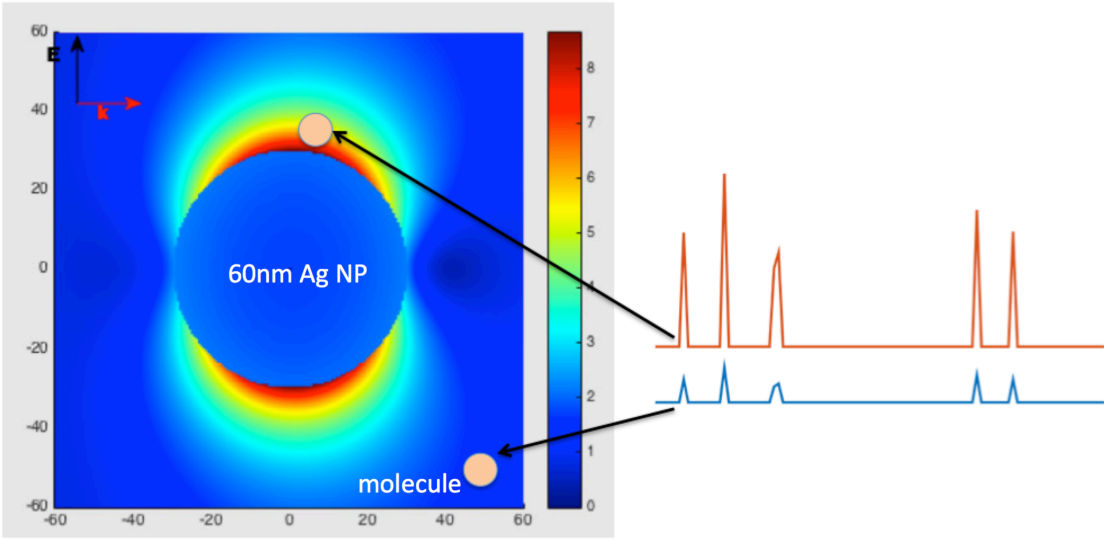

Figure 2.14 Schematic showing the surface enhanced Raman spectroscopy by Ag NP. A molecule near the surface of Ag NP has greater Raman signal (orange) due to electric field enhancement than the one away from enhanced field (blue).

2.4 Bioimaging with plasmonic nanostructures

Contrast agents in bioimaging are necessary tools for biologists and pathologists. The existing optical bioimaging contrast agents for cell labeling are fluorescent molecules, QDs, plasmonic NPs, etc. Actually, there is a tremendous effort in the development of multiplexed imaging with different types of multicolor labellers to enhance the efficiency of differentiating cellular phenotypes. Therefore, in this section, we discuss various contrast biomarker agents and introduce some examples of multiplexed bioimaging techniques.

2.4.1 Contrast agents for cell imaging

In a general manner, there are two ways of targeting cells or organs for bioimaging applications. The first one, more complicated, involves genetics modification and the production of fluorescent protein such as the well-known green fluorescent protein[108] for which Doctor Tsien received the Nobel price. The second one, much more straightforward, uses fluorescent monoclonal antibodies and their ability to link specifically to their corresponding cell antigens, which is called immunofluorescence. Although fluorescent monoclonal antibodies are very useful, it has some significant drawbacks. First, they are costly and are very limited in choices of fluorescence types, especially for ones with high quantum yield. Besides, the fluorophores are vulnerable to photobleaching, which makes it very difficult to restudy the same cells from one region after a certain observation time with high exposure from the optical set-up. Moreover, due to the two drawbacks above, when targeting to the antigens with less specificity, the intensity of the fluorescent label and the observation time can be both limiting. QDs[17-20] as one of the promising alternatives show better photostability and were also applied in bioimaging applications. QDs of different compositions exhibit highly defined luminescence when excited in UV region [18]. However, the toxicity of the semiconductor material and the intermittence of the emission signal, referred to as “blinking”, limit the application to cell imaging.

On the other hand, plasmonic nanocrystals such as gold and silver NPs also offer interesting properties for bioimaging, namely high scattering bands under dark-field (DF) microscope mode, absence of blinking and photobleaching. Au NPs are furthermore chemical inert and less toxic with cells. With the technique of surface modification and functionalization with monoclonal antibodies, NPs are able to be used as specific cell labeller, named immunoplasmonics[109]. The

eternal scattering signal permits longer observation and cell tracking[110] study and the tunable plasmonic bands position according to the material geometry and composition allow multiplexed imaging. For example, our group reported immunoplasmonic microscopy with Au, Ag NPs and Au nanorods as biomarkers for cancer cell imaging applications[109]. However, NPs tends to form clusters and deteriorate the imaging homogeneity due to shifted color and stronger intensity. And for standard darkfield imaging, plasmonic NPs are required to be large enough to scatter sufficient light to be seen under the optical microscope, which increase the difficulty of synthesis. Fortunately, surface modification can be done with plasmonic NPs to increase their stability inside a complex medium. Polyethylene glycol (PEG) and Polyvinylpyrrolidone(PVP) are two frequently used polymers to modify the NP surface so that the precharged NP surface cannot be absorbed to cell surface easily or due to the hindrance of the polymer on surface the NPs tend not to aggregates easily[111]. In Table 2.2, typical candidates for contrast agents are listed and compared.

Table 2.2 Typical contrast agents in bioimaging.

Contrast agents	Advantages	Disadvantages	References
Fluorophore (immunofluorescence)	Mature and widely used, standard methods for examination	Low intensity, photobleaching, complexed procedure with indirect immunofluorescence, spectral overlapping	[112-114]
QDs	Defined peaks, uniform exitation	Blinking, toxicity	[17, 18, 20]
Ag NPs	Strongest scattering signal, plasmonic properties	Toxicity, low chemical stability, resonance in blue so that difficult for signal collection and in vivo application	[115-117]
Au NPs	Strong scattering signal, plasmonic properties, biocompatibility	Broad plasmonic band, resonance in green and yellow so that difficult for in vivo application, heat generation with high absorption	[13, 24, 26, 28, 118, 119]
Au nanorod	Near-infrared emission, in vivo application	Complex synthesis control, two plasmonic peaks, broad spectra	[23, 118-121]
Hybrid structure (core-shell)	Flexible properties for different applications, e.g. Au shell for near-infrared emission	Complexed synthesis control, optical property highly sensitive to structure	[6, 122-124]

2.4.2 Multiplexed imaging

In general, due to the spectral overlapping of the tissue fluorescence, it is difficult to visualize the complex biological structure[125]. Multiplexed imaging is thus very useful for carrying more components information at the same time for better analysis and more certainty. As discussed in the previous section, fluorophores [126], QDs[18, 127] plasmonic NPs[28, 109, 128] and core-shell structures can all be used as multiplexed imaging contrast agent.

Shown in Figure 2.15, the fluorescence-based multiplexed imaging technique is well developed even though the capacity of multiplexed analysis is up to seven colors for labeling different antibodies. [109, 126] The protocol for fluorescence-based multiplexing is available on the MultiOmyx™ platform. As a general advantage of multiplexed imaging, higher diagnostic accuracy can be achieved when synchronously labeling cells with several antibodies that can be identified. By using such technique, the example shows that it is able to directly reveal cancer cells in a complex microenvironment. For multiplexed imaging, the three most important aspects of contrast agents are sensitivity, stability and multiplexing capability. Although being developed a lot, fluorescence has its shortcomings in all these three aspects: the limited fluorophore number per antibody confines its imaging sensitivity; the photobleaching phenomenon indicate its poor stability; the broad emission spectra width limits its multiplexing capability.[126] In order to explore the possible choices of multiplexing, the alternatives such as plamsonic NPs were investigated for selective labeling and imaging[28, 109, 128].

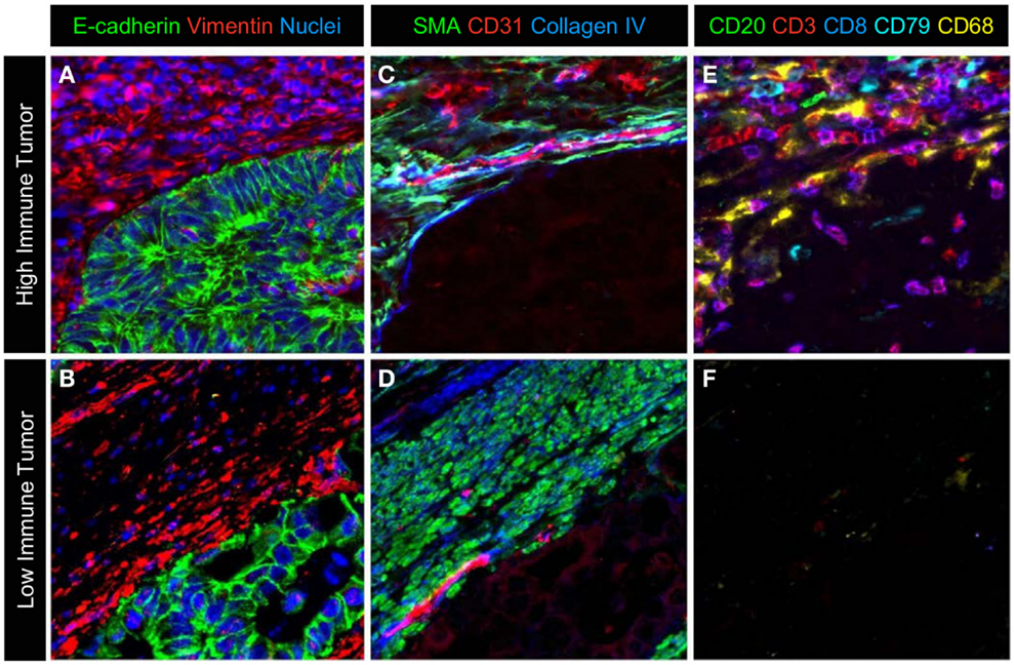

Figure 2.15 A typical example of multiplexed imaging by immunofluorescence for different cell types in the microenvironment. Reprint from[126] © 2014 Gerdes, Sood, Sevinsky, Pris, Zavodszky and Ginty.

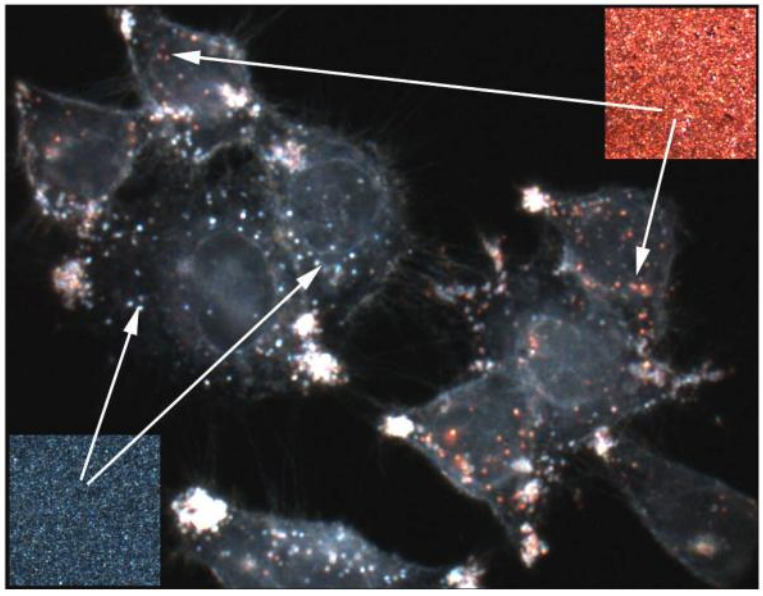

Figure 2.16 An example of plasmonic-based multiplexed imaging. Panc-1 cells were labeled with antibody conjugated Au NRs and Ag NPs. Two insets are dark field images taken from Au NRs (up-right) and Ag NPs (bottom-left) on a glass slide. Reprint from [128] Copyright © 2009, American Chemical Society

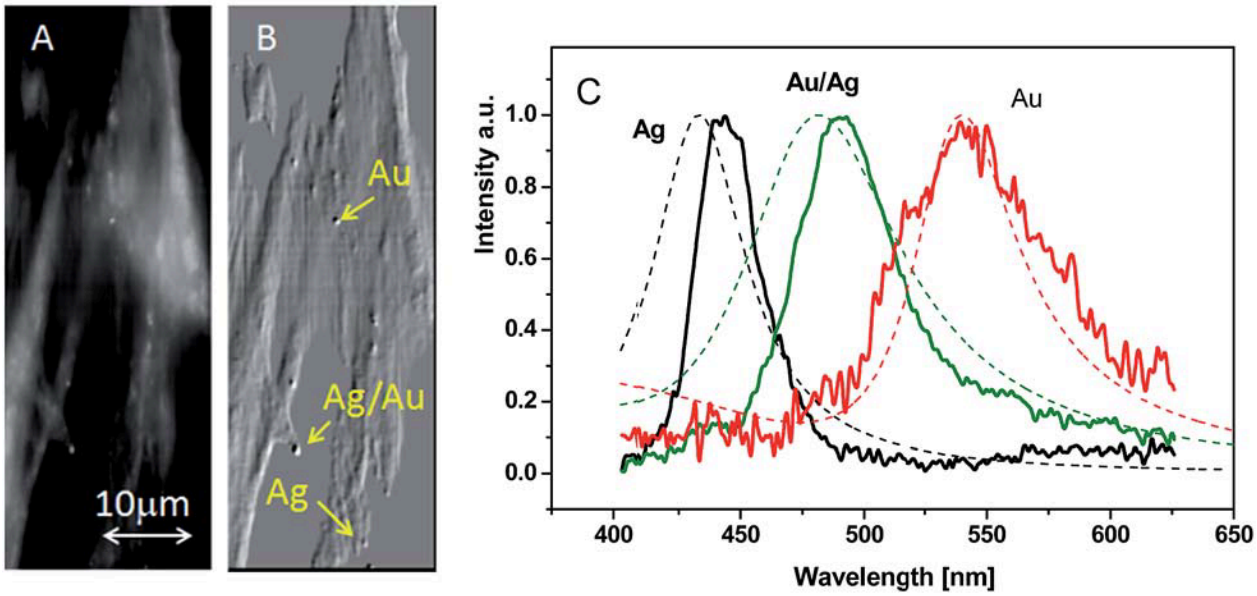

Figure 2.17 Hyperspectral scan of cell-NP complex region in reflected light mode. Individual NP scan be indentified with scattering spectrum as Au, Ag or 50/50 Au/Ag NPs.[28]Copyright © 2014, Royal Society of Chemistry

Multiplexed imaging with plasmonic nanostructures is on the other hand scattering-based imaging and typically up to 3 types of labellers are used for a single sample: Au NP, Ag NP and Au nanorod. [109, 128] It is a popular combination in spite of the usual broadness of the extinction peak because the resonance position is separated enough to be distinguished (Ag NP~480nm, Au NP~590nm, Au rod~700nm). Figure 2.16 shows an example of multiplexed cell imaging with these three labellers. The separated plasmonic peak positions make them easy for fast identifications and the strong scattering signal gives a good imaging sensitivity. The possibility of surface modification of these NPs paves way for antibody functionalization and they are suitable for cell targeting experiments, as shown exactly in Figure 2.16. However, the multiplexing capability with gold, silver and nanorod gives only three possibilities as presented in Figure 2.16. It is manageable for more colors by adjusting the geometry of nanorod, but if we want to have more choices of colors in the visible range, we would like to use Au/Ag alloy NPs.

With the developed synthesis method of Au/Ag alloy NP with larger size and fine distribution, our group studied multiplexing with Au, Ag and Au/Ag alloy NPs with hyperspectral imaging set-up (Figure 2.17).[28] In fact, in terms of Au/Ag alloy core, with its tunable plasmonic

resonance frequency according to composition ratio of Au/Ag, the multiplexed imaging application can be fulfilled by multicolor cell labels with hyperspectral setup.

The thesis is focused mainly on plasmonic core silica shell NPs, especially Au/Ag alloy core silica shell NPs with the same set-up of hyperspectral imaging. The aim of hyperspectral imaging is to obtain a full spectrum of each image pixel for identification or detection of materials in the sight of view; in tour case, it is to obtain the scattering spectra of individual NPs and define its composition. Shown in Figure 2.18, the hyperspectral sensor acquires the spectrum information for each pixel of the slit area and a visual image, either for a single wavelength or for all wavelengths, can be reconstructed to maintain the color information of the material in the area of view.

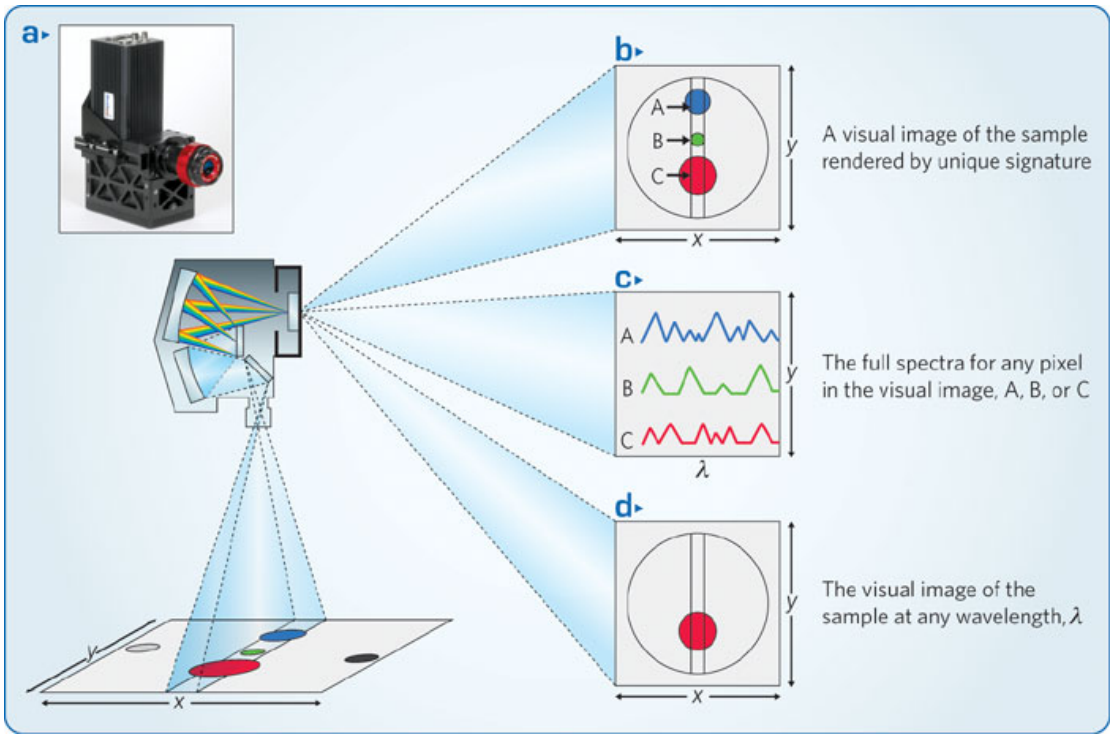

Figure 2.18 (a), One of Headwall's high-efficiency hyperspectral sensors. (b), Visual image of the sample rendered by unique signature. (c), The full spectra for any pixel in the image, A, B or C. (d) Visual image of the sample at any wavelength λ.[129] Copyright © 2009, Rights Managed by Nature Publishing Group

Gold-silver alloy nanoparticles are very promising contrast agent for hyperspectral imaging multiplexed identification due to their specific spectrum information related to the Au/Ag

composition. Patskovsky and his coworkers reported a hyperspectral reflected light microscopy with gold-silver alloy NPs as multiplexed cell labeller[28]. The spectral information obtained by the microscope is essential for efficient multidetection of target and identification of cells. In addition, for an alloy-core silica-shell NPs incorporated with fluorescent molecules in the shell, multimode of detection can be conducted thus further increasing the choice of biomarkers. This part is the main contribution of this thesis and is discussed in more details in the following chapters.

CHAPTER 3 METHODOLOGY

This chapter details the experimental methodology, including the synthesis of alloy NPs and the core-shell NPs, the characterization conditions for UV-visible spectra, TEM and EDS measurement. We will also cover the NPs size measurements statistics as well as the sample preparation for optical microscopic imaging. In general, the presented results are very representative and reproducible, while attentions must be paid to some manipulations.

3.1 Synthesis of alloy NPs and core-shell NPs

The synthesis methods of alloy NPs comes from the seeded growth method [31]. The precalculated chemical reagents were added according to the ratio needed. First of all, 13nm Au seeds have to be synthesised in a solution by boiling 30mL water with 300 μL 30mM $HAuCl_4$ and 200 μL 170mM sodium citrate solution. After 5 minutes reaction, the color of the solution changes to rubber red, we can stop the reaction by cooling down the solution and then we add deionized water untill 30mL for a precise gold atomic concentration of 300 μM. Then typically for the 50/50 Au/Ag alloy NPs synthesis, since gold and silver composition ratio is 1, we added 225μL 30mM $HAuCl_4$ solution and the same amount of 30mM $AgNO_3$ solution to a 100mL prepared 13nm diameter Au NP solution with an atomic concentration of 30 μM. Then we added 900 μL of the reducing agent sodium citrate of 170mM concentration, taking account of the preexisted citrate ions for Au seeds formation. The reaction requires a temperature of 100℃ for 1 hour and the product is thus an intermediate ~30nm diameter alloy NP. In order to further grow larger NPs, we need to restart the reaction with the as-prepared product, namely 30nm alloy NPs, to act as Au seed in the previous synthesis.

Once the alloy NPs were prepared, the NPs need to be transferred to EtOH for further silica coating by performing centrifugation at about 5000 to 10000 relative centrifugal force (rcf) of solution to exchange the supernatant from water to EtOH. In our experiment, we picked 8000 rcf constantly for better reproducibility. However, the alloy NPs are citrate coated so that they can be dispersed properly. For the purpose of stability, while it is risky to exchange all of the water from alloy NPs solution, if we keep too much water, it can affect the polymerization rate of silica precursor (TEOS) by resolving much of the catalyst ammonia thus resulting in core-free silica NPs or uncoated alloy NPs rather than alloy core silica shell NPs. Empirically, we take out half

of the water supernatant and keep some citrate ions for stability. For the silica coating, we added 4mL alloy NPs (atomic concentration 150 μM), removed 2mL water and put 2mL EtOH instead. 1.5 μL TEOS and 625 μL 30% ammonia solution were added gently, preventing any oxygen incorporation. Then, the solution was filled with EtOH to 16mL, ending up with a water/EtOH ratio of 1:7. The reaction can still occur, even if the water/EtOH ratio slightly varies, for example from 1:3 to 1:8, with the total reaction volume of 16mL to 20mL.

In order to incorporate fluorophores in silica shell, the fluorescent precursor FITC-APS and RBITC-APS need to be presynthesized following a similar protocol. They were all prepared in DMF with triethylamine as a catalyst. Typically 4mg(5,7 μmol) FITC was mixed with 114μL DMF, 2μL Triethylamine and 2μL APS in a light proof tube. The reaction was performed at 50℃ with vibration for 3 hours. Then the solution was diluted in 1mL EtOH. Similarly, RBITC 3mg was mixed with 4μL APS in 120μL DMF, 2μL Triethylamine and rest was the same. The prepared solutions were added to the main reaction 30 minutes after the addition of TEOS and ammonia.

The important thing is to use a proper concentration of TEOS and ammonia (the silica precursor and catalyst) in the solution to guarantee an efficient silica shell growth without generating core-free shells and multi-core NPs. More details about how to fabricate highly uniform core-shell NPs will be demonstrated in Chapter 5. After 24h reaction, core-shell NPs are ready for characterization and further functionalization.

3.2 Optical characterization conditions

The optical characterizations of NPs include UV-visible spectra of NPs absorbance in solution and fluorescence intensity measurements. For these characterizations, the definition of a stable background is important in order to obtain reliable results.

For UV-visible spectra detection, we separately measure the absorbance of medium and the absorbance of NPs solution. By comparing two absorbance spectra, we can get the neat absorbance spectra of NPs. we firstly added 300 μL medium, typically water, and 300 μL NP solution to a microplate. By subtracting absorbance of the medium (water), we can finally obtain the absorbance of NPs in water. The concentration of NPs is a factor that can influence the final

results of UV-visible spectra. Since the spectrometer has a detection limit, we need to keep the solution to an appropriate concentration to obtain a measurable signal.

Fluorescence intensity measurements are similar to UV-visible spectra measurements, except that it is needed to use not only a blank control (water), but also some negative controls (alloy NPs solution without fluorescent shell and medium of fluorescent core-shell NPs). Since we want to make sure the measured fluorescent peak is due to the fact that the NPs are fluorescent and fluorophores are well embedded inside silica shell of NPs rather than some free fluorophores in the medium out of NPs give fluorescent intensity, we have to make sure that the medium where NPs are dispersed contains no free fluorophores. The centrifugation and washing is necessary and after three times of washing we can put supernatant as the background of fluorescent intensity measurements. For the same reason, we need also to verify the fluorescent property of bare alloy NPs without fluorophore-embedded silica shell. The results shown in following chapters indicate that the negatives controls stay negative as expected.

Similar to UV-visible measurements, the concentration of NPs cannot be controlled precisely, therefore it is necessary to normalize the intensity for comparing results from different types of fluorophores.

3.3 Transmission electron microscopy characterization and analysis

The structural examination of core-shell NPs was performed by TEM imaging. The transmitted electrons diffraction can easily create different contrast for metallic core and silica shell. For imaging condition, 200kV accelerating voltage was used at typical magnifications from 10kX to 100kX. The compositional analysis of metallic core was realized by EDS in order to track the variation of Ag/Ag ratio before and after silica coating process steps. The electronic beam was spread to cover a single particle core but limited to prevent covering too much the silica shell. Although the shell composition is supposed to be SiO_2 and would not influence the Au/Ag ratio of the core, the observed Ag leaking out of the metallic core during silica coating may results in some tiny Ag nanoparticle attachment to the shell, thus affecting the core composition determination. EDS spectra of 5 individual NPs were checked for four types of samples, namely 10/90 and 50/50 Au/Ag alloy NPs respectively before and after silica coating, and the acquisition counts was around 2000 with a processing time of 4 and dead time of ~40%.

For better representativeness, the size measurements were carried out based on 100 NPs sized from TEM images. The measurements were manipulated manually with a fitted ellipse of major and minor axis. The equivalent radiuses were calculated to have a circle with the same area of the fitted ellipse.

3.4 Sample preparation for imaging

For individual NPs identification, the NPs in the field of view need to be neither too crowded with high chance of aggregations, nor too scarce without all representative types of NPs (different core compositions and different fluorescent colors). In order to have a suitable concentration of NPs in an imaging area, the precalculation of the NPs concentration is very important. Since we have concentrated enough NPs solution (~10^9 particles/ mL, more details given in Chapter 4), we can design the appropriate dilution extend. Moreover, the NPs tend to aggregate in solution and that becomes even more severe when they leave the solution and get exposed to air. So it is necessary to use some stabilizer or surface modification to suppress the aggregations and here we use PVP to create some space between NPs.

The NPs were prepared in a 3mg/mL PVP water solution and added 50μL in 300 μL pure EtOH. 2 μL out of which was spread on a glass slide on approximately 0.25 cm^2 to obtain a concentration of NPs of about 100 NPs/square in the field of view under the microscope ($112\mu m \times 112\mu m$). However, due to the EtOH evaporation, the NPs concentrate near the border of the drop area, where the picture was taken because of the larger concentration.

CHAPTER 4 ARTICLE 1:FLUORESCENCE AND SCATTERING DUAL-MODE MULTIPLEXED IMAGING WITH GOLD-SILVER ALLOY CORE SILICA SHELL NANOPARTICLES

This chapter is a transcription of the article submitted for publication in Journal of Physical Chemistry C. It demonstrates multiplexed imaging application of Au/Ag alloy core fluorescent silica shell NPs. The optical properties and fluorescence and darkfield (DF) dual-channel detection process are discussed in detail. The supporting information is behind the main text where characterizations of fluorescence, NPs concentration, MEF factor and cell targeting applications are discussed.

4.1 Authors

Siyu Tu[1], Danny Brouard[2], David Rioux[1], Josée Perreault[2] and Michel Meunier[1]

[1]Department of Engineering Physics, École Polytechnique of Montréal, Montréal, QC, Canada

[2]Research and Development, Héma-Québec, Québec, QC, Canada

4.2 Abstract

Gold-silver alloy core silica shell nanoparticles (Au/Ag@SiO_2 NPs) with fully accordable photophysical properties were developed and used as contrast agent for multiplexed cell imaging applications. Using a seed growth strategy, these nanoparticular labels can be designed to suit specific experimental needs and be clearly identified based on their distinctive combination of scattering and fluorescence colors. In this paper, the multiplexed cell imaging capabilities of Au/Ag@SiO_2 NPs are presented using four different combinations of core composition and fluorescence colors. In a proof of concept experiment, 86% of total nanoparticles were correctly identified by optical microscope with a system offering fluorescence and darkfield detection capabilities. This multiplatform identification strategy was successfully applied for the detection of four different nanoparticular architectures in cell imaging experiments.

KEYWORDS: Contrast agent, core-shell nanoparticle, multiplexing, gold-silver alloy, plasmonic enhanced fluorescence.

4.3 Introduction

During the last decades, nanotechnology has emerged as one promising research field leading to the development of multiple nanoparticular architectures currently used in an extended range of imaging, sensing and catalyst applications, among many others.[84, 130-136]. Metallic nanoparticles (NPs) have attracted much attention because of their outstanding photophysical properties highlighted in various biomedical applications.[28, 137-140] In this paper, the plasmonic properties of greatly uniform gold-silver alloy NPs were exploited for the design of superluminescent contrast agents for multiplexed analysis in cell sorting and cell imaging applications. Cell analysis is an integral part of biochemical experiments and numerous techniques are available to obtain relevant information on cell identity, structure, function or current state.[141-147] Plentiful applications involve protein quantification, structural staining and, for the purpose of this work, immunofluorescence labelling which takes advantage of the antibody-antigen recognition reaction. The use of fluorophore-labelled antibodies to highlight specific intra- or extra-cellular antigens has led to the development of cell characterization assays for fluorescence microscopy and flow cytometry applications. In the case of studies dealing with weakly expressed antigens or rare events detection issues, the use of highly luminescent and time-stable fluorophores is recommended to maximise detectability and the signal to background ratio. Moreover, most cell characterization experiments involve the use of multiple cell-labelling moieties together to obtain various information on cell populations simultaneously. Multiplexed analysis is however limited by the ability of the sensing system to isolate each cell labels in a single detection channel with minimal crosstalk. In the case of fluorescence-based detection techniques for example, one must consider the use of fluorophores with narrow emission bands to minimise spectral overlap leading to experimental issues and complex results interpretation.

Fluorescent dyes are commonly used as labels but they tend to suffer from photobleaching and large excitation and emission bandwidths [109, 148], thus limiting their use to very short observation time in the case of microscopy experiments or to fewer detection channels (<7 colors)[16] for flow cytometry applications. The use of quantum dots (QDs) for antibody

labelling has emerged as an alternative strategy for multiplexed analysis because of their narrow and tuneable emission band.[16, 149, 150] However, the fluorescence intermittency (blinking) and potential toxicity limit their use as reliable contrast agents for biological applications.[16, 109, 151, 152] Plasmonic nanomaterials, more especially gold or silver NPs (AuNPs and AgNPs), have been applied to a wide range of applications including labels for cell tagging applications.[115, 153] for cell tagging applications. Amongst others, metallic NPs used as contrast agents was previously reported for optical, electronic, X-ray or magnetic resonance image observations[154-156] and as fluorescence quenchers or signal enhancers within a variety of fluorescent core-shell architectures.[66, 79, 157] Recently, multiple research groups have shown interest in the unique photophysical properties of plasmonic NPs for multiplex analysis.[22, 28, 128, 140] For example, the scattering band of plasmonic active NPs can be adjusted by the modification of their size, composition or geometrical shape.[30, 158, 159] . Unlike fluorescence or quantum dots luminescence, scattering does not present any kind of dark state or blinking and is not subject to photobleaching allowing extended observation periods under low intensity illumination, thus improving the signal to background ratio for better detection contrast. For example, Bergeron et al. reported the use of a reflected light microscope dedicated to plasmonic imaging for multiplexed analysis of cancer cells using Au and Ag NPs together with Au nanorods as contrast agents.[109] This study has motivated the development of a NP system offering the fully accordable plasmonic and fluorescence properties for improved multiplexed possibilities. Recently, our group has proposed a gold-silver alloy NP (Au/AgNPs) synthesis based on a seed growth approach offering remarkable features in terms of size and composition adjustability[30]. Au/AgNPs with different size diameters generating predetermined scattering colors were successfully prepared, observed and identified under DF microscopy.[28]

The presence of metallic structures near fluorescent dyes is known to improve their photophysical properties. Noble metal such as gold and silver are frequently being used to increase fluorescence signals due to near-field photophysical interactions, a phenomenon called metal enhance fluorescence (MEF).[78, 89, 160]. When there is MEF, the fluorophore excitation and emission rates increase as its excited state lifetime reduces which lead to an apparent increase of quantum yield and photostability. Nanoparticular core-shell architectures with dye-doped silica shells have been designed to exploit the advantages of MEF over commonly used fluorescent molecules.[25, 66, 157, 161, 162] Core-shell NPs can be ingeniously designed to

position fluorophore molecules at a precise distance from the NP surface to maximise fluorescence and avoid metallic quenching.[102] Moreover, the presence of a silica-shell around the metallic core improves the NP colloidal stability[69] and maximise the surface modification possibilities; thanks to the now well-known silica processing chemistry.[163]

In this paper, we propose alloy-core and fluorescent silica-shell NPs (Figure 4.1) as contrast agents in a multiplatform detection strategy for improved multiplex detection capabilities. The idea is to develop an accordable NP system exhibiting highly controlled fluorescence and plasmonic scattering features. In a proof of concept study, silver core and silica shell NPs($Ag@SiO_2$) along with 50/50 Au/Ag alloy core silica shell NPs($Au/Ag@SiO_2$) were prepared. Using a simple chemistry reaction, fluorophores molecules (fluorescein isothiocyanate (FITC) or rhodamine B isothiocyanate (RBITC) were covalently incorporated inside the silica shell.(Table 4.1) resulting in four different color combinations of contrast agents that can be differentiated using fluorescence and dark field microscopy.

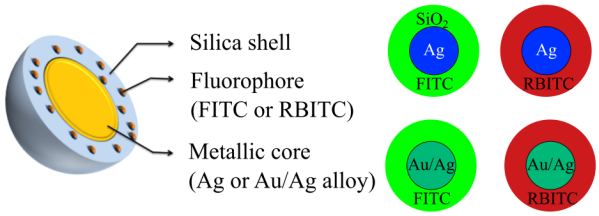

Figure 4.1 Schematic of alloy-core and fluorophores embedded silica-shell nanoparticle and four types of core-shell NPs used as contrast agent.

Table 4.1 Four types of core-shell NPs as contrast agent

Core	AgNPs		Au/AgNPs	
Fluorophore	FITC	RBITC	FITC	RBITC
NPs	$Ag@SiO_2$+FITC	$Ag@SiO_2$+FITC	$Au/Ag@SiO_2$+FITC	$Au/Ag@SiO_2$+RBITC

Table 4.1 Four types of NPs synthesized with Ag and 50/50 Au/Ag alloy core coating with silica shell and embedded with fluorescent dye FITC or RBITC.

4.4 Results and discussions

4.4.1 Structural and composition characterization

Figure 4.2 shows transmission electron microscopy (TEM) images of pure Ag and 50/50 Au/AgNPs before and after the silica shell formation. The silica shell thicknesses are ~12nm and ~27nm for the alloy and silver core-shell NPs respectively. TEM image analysis confirms that there is a decrease in the size of the silver core during the synthesis of $Ag@SiO_2$ NPs (Figure 4.2 (e)) The initial mean diameter of Ag NPs was 70 ± 8nm and was decreased to 55 ± 7nm after the fluorescent silica coating preparation(Figure 4.2 (f)). On the other end, the mean diameter of alloy NPs was not affected by the silica coating synthesis and remained constant at 84 ± 9nm (Figure 4.2 (c)). The size reduction for Ag NPs is probably caused by an etching effect during the Tetraethyl orthosilicate (TEOS) polymerization process catalyzed by ammonia. Indeed, Ung et al[164] have reported a similar effect and attribute the etching effect to the oxidization of silver in presence of ammonia. The same group has also studied the effect of ammonia on small (<30 nm) bimetallic NPs with a 50/50 Au/Ag composition and showed that the etching of Ag is far less severe than in pure Ag NPs,[165] in agreement with the results of Figure 4.2

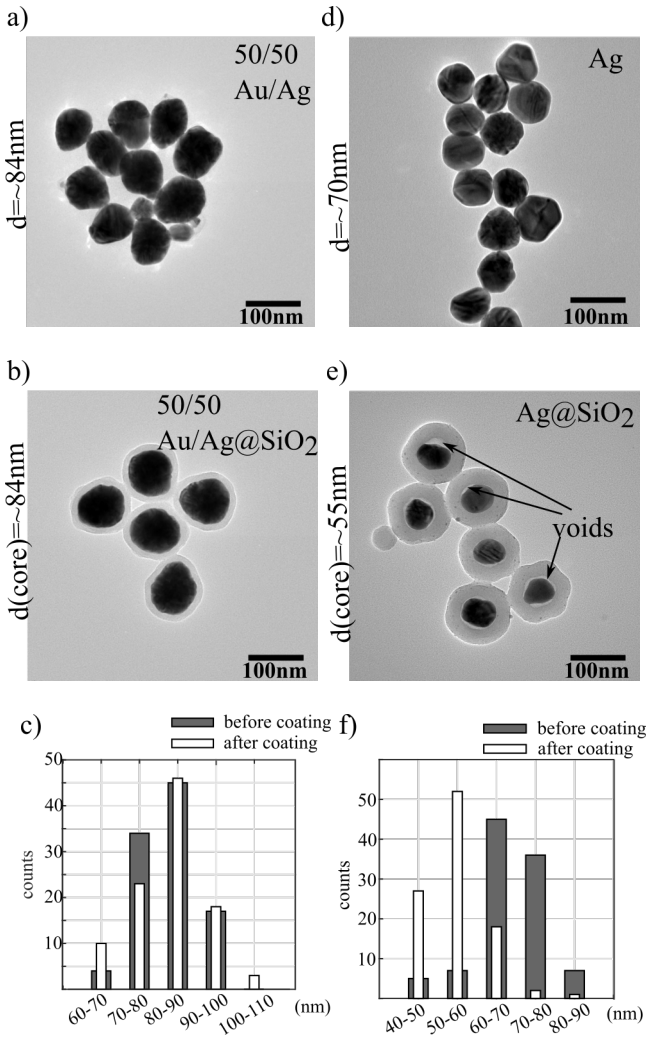

Figure 4.2 TEM images before and after silica coating for (a,b) 50/50 Au/AgNPs and (d,e) pure Ag NPs along with (c,f) their respective size distribution. (e) TEM images for $Ag@SiO_2$ NPs clearly shows voids near Ag cores resulting from etching during the coating process.

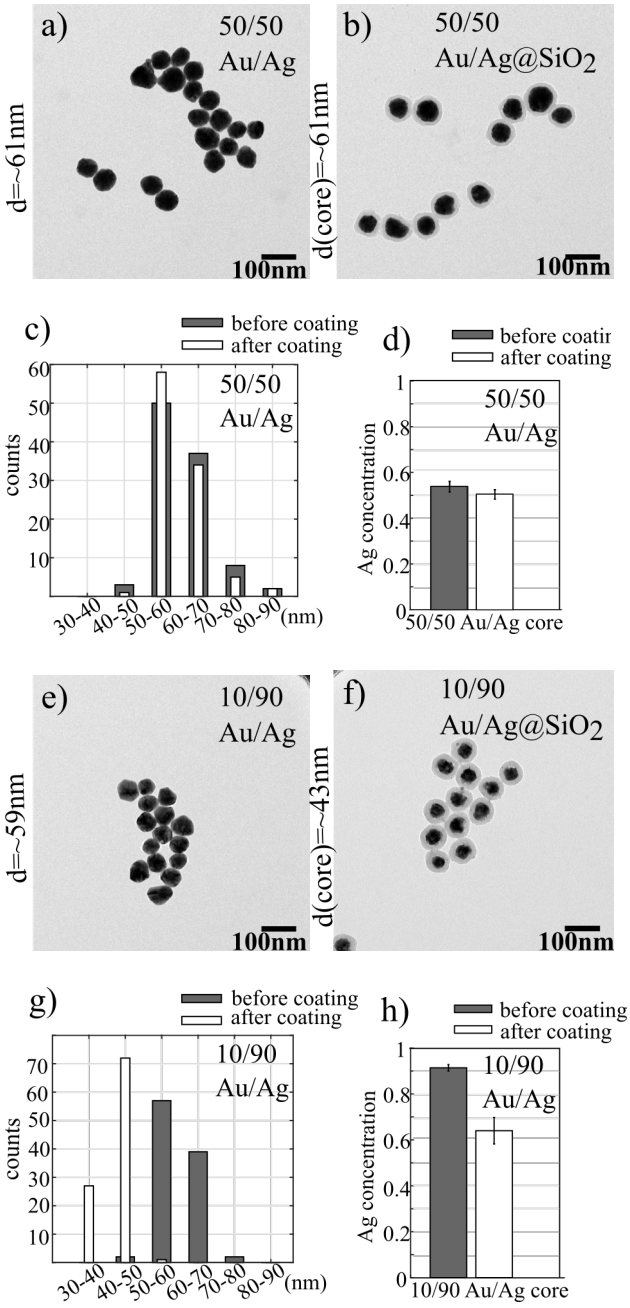

Figure 4.3 TEM images for (a) 61±8 nm 50/50 Au/AgNPs and (e) 59±5 nm 10/90 Au/AgNPs and after coating with silica shell (b) 50/50 Au/Ag@SiO_2 and (f) 10/90 Au/Ag@SiO_2. The respective NP diameter distributions are shown in (c) and (g). Silver concentration bar graph are presented for (d) 50/50 Au/AgNPs and (h) 10/90 Au/AgNPs before and after silica coating based on EDS examination of 5 individual NPs.

To evaluated the core etching effect of the silica coating synthesis for Au/AgNPs, we prepared two types of alloy NPs having similar mean diameters (59±5nm and 61±8nm) with different Au/Ag core composition ratios (10/90 and 50/50). A silica shell was grown on both alloys NPs using the same experimental conditions. Post synthesis TEM images analysis confirmed the etching effect was more important for silver rich alloys NPs. The TEM images analysis results (Figure 4.3 c and g) show a reduction of the core diameter for 10/90 Au/Ag@SiO_2 (59±5nm to 43±4nm) while there was no significant change for 50/50 Au/Ag@SiO_2. The corresponding energy-dispersive X-ray spectroscopy (EDS) results(Figure 4.3 d and h) show a significant 30% reduction in the silver composition for 10/90 Au/Ag@SiO_2 after the silica shell synthesis compared to only ~5% for 50/50 Au/Ag@SiO_2. These results confirm that Au/AgNPs with higher gold ratios are less prone to the core etching process which can take place during the silica coating reaction. The mechanism of Au protecting NP from etching is not entirely clear. Gold could rearrange around silver atoms and because is less affected by ammonia, it would have a protecting effect on silver preventing further etching during the silica-core synthesis, as proposed by Benito Rodríguez-González.[165] Therefore, the higher the gold ratio is for the starting NPs, the easier the silica layer can be generated around the core without any significant core size reduction and apparent voids at the end.

4.4.2 Optical characterization

Characterization of the photophysical properties for gold, silver or alloy nanoparticles were compared to their corresponding theoretical extinction spectra obtained using Mie Theory calculations.[166] The UV-Visible spectra for Ag@SiO_2 and 50/50 Au/Ag@SiO_2 measured before and after the silica coating process are presented at Figure 4.4 and can be compared to their theoretically calculated ones for both FITC and RBITC fluorophores. The dielectric function for Au/AgNPs was taken from Rioux *et al*.[90] and the refractive index for the silica shell was computed using the dispersion equation from Malitson *et al*.[167] Core diameters and silica shell thicknesses considered for calculations were evaluated by TEM image analysis. (details in supporting information)

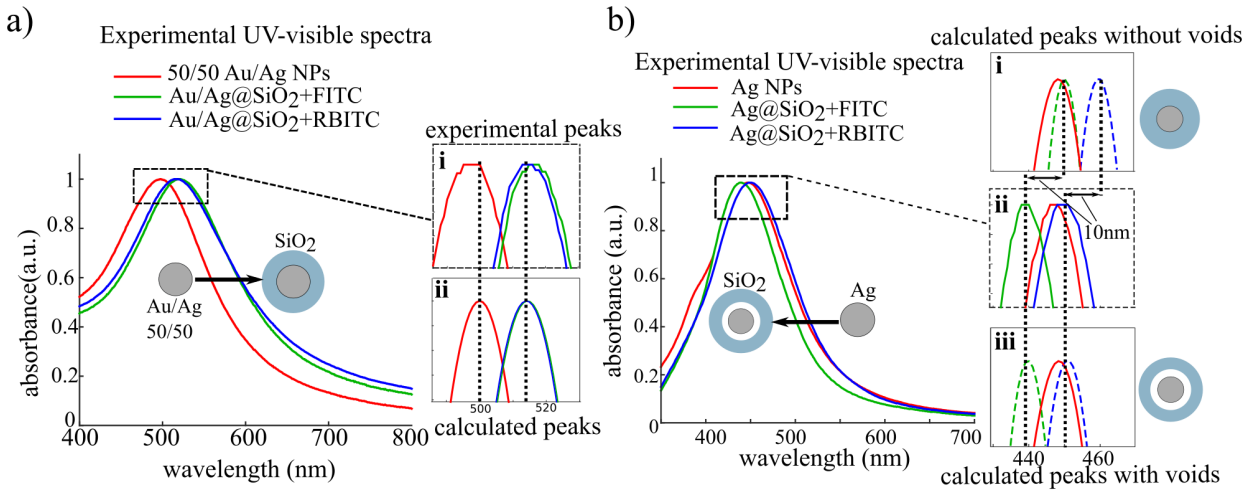

Figure 4.4 Presentation of the experimental and calculated UV-visible spectra for (a) 50/50 Au/AgNPs and (b) Ag NPs before and after the silica shell coating process (with FITC and RIBTC). A ~15nm red shift of the plasmonics band maximum was observed between 50/50 Au/Ag NPs and 50/50 Au/Ag@SiO_2 independently of the fluorophore embedded in the silica shell. The same red shift was smaller (~3nm) for Ag@SiO_2+RBITC and a 6nm blue shift was measured for Ag@SiO_2+FITC. Calculated UV-visible spectra of 50/50 Au/AgNPs (a-ii) and Ag NPs(b-i, b-iii) before and after silica coating are aligned the experiment peaks. For both FITC and RBITC incorporated Ag@SiO_2 NPs, the blue shift of the plasmonics band results from the presence of a void layer between the silver core and the silica shell (b-iii, a 5 nm void was used for this calculation, estimated from TEM images). The schematics show the nanoparticle geometries considered for the calculations.

As expected, a redshift of the plasmonics band is observed for the 50/50 alloy NPs after the silica coating process (Figure 4.4 a) . The ~15 nm redshifts measured for both nanoparticles were confirmed by Mie calculations (Figure 4.4 a-i).[87] An unexpected smaller ~3 nm redshift was recorded for Ag@SiO_2+RBITC NPs and more surprisingly, a ~6 nm blue shift was observed for Ag@SiO_2+FITC NPs. The experimental results observed for Ag@SiO_2 were significantly different from the theoretically expected ones based on nanoparticular core-shell architectures. TEM observations of Ag@SiO_2+RBITC and +FITC samples indicated the presence of voids between the core and the shell (Figure 4.2 e), which have direct impacts on the position of the NPs plasmonics band. The silver-core etching phenomenon may origin from the presence of ammonia during the silica coating process.[168] Consideration of smaller core size diameters

(Figure 4.2 f and Figure 4.3 g) in the calculations could not explained the results observed as there was still a ~10 nm discrepancy with the experimental measures (Figure 4.4 b-i and b-ii). Therefore, reconsideration of the nanoparticular architecture was realised in order to take into account the presence of a 5 nm thick space filled with the NP suspension medium. Using this modified model (see parameters used in supporting information), the calculated spectra for $Ag@SiO_2$+RBITC and +FITC were virtually identical to their counterpart measured experimentally (Figure 4.4 b-ii and b-iii).

Fluorescence characterization for $Ag@SiO_2$ and 50/50 $Au/Ag@SiO_2$ NPs are detailed in supporting info for FITC- and RBITC-embedded core-shell NPs. The MEF factor was measured for $Ag@SiO_2$ NPs with RBITC by comparing the maximum fluorescence intensity of a $Ag@SiO_2$ RBITC solution before and after a complete core etching process using a 250 mM sodium chloride solution. A MEF factor value of 4 was calculated for the $Ag@SiO_2$+RBITC (see supporting information).

4.4.3 Multiplexed imaging

The principal objective of this paper is to present a multiplatform detection approach exploiting the remarkable photophysical properties of alloy-core and fluorescent silica-shell nanoparticles for multiplexed imaging applications. The strategy is based on the use of spectrally distinguishable nanostructures offering multiple combinations of scattering and fluorescence colors. In this proof of concept study, four different color-coded NPs were mixed together and sampled on a glass slide. Single particle identification was accomplished by acquiring the scattering spectra and the fluorescence properties of each nanoparticles. $Ag@SiO_2$ and 50/50 $Au/Ag@SiO_2$ appear blue and green under darkfield microscopy respectively. Their specific color is attributed to the position and shape of their plasmonics band which have maximum at ~450nm for silver core NPs and ~520nm for 50/50 Au/AgNPs. A spectrometer was positioned on the detection path of the optical microscope used in this study in order to acquire the individual scattering spectrum of each nanoparticles. Attribution of the core compositions was realised using each nanoparticle's maximum scattering value. Globally, scattering spectra of twenty-eight particles were recorded has shown in Figure 4.5 c and d**.** On the other end, fluorescence identification was performed by measuring the signal intensities in each detection channel for all nanoparticles (FITC and RBITC)(Figure 4.5 b). Using optical filter sets specific to each

fluorophore, detection thresholds were fixed at three times the standard deviation (pixel to pixel) over the average intensity recorded for a blank sample (nanoparticle free). Figure 4.5 c shows that twenty-four out of twenty-eight NP cores were correctly identified by their scattering maximum resulting in a 86% core-composition differentiation capability. Four NPs, noted as dashed circles 1, 2, 3 and 4 in Figure 4.5 a and b, were not correctly identified because of their higher scattering intensities, broader scattering spectra and more ambiguous peak position compared to the other NPs (Figure 4.5 d); probably as a result of clusters formation. Finally, we observed several isolated fluorescence spots without any scattering signals (noted in yellow triangles). These NPs might be either core-free silica NPs or fluorescent silica fragments that do not produce any coloration under dark-field microscopy.

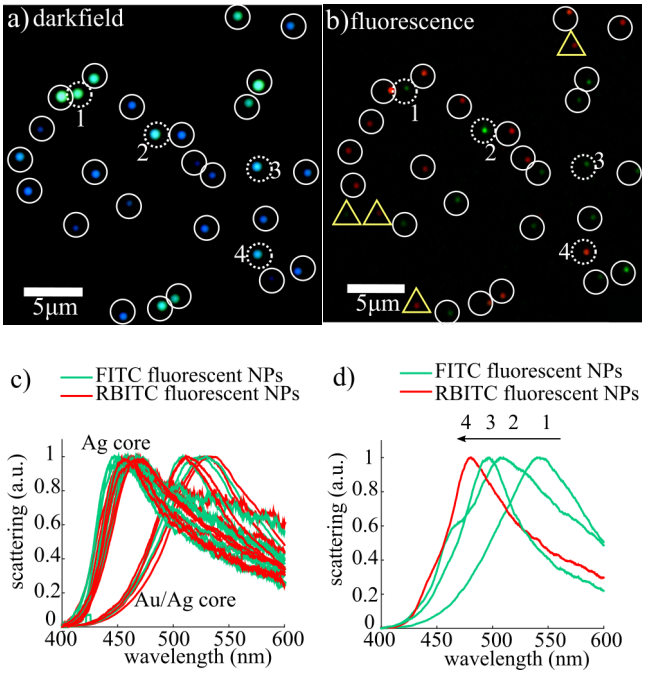

Figure 4.5 (a) Darkfield and (b) fluorescence microscopy images of a Ag@SiO_2 and 50/50 Au/Ag@SiO_2 mixture. (c) Scattering light identification of each identifiable nanoparticles and presentation of the scattering spectra for (d) four specific NPs identified by dashed circles in figures (a). Fluorescence signal from NPs identified by yellow triangles in (b) do not show corresponding scattering signal in (a).

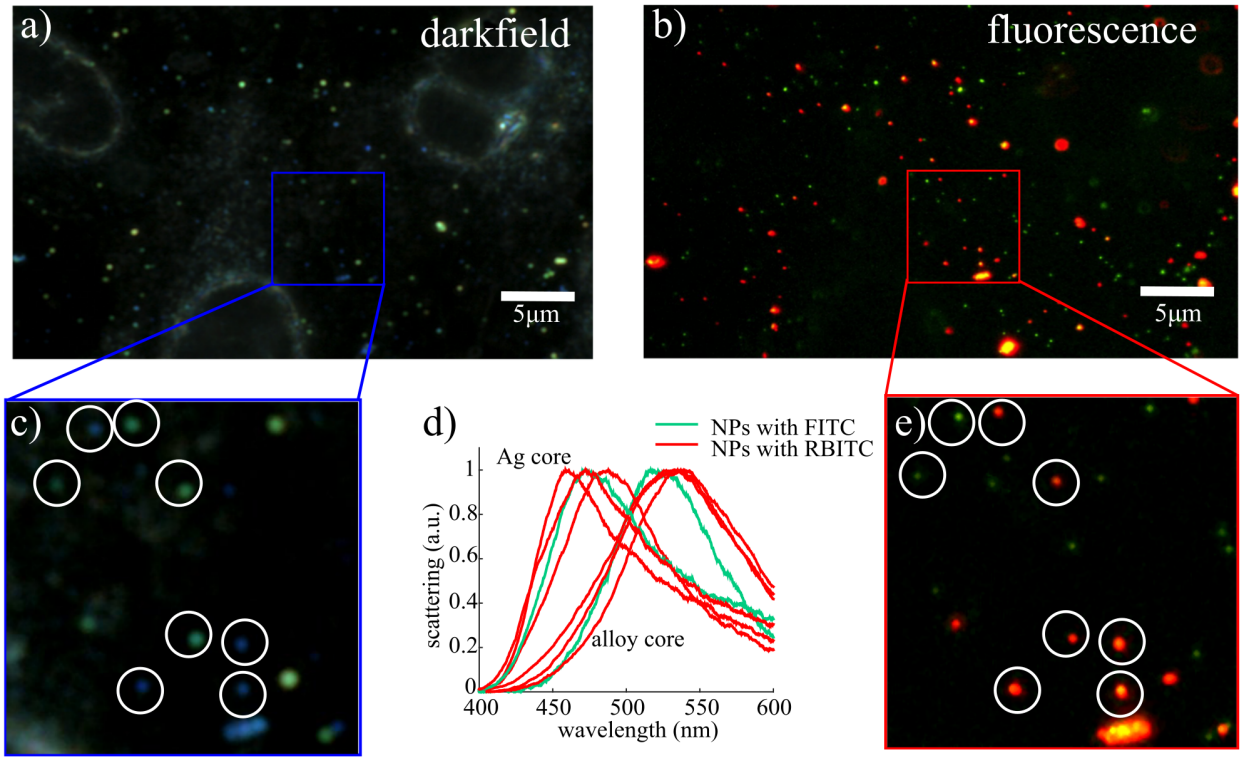

Figure 4.6 (a) Darkfield and (b) fluorescence images of a retinal cells sample (ARPE-19) in presence of a nanoparticles mixture with their respective close-ups view (c and e). (d) Characterization of the scattering and fluorescence properties for eight nanoparticles identified by circles on figures (c) and (e). The four types of color-coded nanoparticles were identified by their scattering spectra and fluorescence properties.

We assessed the performances of fluorescent Au/Ag@SiO_2 as contrast agents for cell imaging applications. A 1:1 mixture of Ag@SiO_2 and 50/50 Au/Ag@SiO_2 NPs with either a FITC (Au/Ag@SiO_2+FITC) or a RBITC (Au/Ag@SiO_2+RBITC) fluorescent silica shell was added to a retina cells sample (ARPE-19). The latter was observed by darkfield and fluorescence microscopy and a representative image of the probed area is presented at Figure 4.6. Stronger photoluminescent spots were attributed to NP clusters; a hypothesis confirmed by darkfield microscopy. Eight circled nanoparticles were characterised and clearly identified by their respective scattering and fluorescence properties (Figure 4.6 c, d, e) on a retina cell with their corresponding core composition (Figure 4.6 c and d). This experiment demonstrates how the fully accordable photophysical properties of alloy core and silica shell nanoparticles can be

exploited in a multiplatform detection strategy for cell imaging applications with multiplexed analysis capabilities.

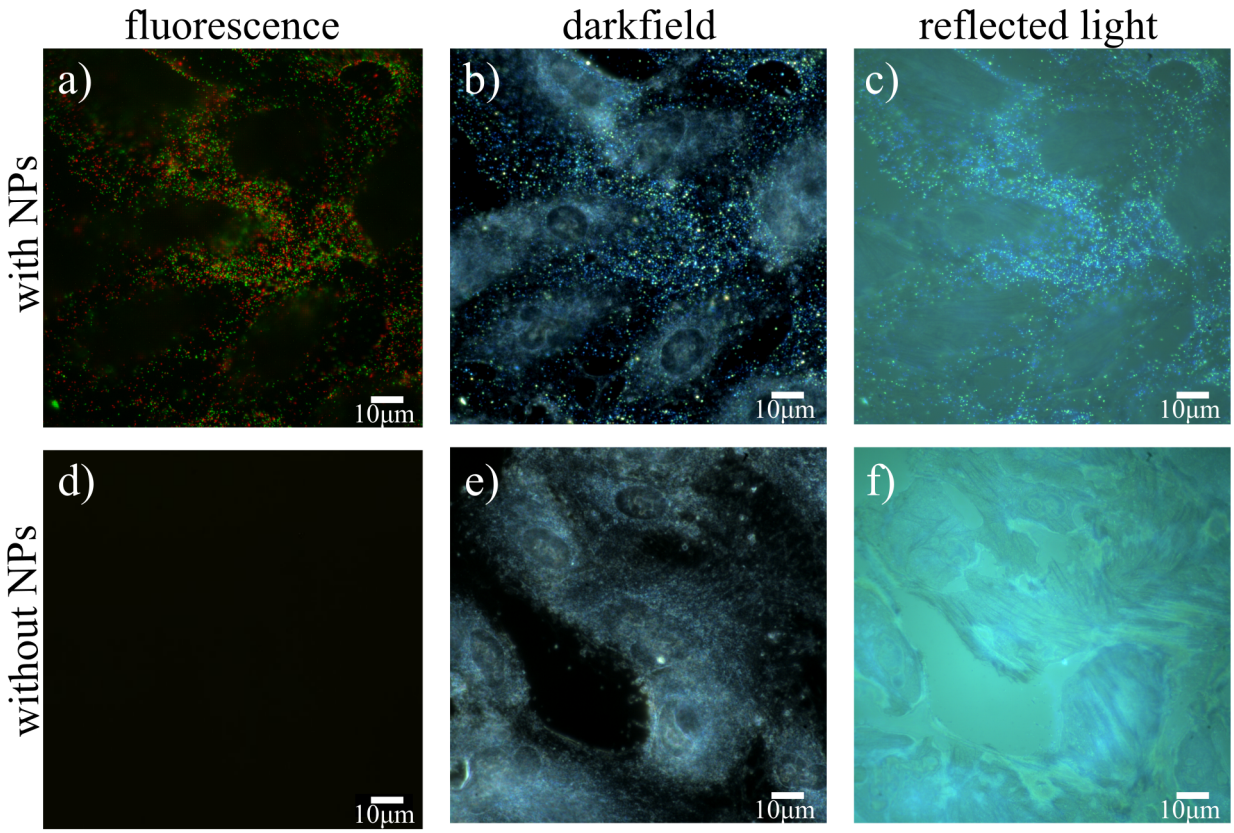

Figure 4.7 (a, d) Fluorescence, (b, e) darkfield and (c,f) reflected light image of a NPs mixture containing four spectrally different types of metallic and alloy-core NPs ($Ag@SiO_2$+ FITC/RBITC, 50/50 $Au/Ag@SiO_2$+FITC/RBITC) in presence of fixed retinal cells (ARPE-19) and their respective controls without nanoparticles (d, e, f).

Reflected light microscopy offers exceptional detection contrast when using NPs as cell labels for imaging applications in highly diffusing media.[12] Fluorescent $Au/Ag@SiO_2$ were added to a retina cells sample and the latter was observed by fluorescence, darkfield and reflected light microscopy. Each image was compared to a nanoparticles free sample (Figure 4.7). This experiment confirms the high potential of alloy-core silica-shell NPs as effective contrast agents for all three modes of optical microscopy. The cells scattering light is stronger under darkfield microscopy making nanoparticle detection and identification more complicated. But rather, the same scattering signal is significantly lower for reflected light without any lost on the nanoparticle signal. Moreover, the depth of field for reflected light microscopy is smaller than

darkfield resulting in a better Z-axis definition and lower background signal. Colocalization of NPs under three different modes of optical microscopy was possible using fluorescent alloy-core silica-shell nanoparticles as contrast agents (Figure 4.7). As an additional proof of concept experiment, fluorescent Au/Ag@SiO_2 were used for cell tagging applications by flow cytometry (See Supporting Information). Using a well-known crosslinking chemistry reaction, specific and nonspecific antibodies to HeLa cells were functionalized at the surface of fluorescent core-shell nanoparticles. The results are promising, despite not being perfect, and are paving the way for further improvements in terms of fluorescence intensity since detection specificity was advantageously compared to the use of regular fluorophore-labelled antibodies.

4.5 Conclusions

Fluorescent alloy-core silica-shell nanoparticles were prepared for cell tagging and imaging applications. The size and composition of the alloy core can be adjusted to control the position and width of the plasmonics band to meet specific experimental needs. Using a well known silica processing reaction, fluorescent silica shells were grown around the alloy nanoparticles making the nanoparticular architecture well suited for multiplexed analysis using a multiplatform detection strategy Retinal cells were observed by fluorescence and darkfield microscopy in the presence of four different color-coded Au/Ag@SiO_2 NPs. Most NPs could be identified by their fluorescence and scattering properties using a simple detection algorithm. Based on this proof of principle study, it is anticipated to achieve higher levels of multiplexing by better controlling the synthesis of Au/Ag alloy NPs to reduce the width of their size distribution thus allowing more scattering colors to be use simultaneously without compromising identification capabilities.[40] Furthermore, quantum dots could be incorporated in the silica shell of Au/Ag@SiO_2 NPs instead of fluorophore molecules. A single excitation wavelength would be needed to generate light from all contrast agents while the narrower emission band of QDs would enhance the multiplexed analysis possibilities of Au/Ag@SiO_2. Finally, the applicability of fluorescent alloy-core silica shell nanoparticles for cell tagging and imaging applications was presented and they offers remarkable and adjustable photophysical properties and they represent a cheaper alternatives to conventional cell labelling moieties in terms of detectability and photostability.

4.6 Experimental section

Materials: Gold-silver alloy NPs with different sizes and compositions were fabricated by a successive seeded growth method of alloy on initial ~15nm Au seeds of.[40] $HAuCl_4$, $AgNO_3$ and trisodium citrate (Na_3Cit) were purchased from Sigma Aldrich. Silver NPs used in this study 0.02mg/mL (~70nm) were received from nanoComposix (#AGCN70). For the fluorescent precursor synthesis, anhydrous N,N-dimethylformamide (DMF, Aldrich #68-12-2), Triethylamine (Aldrich), 3-(aminopropyl)triethoxysilane (APS, Aldrich #919-30-2), fluorescein isothiocyanate (FITC, Aldrich #27072-45-3), Rhodamine B isothiocyanate(RBITC, Aldrich #36877-69-7), CF 647 dye (Aldrich #SCJ4600048) were used as received. For the silica shell coating preparation, Tetraethyl orthosilicate (TEOS Aldrich #78-10-4), 28%-30% $NH_3 \cdot H_2O$ (Aldrich #7664-41-7) and anhydrous ethanol (EtOH) were used as reagent, catalyst and dispersion media respectively. 18 MΩ deionized water was obtained from a EMD Millipore water purifier.

Preparation of fluorescent precursors: FITC-APS and RBITC-APS were prepared following a similar protocol.[169] They were prepared in DMF with triethylamine as a catalyst. Typically 2.2 mg 5.7 μmol) FITC was mixed with 150μL DMF, 2μL Triethylamine and 2μL APS in a light proof tube in continuous agitation at 50℃ for 3 hours. The solution was diluted in 13.5 mL EtOH, resulting in a fluorophore solution at 420 μM. Similarly, RBITC 3mg was mixed with 4μl APS in 150μL DMF, 2μl Triethylamine with all other reagents and reaction conditions being the same.

Preparation of fluorescent AuAg@SiO_2 NPs: 80nm 50/50 Au/Ag and 74nm Ag NPs were used as core. For the fluorescent silica shell synthesis, 4ml of a 50:50 Au/Ag alloy NP aquous solution at ~5×10^9NPs/ml was added directly to 12ml anhydrous EtOH under continuous stirring. Then, 1.2μL of TEOS and 625μL of 30% ammonia solution were added. A small volume of the fluorescent silica precursor (50μl for FITC per example) was added directly to the nanoparticles solution 30 minutes after the start of the silica coating process to reduce the amount of fluorophore quenched because of their close proximity to the metal core. After a 24 hours reaction period, the fluorescent core-shell nanoparticles were clean and dispersed in ethanol and stored at 4°C away from light until their use.

Nanoparticle characterization: UV-visible experiments were carried out on a Epoch Microplate Spectrometer and used to study the plasmonic band evolution and evaluate the colloidal stability of nanoparticle at every steps during synthesis.. The steady-state fluorescence measurements were realised with a Varian Cary Eclipse. The structure of each nanoparticle sample was defined by transmission electron microscopy (TEM, JEOL 2100) and the data were used to generate size distributions and to confirm core-shell morphology. Copper grids (Pacific grid tech, Cu-400CN) were dipped into diluted NPs ethanol solution and air dried before TEM analysis.

DF and fluorescent microscopy images were acquired with an Eclipse Ti microscope (Nikon) equipped with a 100x oil immersion objective (numerical aperture (NA) 0.5–1.3, Nikon) with with a 4.2 megapixel color CMOS camera (xiQ, 2048x2048 pixels) or a QIclick CCD camera (Qimaging, 1392x1040 pixels) for detection and imaging. Two light sources were available, a 100W halogen lamp (Nikon) and the intensilight Epi-fluorescence Illuminator from Nikon for DF and fluorescence applications respectively. FITC (thorlabs, MDF-FITC, excitation filters/emission filters: $475 \pm 35nm/530 \pm 43nm$, Dichroic: 470-490 nm/508-675 nm) and RBITC (Nikon, TRITC/Cy3 long pass filter set, excitation filters/emission filters: $540 \pm 25nm/575nm$ long pass, Dichroic: 565nm) filters were used for fluorescence measurements. The sample preparation method for microscopy experiments was develop to obtain a final NPs concentration of $\sim 1NP/\mu m^2$ in the instrument field of view. The hyperspectral images were acquired using an imaging spectrograph (Shamrock 750, Andor Technology) equipped with an EMCCD camera (Newton 971, 1600x400 pixels, Andor Technology) and a 150 lines per mm grating providing a 242 nm bandpass.

4.7 Acknowledgement

This work was supported by the Nature Science and Engineering Research Council of Canada NSERC. The authors would like to thank Jean-Philippe Masse for the help with the TEM and EDS measurements accomplished at the Center for Characterization and Microscopy of Materials (CM^2).

4.8 Supporting information

4.8.1 Fluorescence detections and MEF factor

Figure 4.8 shows the fluorescence emission spectra of 50/50 Au/Ag@SiO_2 NPs with either FITC (green) or RBITC (red) embedded in the silica shell.

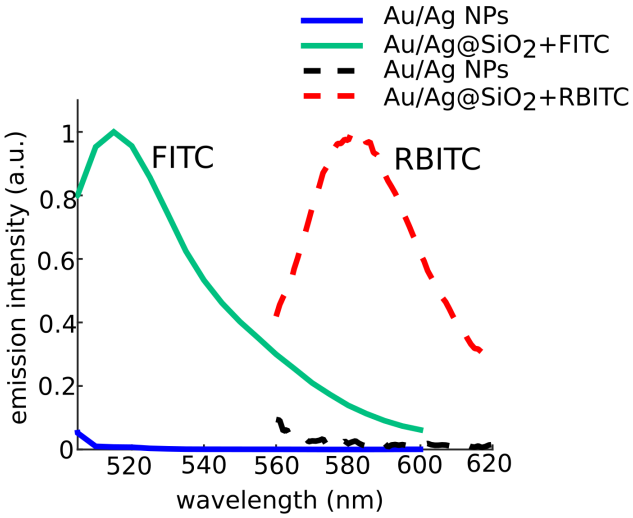

Figure 4.8 Fluorescence emission spectra for 50/50 Au/Ag alloy NPs and for 50/50 Au/Ag@SiO_2 with a fluorescein isothiocyanate (Au/Ag@SiO_2+FITC) or a rhodamine B isothiocyanate (Au/Ag@SiO_2+RBITC) fluorescent silica shells.

4.8.2 Determination of the Metal-Enhanced Fluorescence (MEF) factor

Determination of the MEF factor for alloy core and silica shell NPs was realized by comparing fluorescence intensities between core-shell and core-less nanoparticles.lan[66] For example, the fluorescence intensity of a 2:98 Au/Ag@SiO_2+RBITC sample was measured and then submitted to a core etching process (0.25M sodium chloride solution for 12h). After confirmation of the core etching process by UV-Visible spectroscopy (absence of the plasmonics band), the fluorescence intensity of the core-less nanoparticles sample was measured. The MEF factor, defined as the fluorescence ratio at λ_{max} between core-shell and core-less NPs, was calculated at 4 for 2:98 Au/Ag@SiO_2 +RBITC NPs.

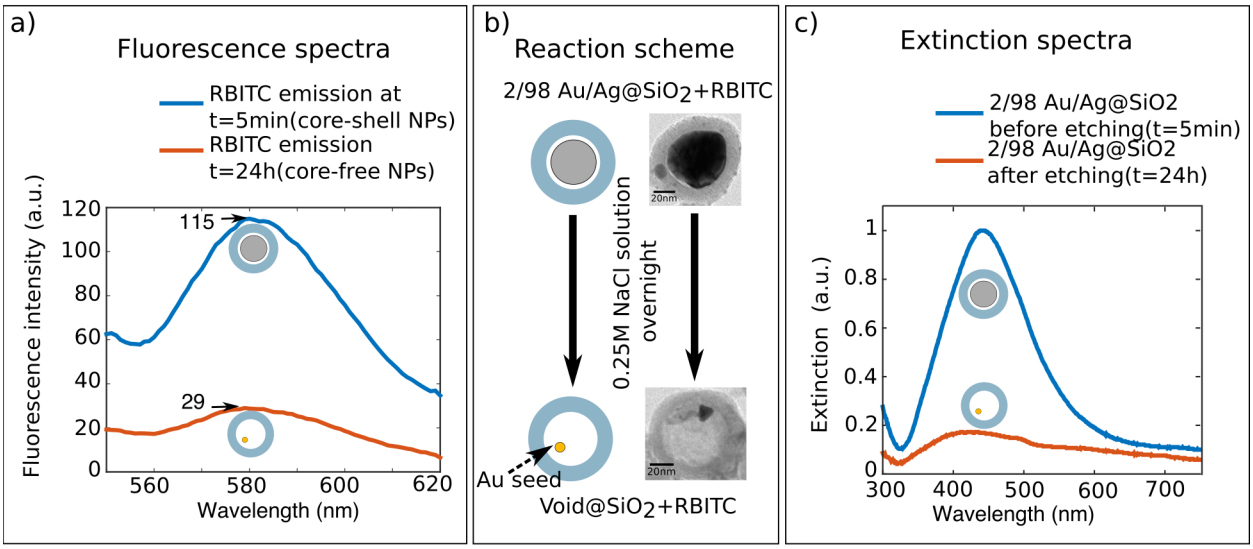

Figure 4.9 (a) Fluorescence spectrum, (b) core-etching reaction scheme supported with TEM images and (c) extinction spectra for 2/98 Au/Ag@SiO_2+RBITC before and after core etching. NPs were dispersed in a 0.25M NaCl solution overnight to complete the etching reaction. A MEF factor of 4.0 was obtained.

4.8.3 Parameters used for absorbance modeling

TEM images confirmed there was a void space between the silver core and silica shell that was generated during the silica shell formation. The presence of a void filled with the nanoparticle suspension medium was considered in the Mie model. Core diameters and silica shell thicknesses for the NPs samples are shown in Table 4.2. We estimated a 5 nm thickness based on our TEM measurements.

Table 4.2 Parametersd used for the Mie calculations

Core and total diameters(nm)	**AuAg@SiO_2 NPs**	**Ag@SiO_2 NPs**
Before silica shell growth	84-84	70-70
FITC	84 - 110	55 – 110
RBITC	84 - 110	62 – 115

4.8.4 Concentration of NPs

Determination of NPs concentrations was calculated by comparing the extinction intensities and extinction cross-sections of NPs sample with those of commercial 70nm Ag NPs (Nanocomposix #AGCN70, NP concentration 9.5×10^9 NPs/mL). A calibration curve for the NPs concentration as function of their extinction is presented at Figure 4.10 Extinction spectrum of nanoparticles prepared in this study compared to the one recorded for a standard 70nm Ag NPs (nanoComposix, 70nm Ag). (b) Normalized extinction intensity measured for different concentrations of 70nm diameter Ag NPs. b. The relative extinction cross-sections of Ag@SiO_2 and Au/Ag@SiO_2 can be calculated using dielectric function of Au/Ag alloy NPs in water.[90] The method precision and exactitude to obtain the NPs concentration depend on losses during cleaning steps, the type of nanoparticles and their tendency to form aggregates. The concentrations results are shown in Table 4.3 Concentrations of Ag@SiO_2 and 50/50 Au/Ag@SiO_2 sample used in imaging.. We assumed that extinction intensity is proportional to concentration and extinction cross-section of NPs.

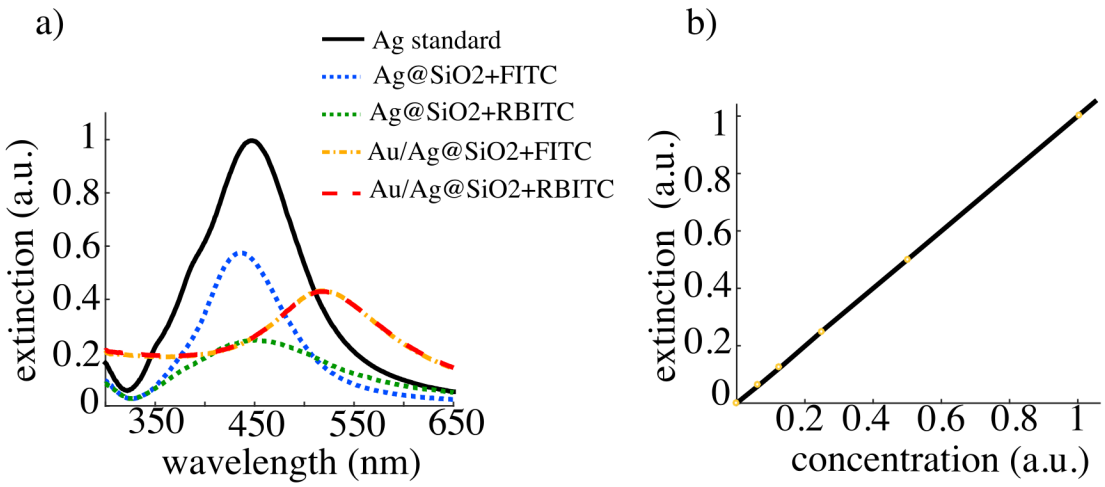

Figure 4.10 Extinction spectrum of nanoparticles prepared in this study compared to the one recorded for a standard 70nm Ag NPs (nanoComposix, 70nm Ag). (b) Normalized extinction intensity measured for different concentrations of 70nm diameter Ag NPs.

Table 4.3 Concentrations of $Ag@SiO_2$ and 50/50 $Au/Ag@SiO_2$ sample used in imaging.

NP type	**Ag@SiO2 +FITC**	**Ag@SiO2 +RBITC**	**50/50 Au/Ag@SiO2 +FITC/RBITC**	**Ag**
Core/Shell diameter(nm)	55/27	62/27	82/12	70
Concentration ($\times 10^9$NPs/mL)	6.6	2.3	3.5	9.5

Note that in Figure 4.10a, the extinction band of $Ag@SiO_2$+RBITC is broader and the maximum intensity is lower and at longer wavelength (>510nm) compared to $Ag@SiO_2$+FITC. A broadening of the extinction band is a sign of aggregation. In the case of 50/50 $Au/Ag@SiO_2$+FITC and +RBITC, the two bands are virtually overlapping.

4.8.5 Retina cells preparation

Human retinal pigment epithelium (ARPE19, from ATCC) cells were cultured in DMEM F12 (10%FBS, 1% Pen Strep) medium and collected at passage 20. The cells were fixed with 100% methanol prior to NP deposition and visualization.

4.8.6 Cell tagging applications and detection by flow cytometry

In a proof of concept experiment, fluorescent Ag@SiO_2 and Au/Ag@SiO_2 NPs were functionalized with monoclonal antibodies using a cross-linker molecule to attached targeting moieties at the NPs surface. HeLa cells were chosen as targets because of their simple culturing process and their well-characterized surface antigens.

Surface functionalization of monoclonal antibodies

Fluorescent alloy-core and silica shell NPs were functionalized with monoclonal anti-CD49e (BD biosciences #557447) and anti-CD44 (BD biosciences #559250) antibodies; both are specific to HeLa cells expressed antigens. The Anti-Nectin-2 monoclonal antibody was used for negative controls since HeLa cells do not express the corresponding cell marker. Fluorophore-labelled monoclonal antibodies (anti-CD49e-PE from BD biosciences #555617, anti-CD44-APC BD biosciences #559250) were used to verify the efficiency of the cross-linking reaction and to confirm specificity of each expressed and unexpressed antigens

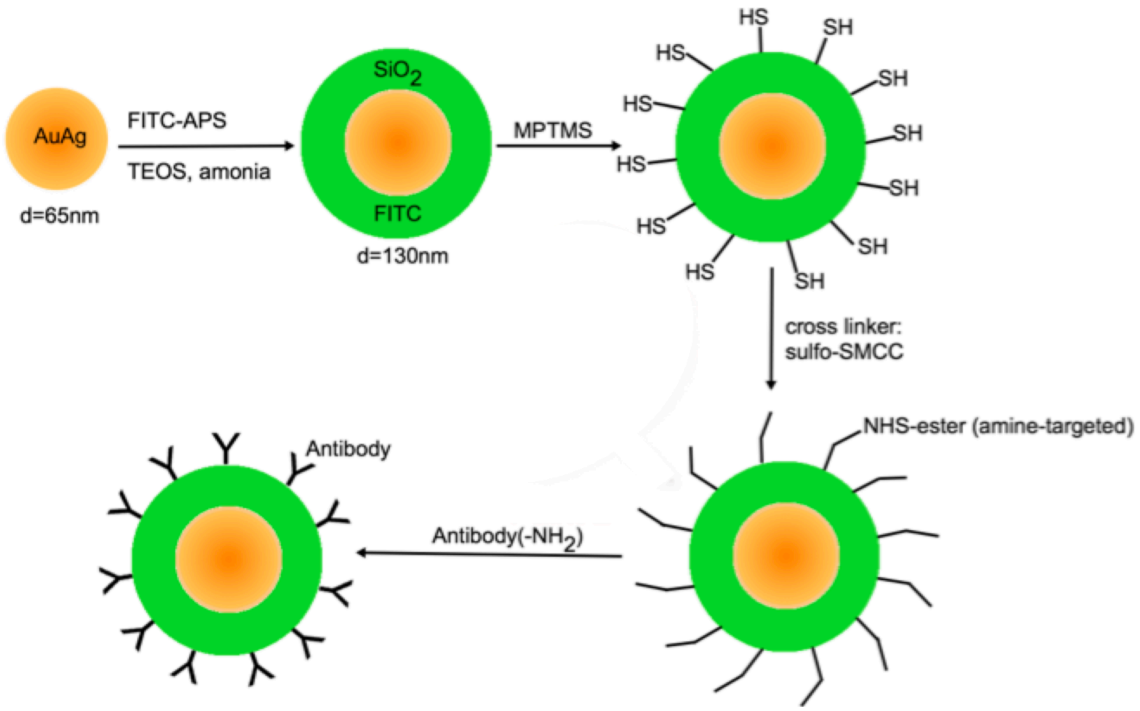

Figure 4.11 Schematic of NPs functionalization with antibodies on the surface

The strategy for the functionalization reaction is presented at Figure 4.11. Starting with fluorescent metal-core silica-shell NPs dispersed in ethanol, a 4 mL sample calculated at ~10^9 NPs/mL was washed with EtOH and deionized water before being dispersed in a final 4mL EtOH volume. The NPs surface was then thiolated by the addition of (3-Mercaptopropyl) trimethoxysilane (MPTMS Aldrich #4420-74-0) to a final concentration of 92 nmol/L under continuous agitation for 3 hours at 60°C. Thiolated NPs were cleaned (8000 g for 10 min) with EtOH and phosphate buffer at pH = 6.8 and finally dispersed in the same initial volume of phosphate buffer. A 2 mg/mL concentration of sulfosuccinimidyl 4-(N-maleimidomethyl) cyclohexane-1-carboxylate (Sulfo-SMCC, ThermoFisher Scientific #22322) in phosphate buffer at pH = 6.8 was used to initiate the cross-linking reaction between the maleimide part of Sulfo-SMCC and sulfhydryl groups of the thiolated NPs. The reaction lasted 2 hours at 60°C under continuous agitation. The NPs solution was washed two times with a phosphate buffer solution at pH8.4 and dispersed in the same solution at an estimated final NPs concentration of ~10^8 NPs/mL. The amine functions of the antibody molecules were let to react with the sulfo-NHS ester function of the cross-linker. Antibodies were added directly to the NPs sample at a 122 nmol/L concentration. The reaction lasted 3 hours at 50°C under continuous agitation. The nanoparticular antibody solutions can be stored for one week at 4°C under dark.

Cell preparation

HeLa cells were grown in RPMI-1640 culture medium (Invitrogen, Burlington, ON, Canada) supplemented with 5% fetal bovine serum (HyClone, Logan, UT, USA) at 37°C in a 5% CO_2 controlled environment. Cells were EDTA-detached (0.5 mM EDTA in PBS without Ca^{2+}/Mg^{2+} (LONZA, Walkersville, MD, USA)) when they reached 80% confluency. Cells were washed using PBS and frozen in 1 mL aliquots of RPMI-1640 containing 10% FBS and 5% DMSO. Cells were rapidly thawed at 37°C and diluted in PBS the day of the experiment. Viable cells count was determined using the Solution 18-AO-DAPI and a Nucleocounter®, NC-250™ (both from Chemometec). Cells were dispersed in multiple eppendor tubes.

Viable cells (650 000 cells/sample) were incubated with the contrast agents (fluorescent antibodies or nanoparticular antibodies) for 120 minutes at 4°C. After two cleaning step with PBS (500 RCF, 5 min), cells were suspended in PBS and measured by flow cytometry (Partec CyFlow-Space and Biosciences BD Accuri™ C6).

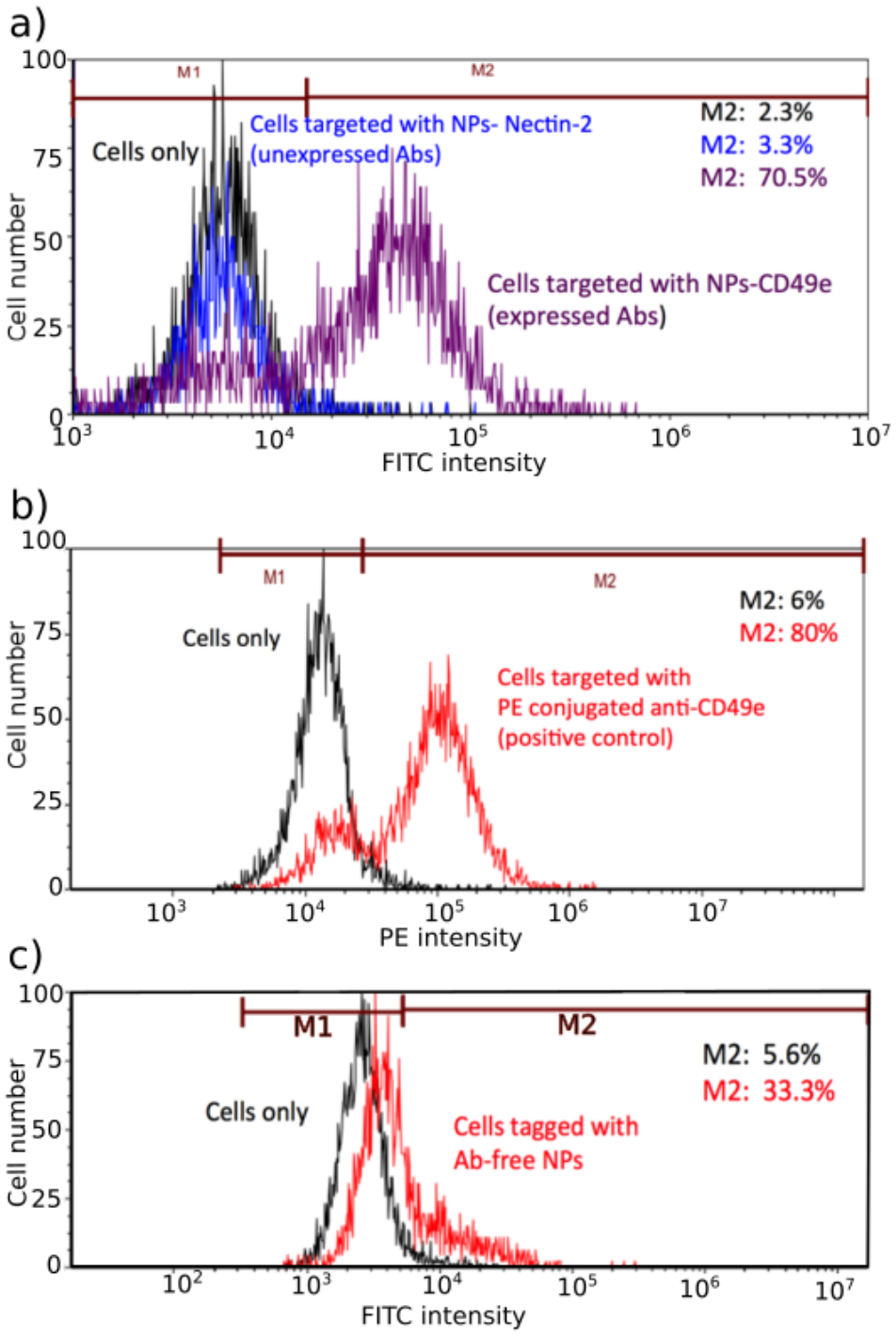

Figure 4.12 (a) Comparison of the intensity histograms for the FITC channel recorded for unlabelled HeLa Cells (black), HeLa cells labelled with specific Anti-CD49e NPs (purple) and HeLa cells labelled with unspecific Anti-Nectin-2 NPs (blue). A shift in the intensity histograms confirms the detection specificity and was used to calculate a 70% cell labeling efficiency for the

nanoparticular antibodies. (b) A fluorophore-labelled monoclonal antibodies (anti-CD49e PE) was used to identify HeLa Cells and under the exact same experimental conditions as (a), the labelling efficiency was calculated at 80%. (c) Antibody-free nanoparticles were used to evaluate how NPs can suffer from non-specific adsorption.

Figure 4.12 demonstrates successful cell tagging applications using fluorescent metal-core silica-shell NPs ($Ag@SiO_2$+FITC) as contrast agent with flow cytometry. A HeLa cells specific antibody (Anti-CD49e) was functionalized at the surface of the nanoparticles to create a nanoparticular antibody. There is no significant difference on the targeting specificity between molecular or nanoparticular antibodies. Experimental results also demonstrated the nanoparticle core composition did not have any influence on the targeting performances of nanoparticular antibodies.

CHAPTER 5 RESULTS AND GENERAL DISCUSSIONS

In the previous chapter, the paper was mainly focused on synthesis, characterizations of fluorescent Au/Ag@SiO_2 NPs and the proof of principle experiments for multiplexed imaging. This chapter aims at tuning the design and improving the quality of fluorescent core-shell nanostructure to maximize its potential for higher multiplexed imaging as contrast agents. The first part covers the possible choices of the peak position of plasmonic core and discussion of better choices for fluorescent emitter inside silica shell. The second part demonstrates possible imaging quality improvement that could be achieved by a better control of the uniformity and shell thickness.

5.1 Choices of plasmonic nanomaterial

As mentioned in previous chapters, Au, Ag and nanorod as multiplexed imaging contrast agents, can be functionalized with specific antibodies and targeted to cells with good identification efficiency[109, 128]. Thanks to seed growth synthesis method[30], the availability of Au/Ag alloy NPs having appropriate size and different compositions offer more choices of colors between LSPR peak position of Au NPs and Ag NPs. Our group has already demonstrated the possibility of multiplexed imaging by distinguishing individual 60nm Au, 50/50 Au/Ag alloy and Ag NPs under darkfield microscope[28]. At minimum, 4 different LSPR wavelengths with Au, 50/50 Au/Ag alloy, Ag and Au nanorod could be used to accomplish higher multiplexed imaging with scattering signal of limited spectral overlap.

Moreover, Au/Ag alloy NPs can be designed with arbitrary Au/Ag composition rations, varying their plasmonic resonance peak positions; nanorods can show tunable peaks by controlling various geometrical factors. Taking all these possibilities into account, the choices of plasmonic color can even increase. The key factor that influences the distinguishability of plamonic-based contrast agents is the plamsonic spectrum bandwidth, affected original sizes, size-distributions for NPs and Au nanorods and composition variation for one another in a batch of alloy NPs. With better control of mentioned factors, we can hope for more possible alloy between gold and silver, for instance, 25/75 Au/Ag, 75/25 Au/Ag. Besides, it is commercially available for 660nm, 800nm and 980nm plamson peak positions for Au nanorod, not to mention the capability of custom design of geometry factors of Au nanorod that shift the plasmon peak between three of them to

generate more possibilities. In summery, we may reasonably imagine 7 plamonic colors (4 from alloys and 3 from nanorods) used simultaneously for multiplexed imaging.

With the idea of the combination of plamonics and fluorescence with a core-shell structure and multichannel detection strategy, we can even extend the multiplexing capacity. Since the limit of fluorescence multiplexing is 7 colors[109], as the reasonable extension of existed reports[109, 128] [28], one can achieve 4×7=28 different markers to be used simultaneously for multiplexing task, as shown in Figure 5.1.

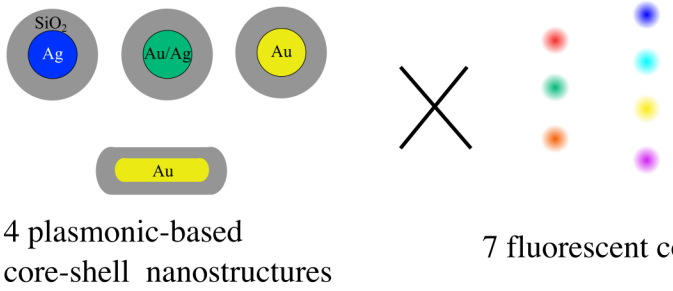

Figure 5.1 Schematics of 28 possible choices of core-shell structural contrast agent based on fluorescence and scattering dual-mode multiplexed imaging strategy.

Since the presence of metallic core largely enhances the fluorescence intensity, as shown in Figure 4.9, the photostability of fluorophore inside the silica shell could also be enhanced. However, for long observation dual-mode multiplexed imaging, it is important to take into account the photobleaching effect and make appropriate choices of fluorophores.

5.2 Choices of fluorescence

For better fluorescent photostability, the effect of MEF on photobleaching was checked with FITC and RBITC near a silver-rich core, the same one used for obtaining MEF factor (Figure 4.9).

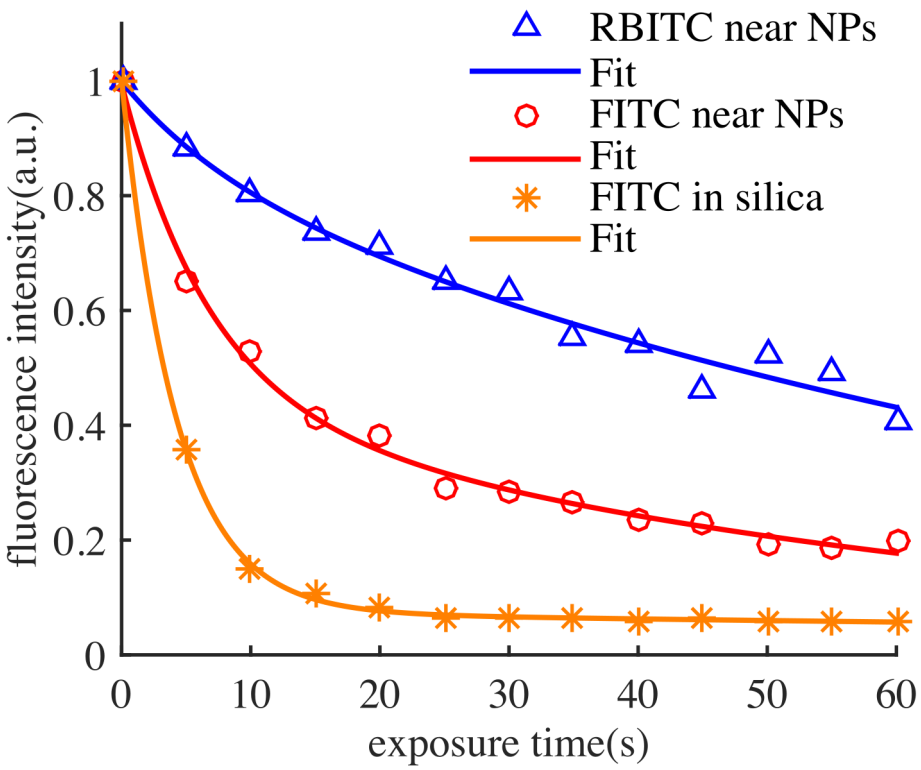

Figure 5.2 Fluorescence decay curves of RBITC and FITC in silica shell with a ~60nm 2/98 Au/Ag alloy and FITC in a hollow shell. Fluorescence intensity were acquired from fluorescent images taken with an Eclipse Ti microscope (Nikon) equipped with a 100x oil immersion objective (numerical aperture (NA) 1.3, Nikon) a QIclick CCD camera (Qimaging, 1392x1040 pixels) and with the same acquisition time (500ms) at 100% light intensity from the fluorescence light source Nikon intensilight Epi-fluorescence Illuminator.

Figure 5.2 demonstrates the photobleaching decay of the RBITC in and FITC in silica shell near metallic surface of core and FITC in hollow silica shell under the same wavelength window (filter excitation at 475 ± 35nm) and intense light exposure. For a single NP, the fluorescent molecules are embedded in the silica shell near a metallic core (~60nm 2/98 Au/Ag alloy NPs). The fluorescence intensities (RBITC and FITC) of from a NP was acquired with an average intensity from 9 pixels in fluorescent images taken every 5 seconds with continuous exposure and the results were shown as blue triangles and red circles for each 5 seconds. Similarly, the results of fluorescence intensity of FITC in hollow shell were also shown in the figure as red yellow stars for each 5 seconds. The experimental results of both conditions were fit to a double-exponential equation. In fact, according to some original work from Szaba Jr et al. the different

accessibility of quencher molecules to the fluorophore and the possible photochemical reaction that destroys the triplet of fluorophore could result in a double-exponential behavior. [170, 171]

From Figure 5.2 we can easily conclude that the FITC molecules near the metallic NP surface decay at a much slower rate than the ones without the presence of metallic core. The results are in agreement with the theory introduced in Chapter 2, that the photostability of fluorescent molecules are enhanced near the surface of NPs where there is an electromagnetic field enhancement. Indeed, since the radiative decay rate of a fluorophore near NPs is increased[27], the quantum yield is thus decreased and so is the lifetime, resulting in an improvement of photostability. This is because there are less time for alternative reactions to occur in the excited state resulting in more excitation-emission cycles prior to photobleaching. [172].

However, the photobleaching in one minute for metal enhanced RBITC is much less compared to the other two cases. These results show equal importance of the choice of more robust fluorophores that are less prone to photobleaching. Yet to fundamentally solve the problem of photobleaching, the combination of plasmonic NPs with QDs is also very interesting alternative. The gold core QDs doped silica shell NPs have been reported [173], and could be developed in some future works. Based on the same strategy, one can easily use 4 types of QDs[174] for multiplexing imaging, thus generating more than 16 possibilities with the combination of plasmonic cores.

5.3 Optimization and control of synthesis

5.3.1 Control of shell thickness

To further improve the fluorescence property near metallic NPs, it is important to be able to control the shell thickness. According to previous studies, fluorophore distance from metallic surface plays an important role to maximise MEF effect[78, 157]. Therefore, it should be important to fabricate alloy core silica shell with different shell thicknesses to better tailor the optical properties of both plasmonic peaks and fluorophores.

In the case of Au/Ag alloy core coating, silica shell thickness can be also controlled with different addition of silica precursor TEOS. The synthesis methods and characterization results of NPs with different compositions and different shell thicknesses are shown in Figure 5.3.

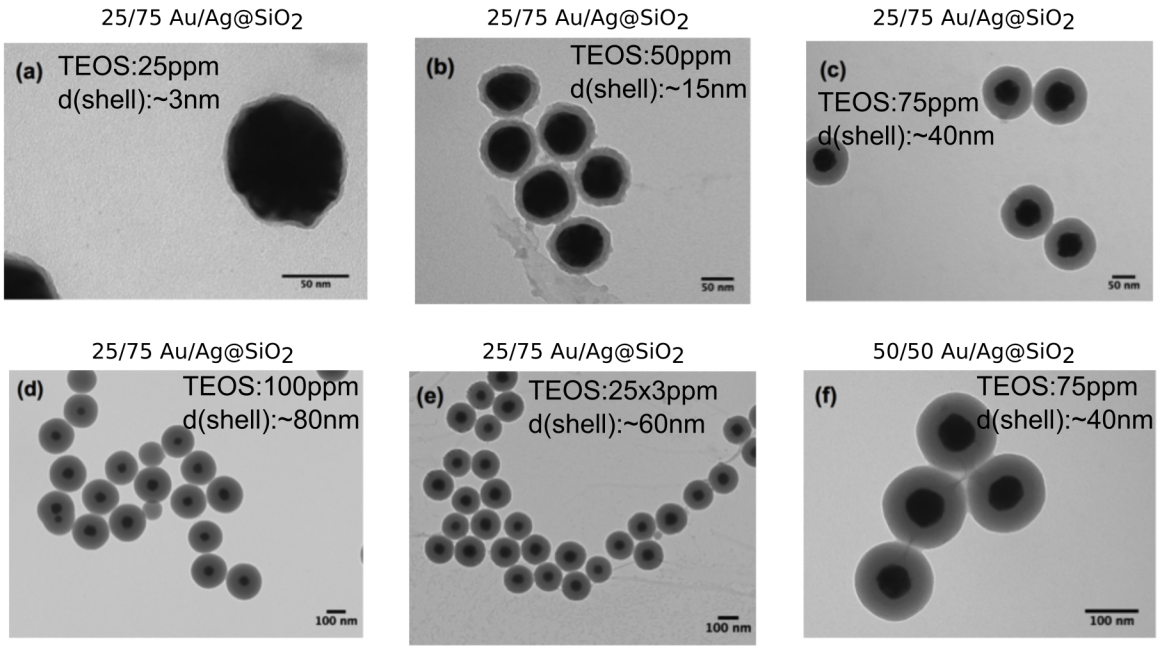

Figure 5.3 TEM images of AuAg@SiO_2 with different size of core and thicknesses of silica shell, where (a)25ppm, (b)ppm, (c,e,f)75ppm, (d)100ppm v/v TEOS were added in solution to coat SiO_2 shell.(a) 25:75 AuAg NPs ~80nm core ~3nm silica shell; (b) 25:75 AuAg NPs ~60nm core ~15nm silica shell; (c) 25:75 AuAg NPs ~60nm core ~40nm silica shell. (d) 25:75 AuAg NPs ~60nm core ~80nm silica shell. (e) 25:75 AuAg NPs ~60nm core ~60nm silica shell; (f) 50:50 AuAg NPs 60nm core 40nm silica shell. In the case of (e), 75ppm TEOS was added 25pm every two hours.

In general, with thicker shell and assuming that the density of fluorophores inside silica shell stays the same, we can load more fluorophores and resulting in a more intense fluorescence. On the other hand, the fluorophores that are too near or attached on the core surface may be quenched because the direct energy transfer to the plasmonic core NPs is favored rather than the radiate decay[94]. However, the large size of NP/SiO_2-shell can cause steric hindrance on cells and less mobility when targeting cells thus decreasing the labeling efficiency in multiplexed imaging.

Furthermore, coating very thick silica shell is hard to generate in a single step without generating core-free silica NPs, which can complicate multiplexed imaging. This problem and solution will be explained in next section in more detail.

5.3.2 Uniformity of core-shell NPs

Identification of NPs in Figure 5.4 was already presented in Chapter 3 (Figure 4.5) to show multiplexing strategy with dual-mode detection platform. Although we cannot exclude that the detection limit in darkfield channel did not allow the detection of some NPs, some core-free dye doped SiO_2 shell can possibly fluoresce without a scattering signal as indicate for examples with yellow triangles in Figure 5.4 b.. Therefore, it is important to improve the uniformity of synthesis product and eliminate core-free dye-doped silica NPs in order to improve the multiplexing efficiency.

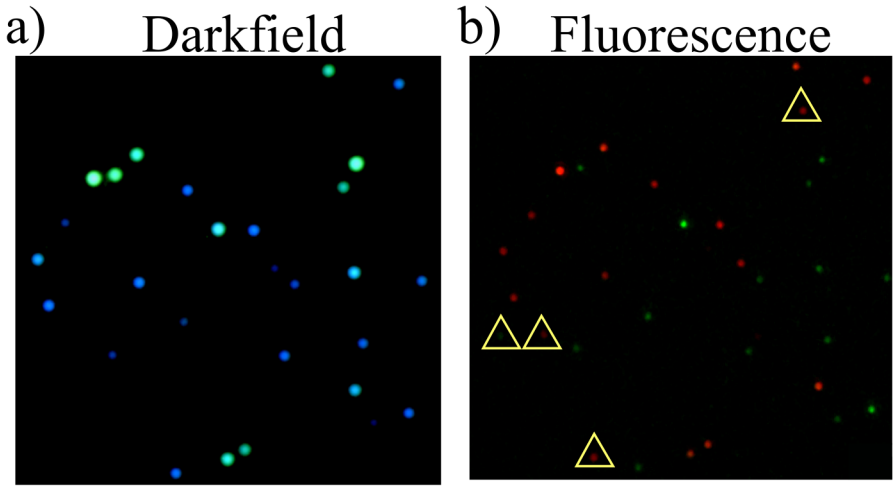

Figure 5.4 a)Darkfield and b)fluorescence imaging of plasmonic core silica shell NPs on same area of a glass slide. The colocalization is good in principle, while 4 fluorescent NPs appears only in the fluorescent channel.

Basically, there are two strategies to deal with the core-free SiO_2 NPs:

1. Physical filtering through centrifugation based on density difference of silica and metallic NPs.
2. Chemical suppression of undesirable nucleation of silica monomers in solution by controlling the amount of silica precursor as well as catalyst.

Both methods were tried and the chemical method gave better results as shown in Figure 5.5.

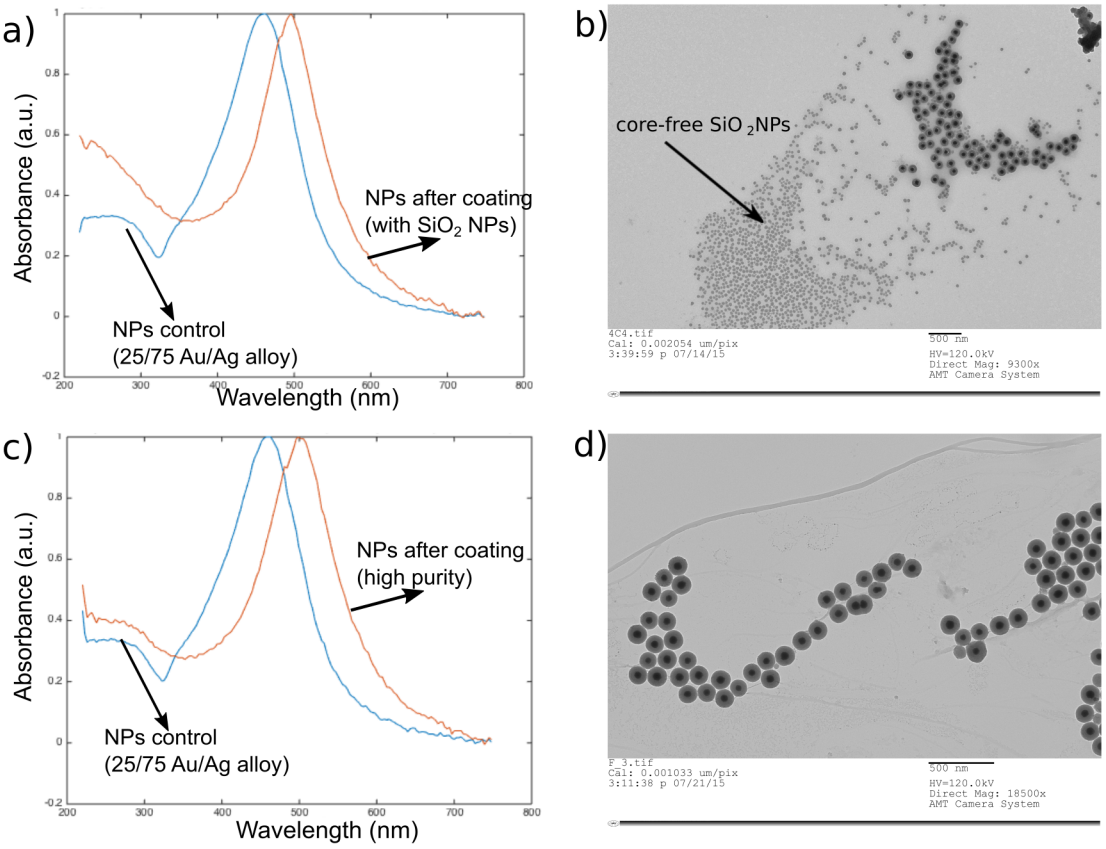

Figure 5.5 UV-visible spectra and TEM results showing the improvement of product uniformity. (a) UV-visible spectra of ~65nm diameter 25/75 Au/Ag NPs before (blue line) and after(red line) silica coating. The UV region indicates the existence of exceeded SiO_2 than silica shell on alloy NPs. (b) TEM image of coated NPs, confirming the existence of core-free SiO_2 NPs. (c) UV-visible spectra of ~65nm diameter 25/75 Au/Ag NPs before(blue line) and after(red line) silica coating under new condition of pre-purification of fluorescent precursor and appropriate chemical amount. (d) TEM image of coated NPs with high uniformity.

To monitor the presence of core free silica shell, on can use the fact that silica absorbs in the ultra-violet (UV) [175]. As shown in Figure 5.5(a), extinction spectrum of prepared Au/Ag@SiO_2 sample has been measured by UV-visible spectrometer. Note obviously that in the region (200nm-300nm), the absorbance of the Au/Ag@SiO_2 (blue line) is twice greater than bare nanoparticles (red line). This suggests that there are a significant amount of silica nanoparticles, confirmed by TEM images (Figure 5.5(b)). Besides, Figure 5.5 (b) shows at the upper right corner an aggregation of silica matrix. Here when we fixed the alloy NPs concentration (typically

~35 μM atomic concentration), an adjustment of the added amount of silica precursor TEOS and catalyst ammonia can considerably improve the purity of product for this synthesis process. The UV-visible spectra show the difference between the core-shell with many core-free silica NPs or silica clusters (Figure 5.5 a) and the highly uniform core-shell NPs (Figure 5.5 c). The key of synthesis depends on two approaches: (i) eliminate silica aggregations before coating by purifying fluorescent precursor and (ii) suppress core-free silica NPs formation during coating. In order to do so, we firstly centrifuged the fluorescent precursor, for example APTES-FITC and take the supernatant as new fluorescent precursor. Then, according to the determined silica thickness, the amount of TEOS, a silica precursor to condense on alloy NPs to form silica shell, needs to be controlled at about 100 ppm v/v during synthesis, which can decrease the undesirable free nucleation in the solution rather than on existing NP surfaces. The TEM image Figure 5.5 (d) confirms the improvement in size uniformity. Using these improved nanoparticles, multiplexed imaging with perfect colocalization in both channel can be obtained as shown in Figure 5.6.

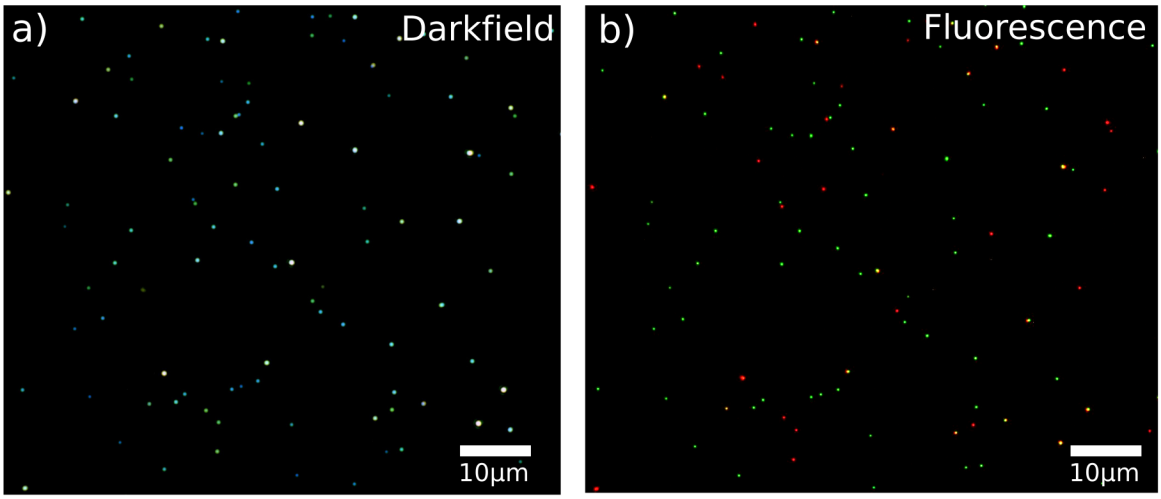

Figure 5.6 Highly uniform Ag@SiO_2 and 50/50 Au/Ag@SiO_2 NPs respectively incorporated with FITC and RBITC were mixed and a 2μL solution was dropped on the glass slide. (a) dark-field and (b) fluorescence image were take at the same area.

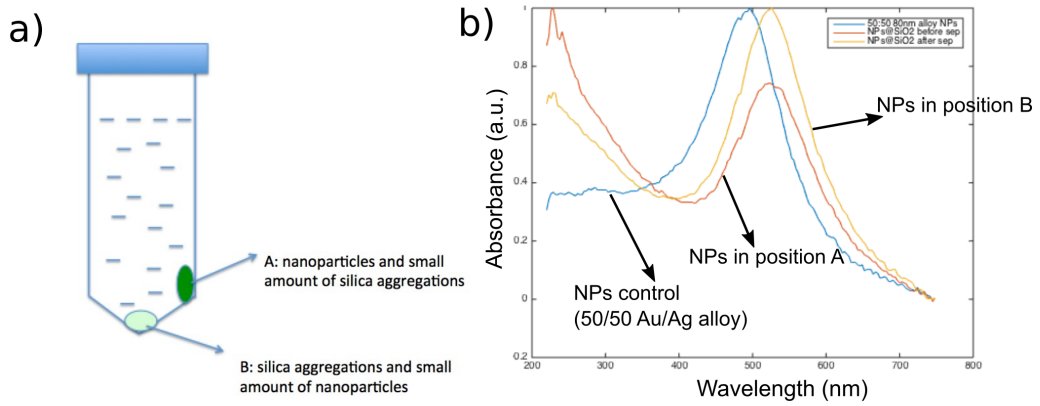

Figure 5.7 Mechanical separation of core-free silica NPs from core-shell NPs. (a) schematic showing two groups of residuals after centrifugation. (b) UV-visible spectra of these two groups and NPs control.

However, by just centrifuging, it is hard to separate most the core-free silica NPs from alloy core silica shell NPs. From Figure 5.7 (b) we can still see two different populations, namely, silica aggregations and NPs. The existing silica NPs cannot only cause problem of imaging as mention previously but also possibly compete with core-shell NPs in the antibody functionalization, resulting in a decrease of functionalization efficiency.

CHAPTER 6 CONCLUSION AND RECOMMENDATIONS

6.1 Main contributions of the thesis

In general, during this work, silica coating approach has been adapted to Au/Ag alloy NPs of 60~80nm diameter to fabricate alloy core silica shell NPs incorporated with fluorophores for multiplexed imaging applications.

The first contribution of this work is the demonstration of a reproducible chemical approach to obtain fluorescent Au/Ag alloy core silica shell NPs. In this work we succeeded in coating 10/90, 25/75 and 50/50 Au/Ag alloy NPs with silica shell with controlled process, to suppress the formation of core-free silica NPs and successfully incorporate different fluorophores in silica shell. During the synthesis, the core etching effect has been shown and discussed. Based on experimental and calculated results, we concluded that higher Au concentrations in the alloy core makes it less vulnerable to be etched by ammonia as the catalyst of silica coating process.

The second contribution of this work is that this new type of core-shell NPs can be designed as contrast agent for multiplexed cellular imaging. A dual-mode detection set-up was developed with the ability of individually distinguishing NPs with the combination of darkfield and fluorescence signals. The identifications of individual NPs on both glass slide and cell culture were demonstrated by determining both the composition with scattering spectrum of each NP and the fluorophore with its filtered fluorescence signal. It is possible to apply these different types of NPs to cell tagging applications as demonstrated by flow cytometry experiments. By using fluorescent alloy core silica shell NPs as contrast agent, this multidetection strategy increases the multiplexed imaging capacity, paving the way to multiplexing colors with all kinds of hybrid nanostructures as contrast agents.

6.2 Recommendations and future work

While we achieved the principal objective of synthesizing and characterising Au/Ag alloy core-shell markers for multiplex imaging, future developments are necessary to improve our technology.

Some of the actual limitations observed during this research include the low fluorescent intensity of prepared core-shell NPs and the limited antibody functionalization efficiency. First, the

fluorescent signal on cells is relatively weak and evanescent for the prepared core-shell NPs. One possible reason is that the incorporation efficiency of fluorescent molecules in the silica shell is too low. In principle, the fluorescence intensity depends on the loaded number of fluorophores inside the silica shell per NP and also the average emission rate for fluorophores. In such core-shell structure, silica shell should be thick enough to incorporate a lot of molecules, resulting in a much higher signal output per NP and MEF enhancement factors. Second, the cell targeting efficiency and the antibody functionalization procedure was not optimized, resulting in low luminescent cells marked with fluorescent NPs. Furthermore, the fluorescent signal from prepared core-shell NPs was already weak, which brought even more difficulty for good contrast in cell tagging applications.

It would be interesting to develop a reliable approach to obtain the MEF factor from Au-rich Au/Ag@SiO_2 NPs, for example 50/50 Au/Ag@SiO_2 NPs. The standard technique to calculate the MEF factor is to use an etching solution to eliminate the metallic core from the fluorescent core-shell NPs and measure the fluorescent intensities with and without the metallic core. For Au/Ag alloy core, however, it is very difficult to perform the etching process properly. In fact, Au/Ag alloy NPs can be etched effectively with only aqua regia but cannot be used in this case because it can destroy the fluorophore with extremely low pH. One possible way to calculate the factor not as precise as the standard approach is to fabricate similar core-free silica NPs structures with same size of etched Ag@SiO_2. The challenge would then be to keep the same fluorophore incorporation efficiency with Au/Ag@SiO_2. Another possible way is to chemically remove the silica shell in order to release fluorophores and measure the intensity after separating them with metallic core.

The fluorescent core silica shell NPs is not yet as strong as direct immunofluorescence with well expressed antibody targeting in terms of cell tagging applications. However, if certain types of receptors are limited, the limitations of immunofluorescence gives a much weaker signal due to the limited number of fluorophores per antibody. In such cases, it is possible to increase the incorporation efficiency of fluorescent core-shell NPs and surpass the fluorophore number limit per antibody, giving a better contrast for less specific receptors in fluorescent channel. In other words, we can exploit the advantage of these core-shell NPs on multiplexed imaging of cell with less specific antibody receptors.

An alternative to the use of fluorophores which might photobleache during long exposure is to incorporate quantum dots (QDs) inside the silica shell to similarly exploit the multiplexing ability of plasmonic core fluorescent shell NPs as more photostable contrast agent.

Improvement of the antibody functionalization of the silica surface of Au/Ag@SiO_2 is also necessary. The cross-linking reaction from linker sulfo-SMCC to antibody mentioned in chapter 3 can be done prior to linking with NPs to better avoid degradation of –NHS ester from sulfo-SMCC and thus improving the antibody binding efficiency. All the other factors, such as temperature, reaction time, incubation time, and antibody type should be tuned to find better conditions to obtain optimised results.

Finally, this hybrid structure combining tunable plasmonics and fluorescence can be extended to include other functional nanomaterials, opening up the possibility of new multifunctional nanodevices. For example, we could even combine a magnetic core and a plasmonic shell with an oxide layer in between, with fluorescent emitters inside the layer to generate signal of 3 modes. We can also load drugs within the porous silica shell or coat alloy core with other types of oxide, for instance TiO_2 to further change the optical properties of the alloy core. New possibilities often lie in the hybrid of different existing techniques. With the recent development of large size Au/Ag alloy NPs, it is anticipated that complex nanostructure containing such nanomaterials will have a bright future.

BIBLIOGRAPHY

1. Roco, M.C., C.A. Mirkin, and M.C. Hersam, *Nanotechnology research directions for societal needs in 2020.* Retrospective and Outlook: Springer, 2010.
2. Baucher, M.-A., et al., *Symposium on Assessing the Economic Impact of Nanotechnology: Synthesis Report.* 2013.
3. Tada, H., T. Kiyonaga, and S.-i. Naya, *Rational design and applications of highly efficient reaction systems photocatalyzed by noble metal nanoparticle-loaded titanium (IV) dioxide.* Chemical Society Reviews, 2009. **38**(7): p. 1849-1858.
4. Maeda, K., et al., *Noble‐Metal/Cr2O3 Core/Shell Nanoparticles as a Cocatalyst for Photocatalytic Overall Water Splitting.* Angewandte Chemie, 2006. **118**(46): p. 7970-7973.
5. Zhou, X., et al., *Surface plasmon resonance-mediated photocatalysis by noble metal-based composites under visible light.* Journal of Materials Chemistry, 2012. **22**(40): p. 21337-21354.
6. Chen, Y., et al., *Core/shell structured hollow mesoporous nanocapsules: a potential platform for simultaneous cell imaging and anticancer drug delivery.* ACS nano, 2010. **4**(10): p. 6001-6013.
7. Kim, J., et al., *Multifunctional uniform nanoparticles composed of a magnetite nanocrystal core and a mesoporous silica shell for magnetic resonance and fluorescence imaging and for drug delivery.* Angewandte Chemie International Edition, 2008. **47**(44): p. 8438-8441.
8. Slowing, I.I., et al., *Mesoporous silica nanoparticles as controlled release drug delivery and gene transfection carriers.* Advanced drug delivery reviews, 2008. **60**(11): p. 1278-1288.
9. Vallet‐Regí, M., F. Balas, and D. Arcos, *Mesoporous materials for drug delivery.* Angewandte Chemie International Edition, 2007. **46**(40): p. 7548-7558.
10. Ibhadon, A.O. and P. Fitzpatrick, *Heterogeneous photocatalysis: recent advances and applications.* Catalysts, 2013. **3**(1): p. 189-218.
11. Sugunan, A. and J. Dutta, *Pollution treatment, remediation and sensing.* Nanotechnology, 2008.
12. Karlsson, H.L., et al., *Copper oxide nanoparticles are highly toxic: a comparison between metal oxide nanoparticles and carbon nanotubes.* Chemical research in toxicology, 2008. **21**(9): p. 1726-1732.
13. Jain, P.K., I.H. El-Sayed, and M.A. El-Sayed, *Au nanoparticles target cancer.* nano today, 2007. **2**(1): p. 18-29.
14. Zhang, J., et al., *Creating new fluorescent probes for cell biology.* Nature reviews Molecular cell biology, 2002. **3**(12): p. 906-918.

15. Luchowski, R., et al., *Single molecule studies of multiple-fluorophore labeled antibodies. Effect of homo-FRET on the number of photons available before photobleaching.* Current pharmaceutical biotechnology, 2008. **9**(5): p. 411-420.

16. Yu, C., H. Nakshatri, and J. Irudayaraj, *Identity profiling of cell surface markers by multiplex gold nanorod probes.* Nano letters, 2007. **7**(8): p. 2300-2306.

17. Chan, W.C. and S. Nie, *Quantum dot bioconjugates for ultrasensitive nonisotopic detection.* Science, 1998. **281**(5385): p. 2016-2018.

18. Chan, W.C., et al., *Luminescent quantum dots for multiplexed biological detection and imaging.* Current opinion in biotechnology, 2002. **13**(1): p. 40-46.

19. Han, M., et al., *Quantum-dot-tagged microbeads for multiplexed optical coding of biomolecules.* Nature biotechnology, 2001. **19**(7): p. 631-635.

20. Gao, X., et al., *In vivo cancer targeting and imaging with semiconductor quantum dots.* Nature biotechnology, 2004. **22**(8): p. 969-976.

21. Tsoi, K.M., et al., *Are quantum dots toxic? Exploring the discrepancy between cell culture and animal studies.* Accounts of chemical research, 2012. **46**(3): p. 662-671.

22. von Maltzahn, G., et al., *SERS‐coded gold nanorods as a multifunctional platform for densely multiplexed near‐infrared imaging and photothermal heating.* Advanced Materials, 2009. **21**(31): p. 3175-3180.

23. Jang, B., et al., *Gold nanorod− photosensitizer complex for near-infrared fluorescence imaging and photodynamic/photothermal therapy in vivo.* ACS nano, 2011. **5**(2): p. 1086-1094.

24. Huang, X., et al., *Cancer cell imaging and photothermal therapy in the near-infrared region by using gold nanorods.* Journal of the American Chemical Society, 2006. **128**(6): p. 2115-2120.

25. Brouard, D., et al., *Label-free biosensing based on multilayer fluorescent nanocomposites and a cationic polymeric transducer.* Acs Nano, 2011. **5**(3): p. 1888-1896.

26. Frigault, M.M., et al., *Live-cell microscopy–tips and tools.* J Cell Sci, 2009. **122**(6): p. 753-767.

27. Lakowicz, J.R., et al., *Radiative decay engineering: 2. Effects of silver island films on fluorescence intensity, lifetimes, and resonance energy transfer.* Analytical biochemistry, 2002. **301**(2): p. 261-277.

28. Patskovsky, S., et al., *Hyperspectral reflected light microscopy of plasmonic Au/Ag alloy nanoparticles incubated as multiplex chromatic biomarkers with cancer cells.* Analyst, 2014. **139**(20): p. 5247-5253.

29. Wustholz, K.L., et al., *Surface-enhanced Raman spectroscopy of dyes: from single molecules to the artists' canvas.* Physical Chemistry Chemical Physics, 2009. **11**(34): p. 7350-7359.

30. Rioux, D. and M. Meunier, *Seeded growth synthesis of composition and size-controlled gold–silver alloy nanoparticles.* The Journal of Physical Chemistry C, 2015. **119**(23): p. 13160-13168.

31. Rioux, D. and M. Meunier, *Preparation process of alloy nanoparticles, involves repeating addition of salts of metals and reducing agent to alloy seed, number of time until desired size of alloy nanoparticle is reached*. POLYVALOR SC (POLY-Non-standard).

32. Graf, C. and A. van Blaaderen, *Metallodielectric colloidal core-shell particles for photonic applications.* Langmuir, 2002. **18**(2): p. 524-534.

33. Graf, C., et al., *A general method to coat colloidal particles with silica.* Langmuir, 2003. **19**(17): p. 6693-6700.

34. Zhang, J., et al., *Plasmon-coupled fluorescence probes: effect of emission wavelength on fluorophore-labeled silver particles.* The Journal of Physical Chemistry C, 2008. **112**(25): p. 9172-9180.

35. Papavassiliou, G.C., *Surface plasmons in small Au-Ag alloy particles.* Journal of Physics F: Metal Physics, 1976. **6**(4): p. L103.

36. Sanchez-Ramirez, J.F., et al., *Synthesis and optical properties of Au-Ag alloy nanoclusters with controlled composition.* Journal of Nanomaterials, 2008. **2008**.

37. Lee, I., S.W. Han, and K. Kim, *Production of Au–Ag alloy nanoparticles by laser ablation of bulk alloys.* Chemical Communications, 2001(18): p. 1782-1783.

38. Besner, S. and M. Meunier, *Laser synthesis of nanomaterials*, in *Laser Precision Microfabrication*. 2010, Springer. p. 163-187.

39. Peng, Z., et al., *Laser-assisted synthesis of Au-Ag alloy nanoparticles in solution.* The Journal of Physical Chemistry B, 2006. **110**(6): p. 2549-2554.

40. Takatani, H., et al., *Characterization of noble metal alloy nanoparticles prepared by ultrasound irradiation.* Reviews on Advanced Materials Science, 2003. **5**(3): p. 232-238.

41. Gonzalez, C.M., Y. Liu, and J.C. Scaiano, *Photochemical Strategies for the Facile Synthesis of Gold− Silver Alloy and Core− Shell Bimetallic Nanoparticles†.* The Journal of Physical Chemistry C, 2009. **113**(27): p. 11861-11867.

42. Link, S., Z.L. Wang, and M.A. El-Sayed, *Alloy formation of gold-silver nanoparticles and the dependence of the plasmon absorption on their composition.* The Journal of Physical Chemistry B, 1999. **103**(18): p. 3529-3533.

43. Mallin, M.P. and C.J. Murphy, *Solution-phase synthesis of sub-10 nm Au-Ag alloy nanoparticles.* Nano Letters, 2002. **2**(11): p. 1235-1237.

44. Turkevich, J., *Colloidal gold. Part II.* Gold bulletin, 1985. **18**(4): p. 125-131.

45. Turkevich, J., P.C. Stevenson, and J. Hillier, *A study of the nucleation and growth processes in the synthesis of colloidal gold.* Discussions of the Faraday Society, 1951. **11**: p. 55-75.

46. Frens, G., *Controlled nucleation for the regulation of the particle size in monodisperse gold suspensions.* Nature, 1973. **241**(105): p. 20-22.

47. Wen, T., L.N. Brush, and K.M. Krishnan, *A generalized diffusion model for growth of nanoparticles synthesized by colloidal methods.* Journal of colloid and interface science, 2014. **419**: p. 79-85.

48. LaMer, V.K. and R.H. Dinegar, *Theory, production and mechanism of formation of monodispersed hydrosols.* Journal of the American Chemical Society, 1950. **72**(11): p. 4847-4854.

49. Perrault, S.D. and W.C.W. Chan, *Synthesis and surface modification of highly monodispersed, spherical gold nanoparticles of 50− 200 nm.* Journal of the American Chemical Society, 2009. **131**(47): p. 17042-17043.

50. Steinigeweg, D. and S. Schlücker, *Monodispersity and size control in the synthesis of 20–100 nm quasi-spherical silver nanoparticles by citrate and ascorbic acid reduction in glycerol–water mixtures.* Chemical Communications, 2012. **48**(69): p. 8682-8684.

51. Schneider, S., et al., *Reproducible preparation of silver sols with uniform particle size for application in surface‐enhanced Raman spectroscopy.* Photochemistry and photobiology, 1994. **60**(6): p. 605-610.

52. Brown, K.R. and M.J. Natan, *Hydroxylamine seeding of colloidal Au nanoparticles in solution and on surfaces.* Langmuir, 1998. **14**(4): p. 726-728.

53. Chan, J.M., et al., *PLGA–lecithin–PEG core–shell nanoparticles for controlled drug delivery.* Biomaterials, 2009. **30**(8): p. 1627-1634.

54. Pan, J., D. Wan, and J. Gong, *PEGylated liposome coated QDs/mesoporous silica core-shell nanoparticles for molecular imaging.* Chemical Communications, 2011. **47**(12): p. 3442-3444.

55. Sasaki, K., et al., *Core‐Protected Platinum Monolayer Shell High‐Stability Electrocatalysts for Fuel‐Cell Cathodes.* Angewandte Chemie International Edition, 2010. **49**(46): p. 8602-8607.

56. Chen, X., et al., *Coherency strain effects on the optical response of core/shell heteronanostructures.* Nano Letters, 2003. **3**(6): p. 799-803.

57. Liu, W., et al., *Gold nanorod@ chiral mesoporous silica core–shell nanoparticles with unique optical properties.* Journal of the American Chemical Society, 2013. **135**(26): p. 9659-9664.

58. Ma, Y., et al., *Au@ Ag core− shell nanocubes with finely tuned and well-controlled sizes, shell thicknesses, and optical properties.* ACS nano, 2010. **4**(11): p. 6725-6734.

59. Chen, G., et al., *Bifunctional catalytic/magnetic Ni@ Ru core–shell nanoparticles.* Chemical Communications, 2011. **47**(22): p. 6308-6310.

60. Jiang, H.-L., et al., *Synergistic catalysis of Au@ Ag core− shell nanoparticles stabilized on metal− organic framework.* Journal of the American Chemical Society, 2011. **133**(5): p. 1304-1306.

61. Mazumder, V., et al., *Core/shell Pd/FePt nanoparticles as an active and durable catalyst for the oxygen reduction reaction.* Journal of the American Chemical Society, 2010. **132**(23): p. 7848-7849.

62. Jiang, H.-L., T. Akita, and Q. Xu, *A one-pot protocol for synthesis of non-noble metal-based core–shell nanoparticles under ambient conditions: toward highly active and cost-*

effective catalysts for hydrolytic dehydrogenation of NH 3 BH 3. Chemical Communications, 2011. **47**(39): p. 10999-11001.

63. Zhang, X. and Z. Su, *Polyelectrolyte‐Multilayer‐Supported Au@ Ag Core‐Shell Nanoparticles with High Catalytic Activity.* Advanced Materials, 2012. **24**(33): p. 4574-4577.

64. Wang, L., et al., *Plasmonics and Enhanced Magneto-Optics in Core− Shell Co− Ag Nanoparticles.* Nano letters, 2011. **11**(3): p. 1237-1240.

65. Ghosh Chaudhuri, R. and S. Paria, *Core/shell nanoparticles: classes, properties, synthesis mechanisms, characterization, and applications.* Chemical reviews, 2011. **112**(4): p. 2373-2433.

66. Aslan, K., et al., *Fluorescent core-shell Ag@ SiO2 nanocomposites for metal-enhanced fluorescence and single nanoparticle sensing platforms.* Journal of the American Chemical Society, 2007. **129**(6): p. 1524-1525.

67. Jankovic, V., et al., *Active layer-incorporated, spectrally tuned Au/SiO2 core/shell nanorod-based light trapping for organic photovoltaics.* ACS nano, 2013. **7**(5): p. 3815-3822.

68. Zhang, F., et al., *Fabrication of Ag@ SiO2@ Y2O3: Er nanostructures for bioimaging: tuning of the upconversion fluorescence with silver nanoparticles.* Journal of the American Chemical Society, 2010. **132**(9): p. 2850-2851.

69. Liz-Marzán, L.M., M. Giersig, and P. Mulvaney, *Synthesis of nanosized gold-silica core-shell particles.* Langmuir, 1996. **12**(18): p. 4329-4335.

70. Rahman, I.A. and V. Padavettan, *Synthesis of silica nanoparticles by sol-gel: size-dependent properties, surface modification, and applications in silica-polymer nanocomposites—a review.* Journal of Nanomaterials, 2012. **2012**: p. 8.

71. Brinker, C.J. and G.W. Scherer, *Sol-gel science: the physics and chemistry of sol-gel processing*. 2013: Academic press.

72. Ahsani, M. and R. Yegani, *Study on the fouling behavior of silica nanocomposite modified polypropylene membrane in purification of collagen protein.* Chemical Engineering Research and Design, 2015. **102**: p. 261-273.

73. Lismont, M., C.A. Páez, and L. Dreesen, *A one-step short-time synthesis of Ag@ SiO 2 core–shell nanoparticles.* Journal of colloid and interface science, 2015. **447**: p. 40-49.

74. Branda, F., *The Sol-Gel Route to Nanocomposites*. 2011: INTECH Open Access Publisher.

75. Niitsoo, O. and A. Couzis, *Facile synthesis of silver core–silica shell composite nanoparticles.* Journal of colloid and interface science, 2011. **354**(2): p. 887-890.

76. Buckley, A. and M. Greenblatt, *The sol-gel preparation of silica gels.* J. Chem. Educ, 1994. **71**(7): p. 599.

77. Lin, J., *The effect of catalysts on TEOS hydrolysis-condensation mechanism.* Journal of Inorganic Materials, 1997. **12**: p. 363-369.

78. Lessard-Viger, M., et al., *FRET enhancement in multilayer core− shell nanoparticles.* Nano letters, 2009. **9**(8): p. 3066-3071.

79. Liu, S. and M. Han, *Synthesis, functionalization, and bioconjugation of monodisperse, Silica‐Coated gold nanoparticles: Robust bioprobes.* Advanced Functional Materials, 2005. **15**(6): p. 961-967.

80. Plueddemann, E.P., *Chemistry of silane coupling agents*, in *Silane coupling agents*. 1991, Springer. p. 31-54.

81. Melo, E., M. Aires-Barros, and J. Cabral, *Reverse micelles and protein biotechnology.* Biotechnology annual review, 2001. **7**: p. 87-129.

82. Fan, H., et al., *Self-assembly of ordered, robust, three-dimensional gold nanocrystal/silica arrays.* Science, 2004. **304**(5670): p. 567-571.

83. Bae, D.-S., et al., *Synthesis of Ag/SiO2 nanosize particles by reverse micelle and sol-gel processing.* Metals and Materials International, 2001. **7**(4): p. 399-402.

84. Guerrero‐Martínez, A., J. Pérez‐Juste, and L.M. Liz‐Marzán, *Recent progress on silica coating of nanoparticles and related nanomaterials.* Advanced materials, 2010. **22**(11): p. 1182-1195.

85. Yang, H., P.H. Holloway, and S. Santra, *Water-soluble silica-overcoated CdS: Mn/ZnS semiconductor quantum dots.* The Journal of chemical physics, 2004. **121**(15): p. 7421-7426.

86. Lu, H., et al., *Synthesis of Ag@ SiO 2 hybrid nanoparticles templated by a Triton X-100)/1-hexanol/cyclohexane/H 2 O water-in-oil microemulsion.* CrystEngComm, 2013. **15**(33): p. 6511-6517.

87. Mie, G., *Beiträge zur Optik trüber Medien, speziell kolloidaler Metallösungen.* Annalen der physik, 1908. **330**(3): p. 377-445.

88. Schwarz, J.A., C.I. Contescu, and K. Putyera, *Dekker encyclopedia of nanoscience and nanotechnology*. Vol. 3. 2004: CRC press.

89. Eustis, S. and M.A. El-Sayed, *Why gold nanoparticles are more precious than pretty gold: noble metal surface plasmon resonance and its enhancement of the radiative and nonradiative properties of nanocrystals of different shapes.* Chemical society reviews, 2006. **35**(3): p. 209-217.

90. Rioux, D., et al., *An analytic model for the dielectric function of Au, Ag, and their alloys.* Advanced Optical Materials, 2014. **2**(2): p. 176-182.

91. Bohren, C.F. and D.R. Huffman, *Absorption and scattering of light by small particles*. 2008: John Wiley & Sons.

92. Halas, N.J., *Plasmonics: an emerging field fostered by Nano Letters.* Nano letters, 2010. **10**(10): p. 3816-3822.

93. Geddes, C.D. and J.R. Lakowicz, *Editorial: metal-enhanced fluorescence.* Journal of Fluorescence, 2002. **12**(2): p. 121-129.

94. Fort, E. and S. Grésillon, *Surface enhanced fluorescence.* Journal of Physics D: Applied Physics, 2007. **41**(1): p. 013001.

95. Anger, P., P. Bharadwaj, and L. Novotny, *Enhancement and quenching of single-molecule fluorescence.* Physical review letters, 2006. **96**(11): p. 113002.

96. Geddes, C.D., et al., *Fluorescence spectral properties of indocyanine green on a roughened platinum electrode: Metal-enhanced fluorescence.* Journal of fluorescence, 2003. **13**(6): p. 453-457.

97. Aslan, K., S.N. Malyn, and C.D. Geddes, *Metal-enhanced fluorescence from gold surfaces: angular dependent emission.* Journal of fluorescence, 2007. **17**(1): p. 7-13.

98. Chen, J., et al., *Development of gold nanoparticle-enhanced fluorescent nanocomposites.* Langmuir, 2013. **29**(5): p. 1584-1591.

99. Bardhan, R., et al., *Fluorescence enhancement by Au nanostructures: nanoshells and nanorods.* ACS nano, 2009. **3**(3): p. 744-752.

100. Fu, Y., J. Zhang, and J.R. Lakowicz, *Plasmon-enhanced fluorescence from single fluorophores end-linked to gold nanorods.* Journal of the American Chemical Society, 2010. **132**(16): p. 5540-5541.

101. Chen, Y., K. Munechika, and D.S. Ginger, *Dependence of fluorescence intensity on the spectral overlap between fluorophores and plasmon resonant single silver nanoparticles.* Nano letters, 2007. **7**(3): p. 690-696.

102. Cheng, D. and Q.-H. Xu, *Separation distance dependent fluorescence enhancement of fluorescein isothiocyanate by silver nanoparticles.* Chemical communications, 2007(3): p. 248-250.

103. Aslan, K., et al., *Fast and slow deposition of silver nanorods on planar surfaces: application to metal-enhanced fluorescence.* The Journal of Physical Chemistry B, 2005. **109**(8): p. 3157-3162.

104. Le Ru, E. and P. Etchegoin, *Principles of Surface-Enhanced Raman Spectroscopy: and related plasmonic effects*. 2008: Elsevier.

105. Xu, D., et al., *Development of chitosan-coated gold nanoflowers as SERS-active probes.* Nanotechnology, 2010. **21**(37): p. 375101.

106. Le Ru, E., et al., *Surface enhanced Raman scattering enhancement factors: a comprehensive study.* The Journal of Physical Chemistry C, 2007. **111**(37): p. 13794-13803.

107. Whitmore, D.D., et al., *High sensitivity surface-enhanced Raman scattering in solution using engineered silver nanosphere dimers.* The Journal of Physical Chemistry C, 2011. **115**(32): p. 15900-15907.

108. Tsien, R.Y., *The green fluorescent protein.* Annual review of biochemistry, 1998. **67**(1): p. 509-544.

109. Bergeron, E., et al., *3D multiplexed immunoplasmonics microscopy.* Nanoscale, 2016.

110. Wang, H.-H., et al., *Fluorescent gold nanoclusters as a biocompatible marker for in vitro and in vivo tracking of endothelial cells.* ACS nano, 2011. **5**(6): p. 4337-4344.

111. Jiang, J., G. Oberdörster, and P. Biswas, *Characterization of size, surface charge, and agglomeration state of nanoparticle dispersions for toxicological studies.* Journal of Nanoparticle Research, 2009. **11**(1): p. 77-89.

112. Swanson, L. and B. Hartman, *The central adrenergic system. An immunofluorescence study of the location of cell bodies and their efferent connections in the rat utilizing dopamine‐B‐hydroxylase as a marker.* Journal of Comparative Neurology, 1975. **163**(4): p. 467-505.

113. Swanson, L., *The projections of the ventral tegmental area and adjacent regions: a combined fluorescent retrograde tracer and immunofluorescence study in the rat.* Brain research bulletin, 1982. **9**(1): p. 321-353.

114. Henle, G. and W. Henle, *Immunofluorescence in cells derived from Burkitt's lymphoma.* Journal of bacteriology, 1966. **91**(3): p. 1248-1256.

115. Ahamed, M., M.S. Alsalhi, and M. Siddiqui, *Silver nanoparticle applications and human health.* Clinica chimica acta, 2010. **411**(23): p. 1841-1848.

116. Lee, K.J., et al., *In vivo imaging of transport and biocompatibility of single silver nanoparticles in early development of zebrafish embryos.* ACS nano, 2007. **1**(2): p. 133-143.

117. Lee, K.-S. and M.A. El-Sayed, *Gold and silver nanoparticles in sensing and imaging: sensitivity of plasmon response to size, shape, and metal composition.* The Journal of Physical Chemistry B, 2006. **110**(39): p. 19220-19225.

118. Sokolov, K., et al., *Real-time vital optical imaging of precancer using anti-epidermal growth factor receptor antibodies conjugated to gold nanoparticles.* Cancer research, 2003. **63**(9): p. 1999-2004.

119. Murphy, C.J., et al., *Gold nanoparticles in biology: beyond toxicity to cellular imaging.* Accounts of chemical research, 2008. **41**(12): p. 1721-1730.

120. Durr, N.J., et al., *Two-photon luminescence imaging of cancer cells using molecularly targeted gold nanorods.* Nano letters, 2007. **7**(4): p. 941-945.

121. Agarwal, A., et al., *Targeted gold nanorod contrast agent for prostate cancer detection by photoacoustic imaging.* Journal of applied physics, 2007. **102**(6): p. 064701.

122. Hu, H., et al., *Multimodal‐Luminescence Core‐Shell Nanocomposites for Targeted Imaging of Tumor Cells.* Chemistry‐A European Journal, 2009. **15**(14): p. 3577-3584.

123. Li, L., et al., *Highly luminescent CuInS2/ZnS core/shell nanocrystals: cadmium-free quantum dots for in vivo imaging.* Chemistry of Materials, 2009. **21**(12): p. 2422-2429.

124. Zimmer, J.P., et al., *Size series of small indium arsenide-zinc selenide core-shell nanocrystals and their application to in vivo imaging.* Journal of the American Chemical Society, 2006. **128**(8): p. 2526-2527.

125. Strack, R., *Highly multiplexed imaging.* Nature Methods, 2016. **13**(1): p. 35-35.

126. Gerdes, M.J., et al., *Emerging understanding of multiscale tumor heterogeneity.* Frontiers in oncology, 2014. **4**: p. 366.

127. Zeng, W.-J., et al., *Quantum dot-based multiplexed imaging in malignant ascites: a new model for malignant ascites classification.* International journal of nanomedicine, 2015. **10**: p. 1759.

128. Hu, R., et al., *Metallic nanostructures as localized plasmon resonance enhanced scattering probes for multiplex dark-field targeted imaging of cancer cells.* The Journal of Physical Chemistry C, 2009. **113**(7): p. 2676-2684.

129. Bannon, D., *Hyperspectral imaging: Cubes and slices.* Nature photonics, 2009. **3**(11): p. 627.

130. Chen, J., et al., *Gold nanocages: engineering their structure for biomedical applications.* Advanced Materials, 2005. **17**(18): p. 2255-2261.

131. Zhu, Y., et al., *Gold nanorod assembly based approach to toxin detection by SERS.* Journal of Materials Chemistry, 2012. **22**(6): p. 2387-2391.

132. Tokonami, S., et al., *Synthesis and bioanalytical applications of specific-shaped metallic nanostructures: A review.* Analytica chimica acta, 2012. **716**: p. 76-91.

133. Larson, D.R., et al., *Silica nanoparticle architecture determines radiative properties of encapsulated fluorophores.* Chemistry of materials, 2008. **20**(8): p. 2677-2684.

134. Kulkarni, A.P., et al., *Plasmon-enhanced charge carrier generation in organic photovoltaic films using silver nanoprisms.* Nano letters, 2010. **10**(4): p. 1501-1505.

135. Lee, S., et al., *Surface-enhanced Raman scattering imaging of HER2 cancer markers overexpressed in single MCF7 cells using antibody conjugated hollow gold nanospheres.* Biosensors and Bioelectronics, 2009. **24**(7): p. 2260-2263.

136. Willner, I. and E. Katz, *Magnetic control of electrocatalytic and bioelectrocatalytic processes.* Angewandte Chemie International Edition, 2003. **42**(38): p. 4576-4588.

137. Lachaine, R., et al., *Rational design of plasmonic nanoparticles for enhanced cavitation and cell perforation.* Nano letters, 2016. **16**(5): p. 3187-3194.

138. Saha, A., et al., *Functionalized plasmonic− fluorescent nanoparticles for imaging and detection.* The Journal of Physical Chemistry C, 2009. **113**(43): p. 18492-18498.

139. MacLaughlin, C.M., et al., *Surface-enhanced Raman scattering dye-labeled Au nanoparticles for triplexed detection of leukemia and lymphoma cells and SERS flow cytometry.* Langmuir, 2013. **29**(6): p. 1908-1919.

140. Seekell, K., et al., *Hyperspectral molecular imaging of multiple receptors using immunolabeled plasmonic nanoparticles.* Journal of biomedical optics, 2011. **16**(11): p. 116003-11600312.

141. Singh, N.P., et al., *A simple technique for quantitation of low levels of DNA damage in individual cells.* Experimental cell research, 1988. **175**(1): p. 184-191.

142. Nicoletti, I., et al., *A rapid and simple method for measuring thymocyte apoptosis by propidium iodide staining and flow cytometry.* Journal of immunological methods, 1991. **139**(2): p. 271-279.

143. Krichevsky, O. and G. Bonnet, *Fluorescence correlation spectroscopy: the technique and its applications.* Reports on Progress in Physics, 2002. **65**(2): p. 251.

144. Cunningham, A.t. and A. Szenberg, *Further improvements in the plaque technique for detecting single antibody-forming cells.* Immunology, 1968. **14**(4): p. 599.

145. Tennant, J.R., *Evaluation of the trypan blue technique for determination of cell viability.* Transplantation, 1964. **2**(6): p. 685-694.

146. Steward Jr, R.L., et al., *Probing cell structure responses through a shear and stretching mechanical stimulation technique.* Cell biochemistry and biophysics, 2010. **56**(2-3): p. 115-124.

147. Spivakov, M. and A.G. Fisher, *Epigenetic signatures of stem-cell identity.* Nature Reviews Genetics, 2007. **8**(4): p. 263-271.

148. Te Velde, E., et al., *The use of fluorescent dyes and probes in surgical oncology.* European Journal of Surgical Oncology (EJSO), 2010. **36**(1): p. 6-15.

149. Bruchez, M., et al., *Semiconductor nanocrystals as fluorescent biological labels.* science, 1998. **281**(5385): p. 2013-2016.

150. Lee-Montiel, F.T., P. Li, and P. Imoukhuede, *Quantum dot multiplexing for the profiling of cellular receptors.* Nanoscale, 2015. **7**(44): p. 18504-18514.

151. El-Sayed, I.H., X. Huang, and M.A. El-Sayed, *Surface plasmon resonance scattering and absorption of anti-EGFR antibody conjugated gold nanoparticles in cancer diagnostics: applications in oral cancer.* Nano letters, 2005. **5**(5): p. 829-834.

152. Wegner, K.D. and N. Hildebrandt, *Quantum dots: bright and versatile in vitro and in vivo fluorescence imaging biosensors.* Chemical Society Reviews, 2015. **44**(14): p. 4792-4834.

153. Ghosh, P., et al., *Gold nanoparticles in delivery applications.* Advanced drug delivery reviews, 2008. **60**(11): p. 1307-1315.

154. Na, H.B., et al., *Development of a T1 contrast agent for magnetic resonance imaging using MnO nanoparticles.* Angewandte Chemie, 2007. **119**(28): p. 5493-5497.

155. Wang, Y., et al., *Photoacoustic tomography of a nanoshell contrast agent in the in vivo rat brain.* Nano Letters, 2004. **4**(9): p. 1689-1692.

156. Kim, D., et al., *Antibiofouling polymer-coated gold nanoparticles as a contrast agent for in vivo X-ray computed tomography imaging.* Journal of the American Chemical Society, 2007. **129**(24): p. 7661-7665.

157. Viger, M.L., et al., *Reduction of self-quenching in fluorescent silica-coated silver nanoparticles.* Plasmonics, 2008. **3**(1): p. 33-40.

158. Burda, C., et al., *Chemistry and properties of nanocrystals of different shapes.* Chemical reviews, 2005. **105**(4): p. 1025-1102.

159. Liz-Marzán, L.M., *Tailoring surface plasmons through the morphology and assembly of metal nanoparticles.* Langmuir, 2006. **22**(1): p. 32-41.

160. Lakowicz, J.R., et al., *Release of the self-quenching of fluorescence near silver metallic surfaces.* Analytical biochemistry, 2003. **320**(1): p. 13-20.

161. Tovmachenko, O.G., et al., *Fluorescence Enhancement by Metal‐Core/Silica‐Shell Nanoparticles.* Advanced materials, 2006. **18**(1): p. 91-95.

162. Dondapati, S.K., et al., *Label-free biosensing based on single gold nanostars as plasmonic transducers.* Acs Nano, 2010. **4**(11): p. 6318-6322.

163. Zhang, Y., et al., *A versatile synthesis route for metal@ SiO 2 core–shell nanoparticles using 11-mercaptoundecanoic acid as primer.* Journal of Materials Chemistry C, 2013. **1**(39): p. 6355-6363.

164. Ung, T., L.M. Liz-Marzán, and P. Mulvaney, *Controlled method for silica coating of silver colloids. Influence of coating on the rate of chemical reactions.* Langmuir, 1998. **14**(14): p. 3740-3748.

165. Rodríguez-González, B., et al., *AuAg bimetallic nanoparticles: formation, silica-coating and selective etching.* Faraday discussions, 2004. **125**: p. 133-144.

166. Lachaine, R., et al., *Computational design of durable spherical nanoparticles with optimal material, shape and size for ultrafast plasmon-enhanced nanocavitation.* ACS Photonics, 2016.

167. Malitson, I., *Interspecimen Comparison of the Refractive Index of Fused Silica*,†.* JOSA, 1965. **55**(10): p. 1205-1209.

168. Li, Z., et al., *Ammonia-free preparation of Ag@ SiO 2 core/shell nanoparticles.* Applied Surface Science, 2015. **345**: p. 122-126.

169. Asselin, J., et al., *Supported core–shell nanobiosensors for quantitative fluorescence imaging of extracellular pH.* Chemical Communications, 2014. **50**(89): p. 13746-13749.

170. Szaba Jr, G., et al., *Epitope mapping by photobleaching fluorescence resonance energy transfer measurements using a laser scanning microscope system.* Biophysical journal, 1992. **61**(3): p. 661.

171. Song, L., et al., *Photobleaching kinetics of fluorescein in quantitative fluorescence microscopy.* Biophysical journal, 1995. **68**(6): p. 2588.

172. Fu, Y., J. Zhang, and J.R. Lakowicz, *Plasmonic enhancement of single-molecule fluorescence near a silver nanoparticle.* Journal of fluorescence, 2007. **17**(6): p. 811-816.

173. Song, J.-T., et al., *Composite silica coated gold nanosphere and quantum dots nanoparticles for X-ray CT and fluorescence bimodal imaging.* Dalton Transactions, 2015. **44**(25): p. 11314-11320.

174. Sapsford, K.E., et al., *Biosensing with luminescent semiconductor quantum dots.* Sensors, 2006. **6**(8): p. 925-953.

175. Kitamura, R., L. Pilon, and M. Jonasz, *Optical constants of silica glass from extreme ultraviolet to far infrared at near room temperature.* Applied optics, 2007. **46**(33): p. 8118-8133.

APPENDIX A – DUAL MODE IMAGING SET-UP

The multiplexed imaging is based on colocalization of NPs in image of both dark-field and fluorescence mode.

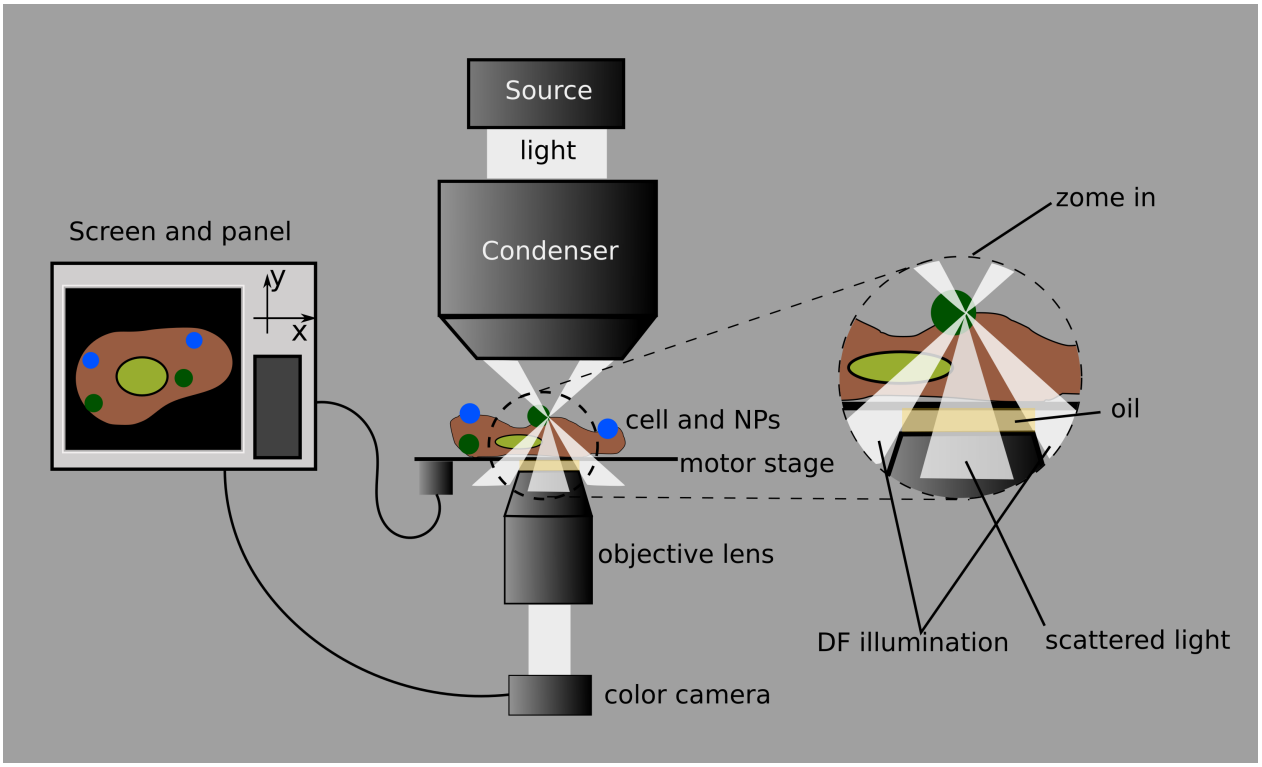

Figure A.1 Schematic assembly dark field with color camera. The dark field condenser illuminates the sample with a hollow cone of light. The microscope objective can only pick up light that has been scattered by the sample. The image is then projected onto the color camera.

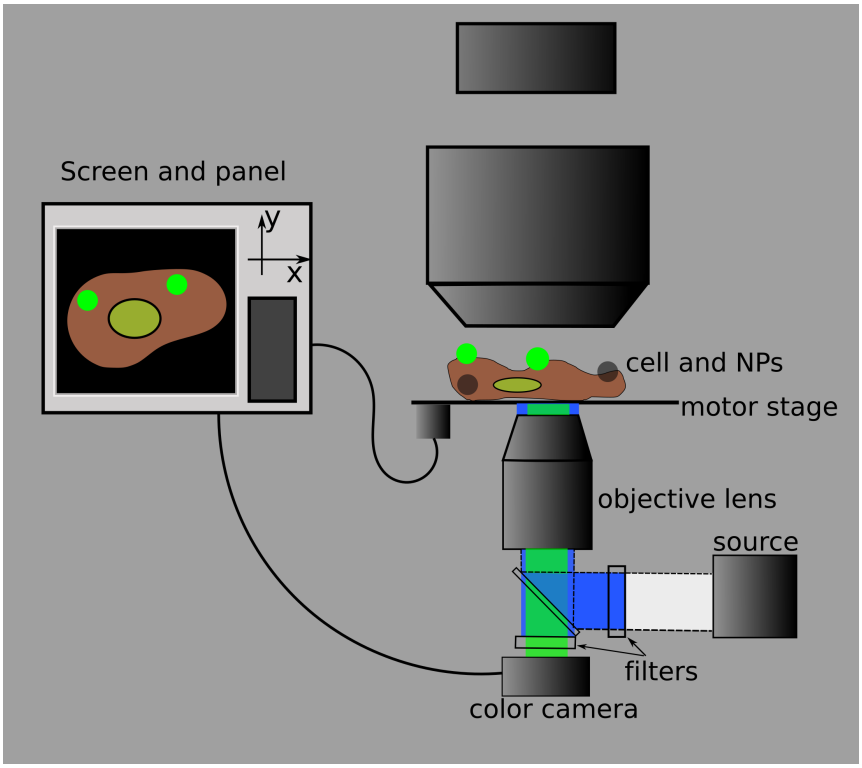

Figure A.2 Schematic of fluorescence microscopy with color camera, white light source illuminate sample from downside and in the scheme, a representation of FITC filter pass the excitation wavelength around 480nm(blue) and emission wavelength around 515nm(green). NPs with other fluorophore are exited and cannot be observed (black on the stage and not visible on screen.